U. S. DEPARTMENT OF COMMERCE
W. Averell Harriman, Secretary
NATIONAL BUREAU OF STANDARDS
E. U. Condon, Director

FEBRUARY 1948
VOLUME 40
NUMBER 2

JOURNAL OF RESEARCH

of the

NATIONAL BUREAU OF STANDARDS

Contents

RP		Page
1858	Lenses of extremely wide angle for airplane mapping. Irvine C. Gardner and Francis E. Washer (Price 10 cents)	93
1859	Effect of annealing and other heat treatments on the pH response of the glass electrode. Donald Hubbard and Gerald F. Rynders. (Price 10 cents)	105
1860	Infrared radiation from a Bunsen flame. Earle K. Plyler. (Price 10 cents)	113
1861	Perforated cover plates for steel columns; compressive properties of plates having ovaloid, elliptical, and "square" perforations. Ambrose H. Stang and Bernard S. Jaffe. (Price 10 cents)	121
1862	Behavior of certain sugars and sugar alcohols in the presence of tetraborates—correlation of optical rotation and compound formation. Horace S. Isbell, Joseph F. Brewster, Nancy B. Holt, and Harriet L. Frush. (Price 15 cents)	129
1863	Effect of inhibitors on the corrosion of zinc in dry-cell electrolytes. Clarence K. Morehouse, Walter J. Hamer, and George W. Vinal. (Price 10 cents)	151
1864	Thermodynamic functions for molecular oxygen in the ideal gas state. Harold W. Woolley. (Price 10 cents)	163

For sale by the Superintendent of Documents, U. S. Government Printing Office, Washington 25, D. C. - Price 40 cents
$4.50 per year on subscription

UNITED STATES GOVERNMENT PRINTING OFFICE, WASHINGTON : 1948

U. S. Department of Commerce
National Bureau of Standards

Research Paper RP1858
Volume 40, February 1948

Part of the Journal of Research of the National Bureau of Standards

Lenses of Extremely Wide Angle for Airplane Mapping

By Irvine C. Gardner and Francis E. Washer

If the illumination of the image produced by a wide angle lens covering a field of 120 degrees follows the cosine-fourth-power law, the illumination at the edge of the field will be one-sixteenth that at the center in the absence of vignetting. By introducing negative distortion, the illumination may be expected to be more uniform from the center to the edge of the field. In particular, if there is no vignetting, and if the diaphragm precedes the lens, there will be uniform illumination, even for a field as great as 180 degrees, if the distortion is such that $r'=f \sin \beta$, where r' is the distance from center of the field to a given image point, β is the corresponding angular distance from the axis in the object space, and f is the focal length corresponding to the part of the image in the neighborhood of the axis.

During the war Zeiss developed a mapping lens with a large amount of negative distortion and a second rectifying system by which undistorted copies could be obtained from the distorted negative made with the camera lens. A German mapping lens and a rectifying unit have been brought to this country, and detailed results of tests made at the National Bureau of Standards are given in this paper. The lens, termed the Pleon, covers a field of 130 degrees, and the distortion closely follows the law $r'=f\ \beta$, the distortion being somewhat less than that of the preceding formula. Measurements of the resolving power, of the effective size of the entrance pupil for different angular distances from the axis, and of the net distortion of the two systems are reported. In a final print there is significant residual distortion resulting from the failure of the distortions of the two systems to exactly annul each other.

I. Introduction

In general, a distortion-free photographic lens forms an image on a plane surface over which the illumination conforms, at least approximately, to the cosine-fourth-power law. According to this law, the illumination, E, of the image at any point in the field when there is no vignetting, is given by the equation

$$E=A_0 \cos^4 \beta, \tag{1}$$

where A_0 is the illumination at the axial point of the field and β is the angle, measured in the object space, between the axis and a chief ray passing through the object point conjugate to the image point under consideration. This law seriously restricts the extent of field that can be usefully covered by a wide angle lens. To illustrate this, a 90-degree field ($\beta=45$-degrees) the ratio of the illumination at the edge of the field to that at the center is 0.25 in the absence of vignetting. Actually, with so large a field angle, vignetting is inevitable and the ratio is probably further reduced to the value 0.12 or possibly even less. If a useful field of 120-degrees were achieved, the ratio would be 0.06 before vignetting is considered. This decrease in illumination from the center outward is a serious disadvantage when using black-and-white emulsion and makes the use of color film, because of its more limited latitude, quite impossible. The illumination over the field can be made uniform by using a variable density filter a short distance in front of the lens and so designed that the illumination at the center of the field is reduced much more than that at the edge. Such a method is undesirable because it greatly reduces the effective speed of the lens and makes longer exposures necessary. Slusareff [1] has called attention to the approximate character

[1] G. Slusareff, J. Phys. USSR **4**, 537 (1941); J. Opt. Soc. Am. **36**, 707 (1946).

771185—48

of the cosine-four-power law and has cited a particular lens, designed by M. Russinoff, for which the illumination varies as the third power of the cosine. In this lens the image is free from distortion, and the desirable departure from the cosine-fourth-power law arises because the entrance pupil, which is conjugate to a diaphragm within the lens, is larger for an oblique entering beam than for an axial entering beam.

II. Wide-Angle Lenses With Negative Distortion

It has been known for some time that a lens with a very large amount of negative distortion forms an image in which the illumination decreases much less rapidly from the center outward than is indicated by the cosine-fourth-power law. This is readily appreciated because, for the peripheral parts of the field, the luminous flux proceeding from a given small object area, for the lens with negative distortion, is concentrated on a region much smaller in area than for a distortion-free lens of the same equivalent focal length with consequent increase in the illumination. Gardner[2] describes a photogrammetric method in which photographs are taken from an airplane with a wide angle lens by which large amounts of negative distortion are introduced and subsequently, by the use of a copying or projection lens, a final print is made that is free from distortion. Merte[3] describes a wide-angle lens in which the first component is a negative meniscus. Distortion is not referred to in the patent, but computation shows that this lens does attain its wide coverage (180 degrees is claimed) by introducing large amounts of distortion. Richter,[4] in the patent which evidently applies to the Pleon lens, describes two wide-angle systems, each of which consists of an achromatic negative meniscus system which introduces large amounts of distortion and a following positive system, relatively free from distortion, which forms a real image in the plane of the photographic emulsion. At present no information is available concerning United States or German patents assigned to the firm of Carl Zeiss and applying to the rectifying system used with the Pleon lens. In the patent literature that has just been discussed, there are several statements concerning the more uniform illumination over the field of view resulting from the presence of large amounts of negative distortion. A quantitative statement of this effect has been given by Gardner[5] and it is shown that if the diaphragm is in front of a photographic lens and if there is no vignetting, the field will be uniformly illuminated, even out to 180 degrees, provided that the distortion is such that

$$r' = f \sin \beta, \tag{2}$$

where r' is the radial distance from the center of the field to a given object point, f is the equivalent focal length corresponding to the scale of imagery in the neighborhood of the axis of the lens, and β is as defined for 1. For a distortion-free lens

$$r = f \tan \beta, \tag{3}$$

and it is evident that the linear distortion corresponding to the angle β in the true field is given by the equation

$$\text{linear distortion} = f(\sin \beta - \tan \beta). \tag{4}$$

Applying eq 4 to a lens of 100-mm focal length, the distortions corresponding to values of β of 45 and 60 degrees are 29 mm (1.14 in.) and 87 mm (3.4 in.), respectively. These values illustrate the extremely large values of distortion that are encountered when uniformity of image illumination is secured by this means.

The lenses of extremely wide angle that have been referred to have the diaphragm within the lens system, and consequently eq 2 does not apply. However, the method by which eq 2 was derived can be applied to a lens system with an internal diaphragm. For such a lens system the relation between distortion and uniformity of illumination must be determined by a computation applied to the design data of the lens under consideration, and no general statement can be made.

III. Wide-Angle Photographs With Large Amounts of Distortion

With the large amounts of distortion that have been considered it is evident that the scale of the photograph becomes rapidly smaller from the center outward, that straight lines not passing through the center become curved lines concave

[2] Irvine C. Gardner, U. S. Patent 2,037,017 (April 14, 1936).
[3] W. Merte, U. S. Patent 2,126,126 (Aug. 9, 1938).
[4] R. Richter, U. S. Patent 2,247,068 (June 24, 1941).
[5] Irvine C. Gardner, J. Research NBS **39**, 213 (1947) RP1824.

toward the center, and that the photographs cannot be assembled directly to form a mosaic. Such photographs may, however, be used in a variety of ways. In Germany the availability of photographs of this character led to the chance discovery that pilots of airplanes are not confused by such distortion if they are provided with photographs on which their location in flight is over the central portion of the picture. It was said that the outer, more distorted portion of the picture served as a "finder", and that the smaller scale, with accompanying loss of detail at the edge of the picture, suggests the loss of detail due to haze and increased distance when far off objects are viewed from a plane. The extremely wide angle lenses, however, were not developed to produce photographs for the use of aviators, and it is not known how extensively the photographs were used for this purpose.

The large amount of radial distortion does not present any obstacle to the use of the photographs, in their original form, for mapping by means of plotted templates or other methods of radial triangulation, although the large negative distortion and the smaller scale to which peripheral points are recorded lessen the precision with which the radial angles can be constructed or the slots cut. With the extremely large coverage of each photograph, it might be possible to orient a series of photographs with a minimum of ground control points, after which a sufficient number of additional points could be interpolated to serve as control for the use of narrower angle distortion-free photographs from which a final map can be constructed. For such a procedure to succeed it would probably be necessary to have a particularly favorable array of very conspicuous landmarks, easily identified from the air and ground, to serve as control points.

In general, however, when a lens of the type under consideration, with large field and large negative distortion, has been developed, it has been the intention to develop an accompanying copying or enlarging lens with a large amount of positive distortion so that the original distorted negative might be copied to produce an undistorted print. It has been mentioned that negative distortion tends to make the illumination more uniform from center to edge. By the same token, positive distortion acts to increase the nonuniformity of illumination beyond that predicted by the cosine-fourth-power law, because the outer parts of the field, which in the natural course of events, would be more faintly illuminated than the center, have the illumination further decreased as a consequence of the greater magnification. For the copying lens, however, this unevenness of illumination is not so detrimental as in the case of the airplane camera lens, because copying is a laboratory process with the source of illumination entirely under control, and the uniformity of illumination in the image can be compensated by illuminating the negative in an appropriate manner.

One might envision the use of the copying lens of the preceding paragraph in a multiplex projector and the direct production of a contour map from the distorted photograph. The unevenness of illumination introduced by the projection lens, however, would introduce difficulties more serious for the multiplex operation than for the production of enlargements, and it appears that they might be insurmountable. On the other hand, the copying lens, instead of producing an enlargement, might be designed to produce a distortion-free diapositive of suitable scale to be used in a multiplex projector.

IV. Pleon Lens

During World War II, Richter, of Zeiss, designed a camera lens and a rectifying lens of the type under consideration. They were designated, respectively, the Pleon lens and the Pleon rectifier. Samples of the lenses and drawings of the optical system were obtained by the intelligence groups working in Germany after the war. Figure 1 is a reproduction from a photograph of the Pleon lens tested. Figure 2 shows the optical system as specified (fig. 2 and table 2) in U. S. Patent 2,247,068 (June 24, 1941). The first two elements form the member A, which is an achromatized lens of the type sometimes referred to as a "field compressor." The lens is designed to cover a full field of 130 degrees. The extreme chief rays entering the negative system and including this angle, after refraction, include an angle approximately 40.7 degrees. (These values are based on ray tracing applied to the design data given in the patent.) This smaller field is then imaged by the second member of the system at B, which is similar to the Metrogen lens in design. The diaphragm is at C, and D represents a filter

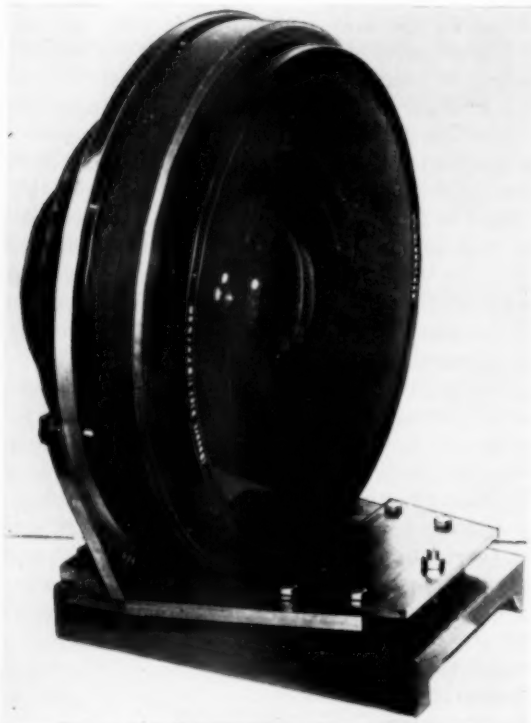

FIGURE 1. *Pleon lens as mounted on a laboratory support for testing.*

The surface shown is the large first surface of the field compressor and is turned toward the object. The diameter of this surface is approximately 1 foot.

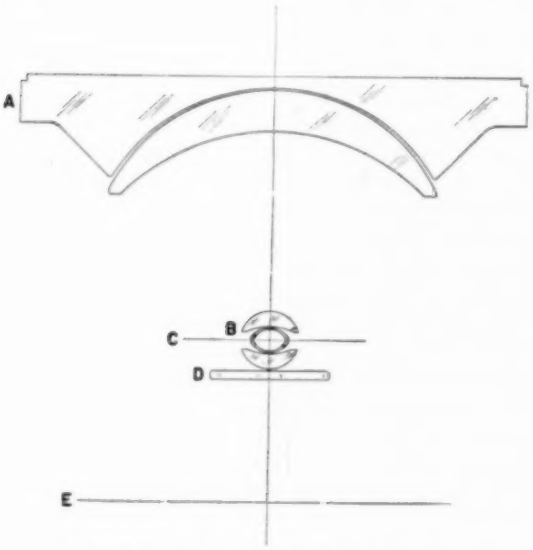

FIGURE 2. *Optical system of the Pleon lens.*

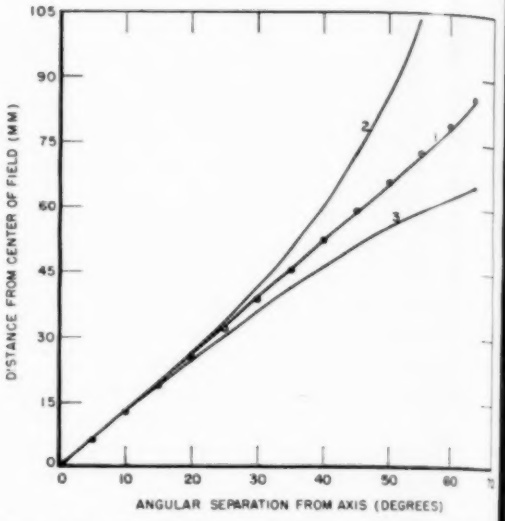

FIGURE 3. *Relation between distance of image point from center of negative and angular displacement of corresponding object point from the axis for the Pleon lens.*

Curve 1 shows results of measurements made on Pleon lens and corresponds respectively to equation $r=f\beta$. Curves 2 and 3 correspond respectively to equation $r'=\tan\beta$ applying to a distortion free lens, and to the equation $r'=f\sin\beta$.

which is an integral part of the lens. The image plane is at E. To give an idea of the size of this lens it may be noted that for a nominal focal length of 72.5 mm, the over-all diameter of the first negative component is 300 mm. and the distance from the plane surface of this component to the second surface of the filter D is 180 mm. In another method of considering this system the negative member A and a portion of the positive power of the second member may be assumed to constitute a Galilean telescope system used backward, which produces an image at an infinite distance but much reduced in angular dimensions. The remaining power of the second member is utilized to form a real image on the photographic emulsion of this intermediate reduced image. The measured equivalent focal length of the camera lens, corresponding to the center of the field, is 72.1 mm. The radius of the negative, corresponding to a half angle of approximately 65 degrees, is 85 mm, and the linear distortion is −68.8 mm. In other words, in the absence of distortion, the radius of the negative corresponding to 65 degrees and the given focal length would be 154 mm from eq 3. The distortion is such that

$$r' = f\beta \qquad (5)$$

where the notation is the same as for eq 2 and 3. This relationship is illustrated by the graph of figure 3. Curves corresponding to the relations, $r = f \tan \beta$ (see eq 3) and $r' = f \sin \beta$ (see eq 2) are also shown in figure 3. The distortion, therefore, is not as great as that of eq 2, but no direct deduction concerning the illumination can be made because the diaphragm is not in front of the lens system, as was specified in the example of section III. Experience shows that the illumination of the field is satisfactorily uniform. The resolving power is excellent, ranging from 82 lines per millimeter at the axis to 18 and 29 for tangential and radial lines, respectively, at 65 degrees.

V. Pleon Rectifier

Two views of the Pleon rectifier are shown in figures 4 and 5. Figure 4 shows the instrument

FIGURE 4. *Pleon rectifier.*

The film to be printed passes through the instrument near the center, the rolls of film resting in the metal pockets on either side. The paper is held flat near the bottom of the instrument by a vacuum back actuated by the small motor-driven exhaust pump at the right. The eyepiece, marked *G*, is part of an auxiliary optical system for centering the negative. The knob, *H*, swings four prisms into position for viewing the collimation marks on the negative in order to center it.

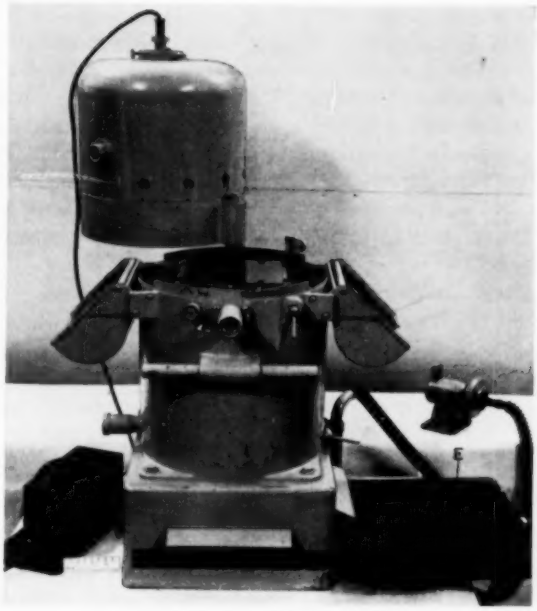

FIGURE 5. *Pleon rectifier.*

The top of the instrument is swung to the left to expose the glass pressure plate by which the negative film is held flat during the operation of printing. The sensitive paper is held flat by the vacuum plate swung out of the instrument in position for loading. The two small doors near the bottom are for the insertion of paddles for dodging the print to compensate for differential illumination of the terrain at the time the exposure was made.

closed in position for making the rectified print. The film to be printed passes through the instrument near the center, the rolls of film resting in the metal pockets on either side. The paper is held flat near the bottom of the instrument by a vacuum back actuated by the small motor-driven exhaust pump at the right. The over-all height of the instrument is approximately 4½ feet. Figure 5 shows the instrument open at the top to expose the glass pressure plate that holds the negative film flat and with the vacuum plate swung out to permit loading the instrument with a sheet of sensitive paper.

Figure 6 shows the optical system of the Pleon rectifier. The lamp, shown at *A*, was apparently a mercury arc of the pressure type, familiar in this country, with the mercury vapor contained in a capsule of fused-quartz. The lamp of the rectifier received from Germany was broken, and a duplicate was not obtainable. The rectifying system is not corrected chromatically, a filter, apparently of cobalt glass, forming a part of the system. The group of parts marked *B* comprises this filter and a

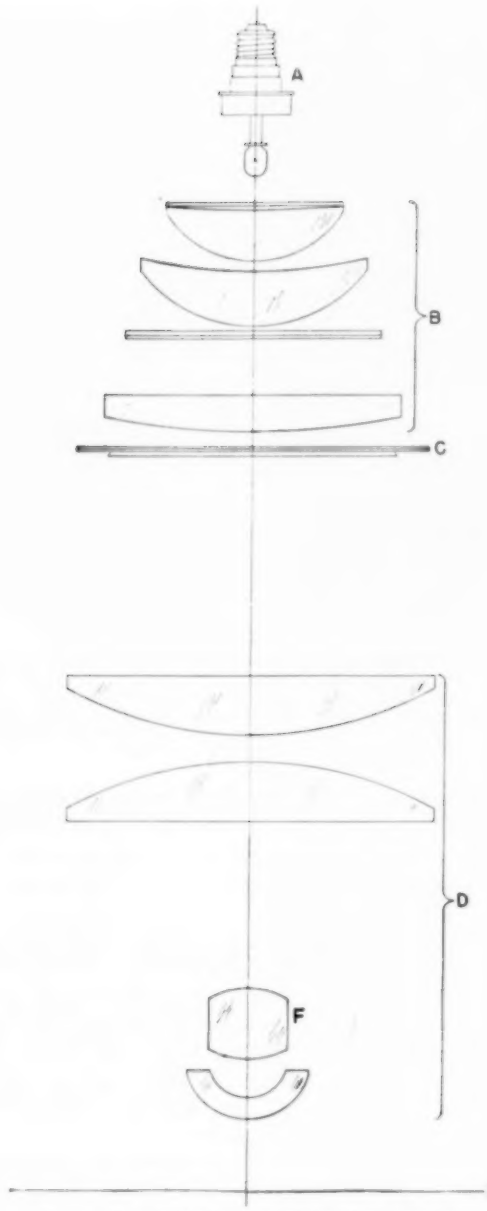

FIGURE 6. *Optical system of the Pleon rectifier.*

condensing system. At C is the stage on which the negative to be copied is placed and also a variable density filter for compensating the otherwise uneven illumination of the image. This filter also failed to arrive from Germany, and an approximate filter was produced by placing a photographic plate at C and exposing it by light transmitted backward through the optical system from E. The rectified image is produced in the plane at E by the projection system marked D. This part of the optical system contains one detail not clearly recognizable from figure 2. Lens F appears to be double convex. Actually, however, the surface nearer E is coated with black opaque paint except for an area on the axis not greater than 1 mm in diameter. This area, which is the limiting diaphragm of the system, is concave, the radius of curvature being approximately equal to that of the first surface of component F. The over-all length of the system, from the mercury capsule of the lamp to plane E, is approximately 110 cm. Figure 4 shows the complete rectifier. With the distortion changing so rapidly from the center outward, it is evident that the axial point of the negative must be carefully alined with the axis of the rectifying system if the resulting print is to be distortion free or even radially symmetrical. To facilitate this adjustment an auxiliary optical system, not shown in figure 6, is provided. Immediately below stage C there are four prisms by which the images, on the negative, of the four camera collimation markers can be simultaneously viewed and brought into coincidence with indexes in the rectifier. In figure 4, G is the eyepiece through which the markers are viewed and H is a knob for throwing the prisms out of the field after the adjustment has been completed. The vacuum plate that holds the paper flat is shown at E. Openings, covered by doors, shown on figure 3, are also provided for inserting a paddle over the printing paper for dodging to compensate for nonuniform illumination of the terrain at the time that the exposure was made.

VI. Measurements on Pleon Lens and the Rectifier

The conjugate distances for the rectifying lens were so adjusted that there was a reduction on the axis of 1:0.82. Consequently, the scale of the rectified print corresponds to an equivalent focal length of 59.1 mm. The resulting circular print for an angle of 65 degrees, if accurately freed from distortion, would have a radius of 126.8 mm. For a point at the edge of the field ($\beta = 65$ degrees), the magnification incidental to the rectification is 4.58 diameters. If the magnification on the axis

were 1:1, the magnification at the edge would be 5.59 diameters. The resolving power of the camera lens was measured at 5-degree intervals. The over-all resolving power of the camera lens and the rectifying system was obtained by computation, the assumption being that the rectifying lens recorded faithfully all detail in the original negative. The final resolving power for any angle (measured in the object space) therefore, is equal to the resolving power of the Pleon lens divided by the magnifying power of the rectifier for the same object ray. On the basis of such computation, the resolving power on the final print is 100 lines per millimeter on the axis, and for 65 degrees it is 4 and 6 lines, respectively, for tangential and radial lines.

In figure 7 the linear distortions are plotted for the camera lens, the rectifying unit, and the combination of the two systems. The values of the distortion for the camera lens have been multiplied by 0.82, corresponding to the axial reduction introduced by the rectifying system before being plotted on figure 7. This having been done, the distortion for the complete process corresponding to any angular distance from the axis is found by adding the ordinates corresponding to the lens and rectifier. It will be noticed that there is a net negative distortion of −4.34 mm at the edge of the resulting print after rectification. This is much too great for photogrammetric purposes. However, this result should be accepted with considerable caution because there is a possibility that camera lens and rectifier were designed to be selectively paired for use, and the two instruments received for test have not had the advantage of such pairing. Nevertheless, certain general considerations stand out. The camera lens has a negative distortion of −68.8 mm at the edge of the field. When the distortion is so large, it is to be expected that not only third order but many higher orders of distortion are present. If the rectifier is to accomplish its purpose in a satisfactory manner it must introduce the same orders of distortion in such magnitudes that each order of distortion in the negative is very closely compensated by a term of the same order in the rectifier. With camera lens and rectifier system so different in design, it is hardly to be expected that complete compensation for all orders can be secured.

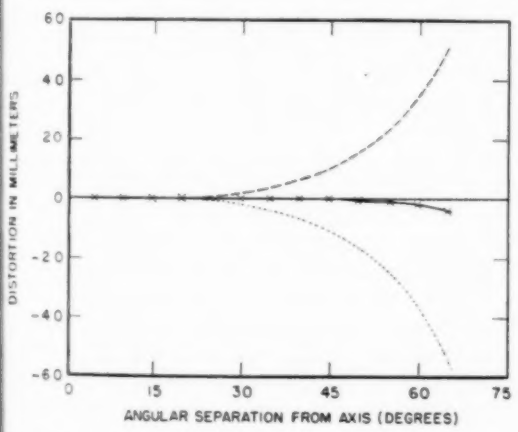

FIGURE 7. *Linear distoration of camera lens, rectifying system, and final rectified print.*

The dotted curve shows the linear distortion of the camera lens, multiplied by 0.82 to reduce the values to the scale of the rectified print. The dashed curve shows the linear distortion of the rectifying system. The full-line curve, obtained by adding the corresponding ordinates of the first two curves, shows the residual distortion in the final print.

The camera lens tested was No. 2801326, nominal focal length 72.5 mm, and maximum aperture ratio 1:8. It bore the Zeiss imprint and was definitely a Zeiss product. The rectifier was No. 200701 and bore the manufacturer's code designation "rln." Ordinarily, Zeiss products, during the war, were marked with the code "blc," but one of the German scientists now in this country affirms that the rectifier was manufactured by Zeiss, despite the code "rln."

1. Focal Lengths

The equivalent focal length and back focal length were found to be 72.13 and 74.78 mm, respectively. This value of the equivalent focal length was obtained from the approximate relation $f=d$ cot 5 degrees, where f is the focal length, d is the distance separating fiducial marks in the images on the negative of targets that are located at 0 and 5 degrees from the lens axis in the object space. These values of the focal length have been selected to give best average definition across the entire negative and do not necessarily correspond to those values of the focal length that give best definition on the axis. The probable errors of these determinations do not exceed ± 0.10 mm.

2. Distortion of Pleon Lens and the Rectifier

The values of the distortion listed in table 1 are measured in millimeters and indicate the dis-

placement of the image from its distortion-free position. A positive value indicates a displacement from the center of the plate. The probable errors for the Pleon lens data do not exceed ± 0.02 mm for the range 0 to 45 degrees; beyond this range the probable error increases rapidly and may be as high as ± 0.20 mm at 65 degrees. The probable errors for the projector lens do not exceed ± 0.03 mm for the range 0 to 45 degrees; beyond this range the probable error increases rapidly and may be as high as ± 1.00 mm at 65 degrees.

TABLE 1. *Distortion of the Pleon lens, rectifier, and final print from rectifier*

Angular separation from the axis	Distance from center of the Pleon lens negative	Distortion in Pleon lens negative	Contributions to distortion in final print		
			Pleon lens (adjusted)	Projection lens (contributed)	Net distortion
Degrees	*mm*	*mm*	*mm*	*mm*	*mm*
0	0.00	0.00	0.00	0.00	0.00
5	6.30	.00	.00	+.02	0.02
10	12.64	−.08	−.06	.12	.06
15	19.02	−.30	−.24	.29	.05
20	25.47	−.78	−.64	.67	.03
25	32.00	−1.62	−1.32	1.41	.09
30	38.64	−3.00	−2.45	2.47	.02
35	45.38	−5.12	−4.19	4.19	.00
40	52.20	−8.32	−6.80	6.88	.08
45	59.08	−13.04	−10.66	10.60	−.06
50	65.91	−19.98	−16.34	15.51	−.83
55	72.68	−30.16	−24.66	23.96	−.70
60	79.22	−45.44	−37.15	35.34	−1.81
65	85.39	−68.80	−56.26	51.92	−4.34

The distortion of the Pleon lens was determined in the usual manner with the aid of the precision lens-testing camera,[6] with the exception that a second setting of the camera bench was necessary to measure the region from 45 to 70 degrees. For the projector lens, a halftone screen with accurately measured spacings was used as target, a deep-blue filter (tricolor C) was placed over the target, and exposure made with a moving lamp instead of the illuminator supplied with the projector. (This method was necessary because the special bulb required for the projector was not available.) The exposure was made on a Panatomic-X plate. Correspondence of the angular values reported for both lenses was accomplished by a series of interpolations, with the distance from the center of the master negative made on the precision lens-testing camera serving as the connecting link. The primary purpose in effecting this correspondence was to permit the distortion of the lens and the projector to be evaluated at the same point on the negative made with the Pleon lens. Thus these values can be used in evaluating the performance of the combination, as is done in the last column of table 1.

3. Resolving Power of the Pleon Lens and the Rectifier

The values of the resolving power, shown in table 2, are given at 5-degree intervals from the center of the field, and, for the Pleon lens, are obtained by photographing test charts comprised of patterns of parallel lines. The series of patterns of the test charts are imaged on the negative with the lines spaced 10, 15, 20, 29, 41, 58, 81, 116, and 163 lines per millimeter. The values marked "tangential" give the number of lines per millimeter in the image on the negative of the finest pattern of the test chart that is distinctively resolved into separare lines when the lines lie perpendicular to the radius drawn from the center of the field. The row marked "radial" gives similar values for the pattern of test lines lying parallel to the radius. Because of the unusual distortion characteristics of this lens, the above series of resolving power values is valid only on the axis of the lens. Therefore, in order to avoid error, line spacings were measured in each image on the negative, and the values of resolving power computed from these measurements.

The value of the resolving power of the projection lens was not measured, but the resolving power in a final print has been computed on the assumption that the projection lens reproduces all detail present in the original negative. Reference to table 2 shows that the distance from the axis to the image of a point at the angular distance β from the axis is closely proportional to β. In the final image, if the distortion is eliminated, the corresponding distance is proportional to $\tan\beta$. Therefore, the instantaneous value of the magnification introduced by the projection lens, corresponding to any value β is $1/1.223\cos^2\beta$, where 1.223 is the reciprocal of the axial magnification introduced by the projection lens. It is, therefore, evident that the formula

[6] I. C. Gardner and F. A. Case, J. Research NBS **18**, 449 (1937) RP984.

TABLE 2. *Resolving power in lines per millimeter*

Angular separation from the axis	Pleon lens (measured)		Projection lens (computed)	
Degrees	*Tangential*	*Radial*	*Tangenital*	*Radial*
0	82	82	100	100
5	82	82	100	100
10	86	83	102	98
15	85	83	97	95
20	72	83	78	90
25	59	81	59	81
30	54	81	50	74
35	55	59	45	48
40	54	47	39	34
45	57	34	35	21
50	39	27	20	14
55	38	29	15	12
60	43	30	13	9
65	18	29	4	6
70	--	31	---	4

$$\text{Resolving power} = 1.223r \cos^2\beta,$$

where r is the resolving power of the Pleon lens corresponding to the value β, is the resolving power of the combination of lens and projector, assuming that no loss of detail is caused by the projection lens. It is, therefore, the maximum resolving power obtainable in the final projected print of a negative made with the Pleon lens, neglecting reductions that may result from aperture limitations. In view of aperture limitation discussed in the description of component F in figure 2, it is possible that the maximum resolving power for the rectifier may not exceed 20 lines per millimeter, which is, however, still adequate for good prints.

4. Effect of Vignetting for the Pleon Lens

In table 3, the vignetting of the Pleon lens is given, together with the comparable quantities for an ideal lens and for a Topogon-type lens. Let A_β be the projected area of the stop opening as viewed from the object space at the angular obliquity β; and let A_0 be the corresponding area of the stop opening as viewed from the object space along the lens axis. Then the ratio A_β/A_0, on the basis of first order imagery, is equal to $\cos\beta$ for the case of the ideal lens having no vignetting. Appreciable vignetting exists in the Pleon lens as the measured value of A_β/A_0 is smaller for it than for the ideal lens. However, for values of $\beta \leqq 30$ degrees, the loss of light by vignetting is much less for the Pleon lens than for the Topogon-type lens.

TABLE 3. *Vignetting of the Pleon lens*

Angular separation from the axis	Relative area of diaphragm stop A_β/A_0		
	Ideal lens (cosine)	Pleon lens	Topogon type lens
Degrees			
0	1.00	1.00	1.00
10	0.98	0.96	0.96
20	.94	.87	.87
30	.87	.80	.72
40	.77	.67	.49
45	.71	.60	.25
50	.64	.52	----------
60	.50	.27	----------
65	.42	.05	----------

Figure 8 reproduces a photograph, reduced approximately 40 percent, as made with the Pleon lens by AAF personnel at Wright Field. At the peripheral parts of the lens, the full possibilities are not realized because of haze. It is obviously desirable to have ideal atmospheric conditions, and possibly to use infrared plates, if the full 130-degree field is to be achieved.

Figure 9 reproduces a rectified print reduced to the same percentage as figure 8. This probably does not represent the best possible print, because of the haze effect in the original negative and also because, as has been mentioned, the lamp and variable density filter designed to be used with the rectifier were not available.

The rectified print (fig. 9) was made by Walter R. Darling, of the National Bureau of Standards, and he is to be commended for the resourcefulness and ingenuity that he showed in obtaining so good a print with an incomplete rectifier.

FIGURE 8. *Photograph from negative exposed in airplane camera with Pleon lens.*

FIGURE 9. *Rectified copy of photograph shown in figure 8.*

This probably does not represent the best obtainable results, because the rectifier, when received in this country, was imperfect, the lamp being broken and the variable density filter missing. Figures 8 and 9 have been reduced in the same proportion from the original prints.

WASHINGTON, September 9, 1947.

U. S. Department of Commerce
National Bureau of Standards

Research Paper RP1859
Volume 40, February 1948

Part of the Journal of Research of the National Bureau of Standards

Effect of Annealing and Other Heat Treatments on the pH Response of the Glass Electrode

By Donald Hubbard and Gerald F. Rynders

The effect of annealing and other heat treatments on the pH response of electrodes prepared from Corning 015 glass has been studied and a comparison made with the accompanying changes in hygroscopicity of the glass. New, unleached electrodes continued to give the correct pH response after being annealed near the critical temperature as indicated by the expansion curve for Corning 015 glass. Electrodes that were leached in 0.1 *N* HCl at 80° C lost much of their pH function when given identical heat treatments. The pH response of a typical glass electrode, held 10 minutes at 500° C after being leached in 0.1 *N* HCl for 6 hours at 80° C, was reduced from 59 millivolts per pH (the theoretical value at 25° C) to 22 millivolts per pH. A few seconds in hydrofluoric acid solution restored the pH function of these "dead" electrodes, showing that the inhibiting effect was confined to the outer surface of the electrode bulbs. Evidence obtained by the interferometer indicated that the thickness of this inhibiting layer was less than 5.8×10^{-6} centimeter. Hygroscopicity determinations made on leached samples of the powdered glass showed that the "sorption" power was greatly reduced by heat treatment, whereas for unleached specimens this property was much less affected. From the evidence obtained it seems reasonable to interpret the loss in pH function shown by glass electrodes on heat treatment as being due to the formation of a thin nonhygroscopic silica-rich layer. The resulting electrodes behaved in a manner similar to electrodes prepared from glasses of low hygroscopicity.

I. Introduction

Considerable confusion exists concerning the effect of annealing (release of strain within the glass) on the pH response of the glass electrode. This confusion has been further increased by nonconventional usage of the term annealing. For example, heat treatment of a glass electrode at 120° C should not properly be classified as annealing, as essentially no release of strain within the glass is brought about until much higher temperatures are attained, [1, 2, 3, 4, 5, 6][1] such as the critical temperature, *CT*, indicated by the expansion curve, figure 2. Nevertheless, heat treatment of an electrode for 15 to 20 hours at 120° C is reported to cause a reduction in pH response that is variable and very slow in disappearing [7]. Also, if the electrode is subjected to prolonged or repeated heating at high temperatures, the hydrogen electrode function may disappear completely [8].

The present investigation was undertaken in order to obtain a clearer understanding of the effect of annealing and other heat treatments on the pH response of the glass electrode, with particular attention being given to the accompanying alteration in hygroscopicity of the glass.

II. Experimental Procedure

The pH response was determined by comparing the experimental electrodes against a well-conditioned glass electrode as the reference electrode and measuring the voltage with a Beckman pH meter, model G. The experimental electrodes were blown as thin walled bulbs [9] of Corning 015 glass (72% SiO_2, 22% Na_2O, and 6% CaO) [10] on the end of soft glass tubing and the bulb filled with mercury for the inner connection [11]. Unless otherwise stated, the electrodes were con-

[1] Figures in brackets indicate the literature references at the end of this paper.

ditioned for at least 1 hour in distilled water. The emf values obtained in Britton-Robinson universal buffer mixture [12] of pH 1.9 were taken as the zero voltage departure [2] and the data of the investigation confined to a pH range over which the glass electrode is known to give reliable readings.

For the purpose of rapid aging, some electrodes were leached in 0.1 *N* HCl at 80.0°±0.2° C in a constant-temperature bath for 6 hours. Following a heat treatment, the electrodes were conditioned again for 1 hour in distilled water before use.

All heat treating was done in a small electrically heated muffle furnace whose temperatures were measured to an accuracy of ±10° C. The annealing schedule consisted of holding the electrodes for 10 minutes at or a few degrees above the critical temperature of Corning 015 glass, cooling slowly to 400° C and then more rapidly to room temperature.

The hygroscopicity data were obtained from the weight of moisture "sorbed" [14, 15] by powdered samples (approximately 1.5 g) of the glass that passed a Tyler standard 150 mesh sieve. This powder was exposed to the high relative humidity (approximately 98%) maintained by a saturated solution of $CaSO_4.2H_2O$, thermostated at 25° C. The results are reported in terms of grams of water sorbed per cubic centimeter of glass, calculated as follows:

$$\frac{\text{weight of water sorbed} \times \text{density of glass}}{\text{weight of sample}}$$

III. Results and Discussion

1. Effect of Annealing

To ascertain what effect true annealing (release of strain) has on the behavior of the glass electrode, 12 electrodes of Corning 015 glass were prepared for study and their uniformity of pH responses determined after 1-hour conditioning in distilled water. Nine of them showed no departure from the theoretical value over the range pH 1.9 to pH 9.2, and none of the remaining three exhibited a departure greater than 3 mv over this range (curve *A*, fig. 1). Two of these electrodes were heated above the critical temperature (500° C)

[2] Theoretically, the potential difference between the hydrogen electrode and the experimental glass electrode in a hypothetical solution, normal with respect to hydrogen ions, should have been used as the zero potential [13]. This would have involved experimental difficulties that would add little or nothing to the present data except to displace the departure curves along the pH axis.

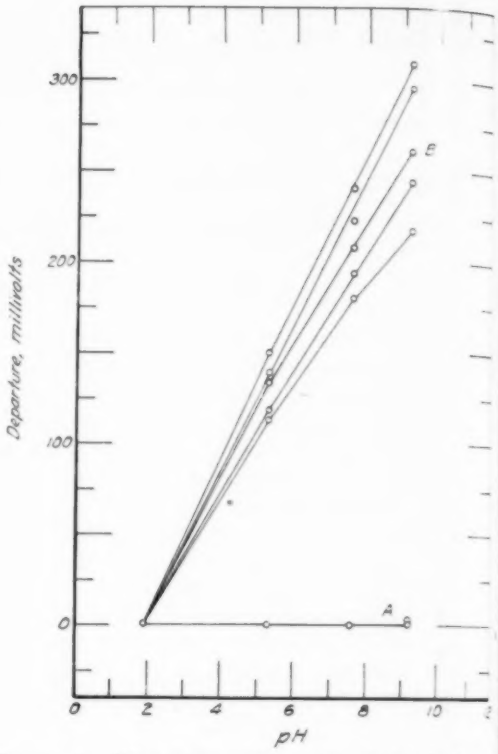

FIGURE 1. *Effect of annealing on the hydrogen electrode function of the glass electrode.*

A, Composite curve of voltage departure for glass electrodes; (1) at time of preparation; (2) unleached and annealed at 500° and 550°C; (3) after leaching in 0.1 *N* HCl at 80° C; (4) after treatment of "dead" electrodes with hydrofluoric acid. *B*, Voltage departures of five electrodes after being leached in 0.1 *N* HCl for 6 hours at 80° C and then annealed below 550° C.

but below the deforming temperature (550° C) indicated by the expansion curve for Corning 015 glass, curve *B* of figure 2,[3] obtained by the interferometer procedure [4, 17].

After holding for 10 minutes,[4] the temperature of the muffle was allowed to fall slowly to 400° C (curve *A*, fig. 2), followed by a more rapid cooling to room temperature. These two electrodes, upon being soaked for 1 hour in distilled water, showed no voltage departures (errors) over the range pH 1.9 to pH 9.2 and continued to coincide with curve *A*, figure 1.[5] To emphasize these

[3] The expansion curve for this specimen of Corning 015 glass exhibited a less pronounced critical region than is shown by many other glasses [4, 5, 6].

[4] As the electrodes were very thin, the time for temperature equilibrium to be attained throughout the specimen was very short. However, a holding period of 10 minutes was adopted for the sake of uniformity of procedure and also as it was a period sufficiently short to avoid devitrification [8].

[5] The initial emf readings of unleached electrodes at pH 1.9 were different before and after annealing and other heat tretament, but the pH response, mv per pH, remained unaffected.

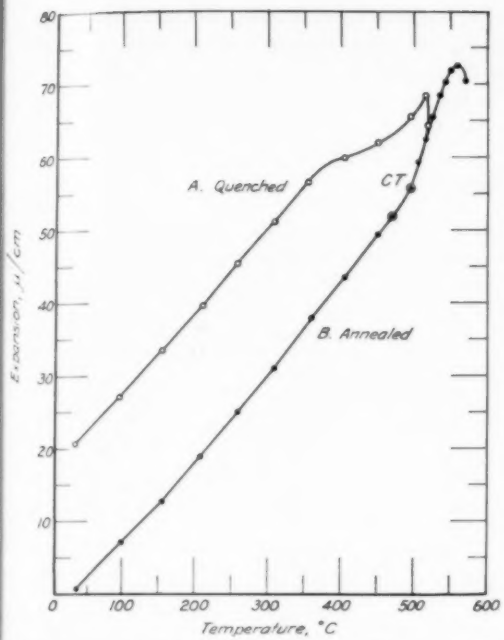

FIGURE 2. *Thermal expansion curve of Corning 015 glass.*
A, quenched; *B*, annealed. (Expansion data taken by J. B. Saunders).

results further, one of the electrodes was reheated to the deforming temperature, 550° C, and held for 3 hours before cooling slowly through the annealing range. The bulb was badly deformed by this treatment, but showed no failure of electrode function.

These data indicate that neither annealing nor high temperatures have any pronounced effect, either beneficial or detrimental, on the performance of virgin glass electrodes.

Five of the electrodes from the series were leached 6 hours in 0.1 *N* HCl at 80° C. These electrodes, at the end of the leaching period, still gave pH responses coinciding with curve *A*, figure 1. Upon being heated near 550° C and cooled according to the previous annealing schedule, these electrodes lost much of their electrode function (table 1, curves *B*, fig. 1) and behaved similarly to electrodes prepared from a glass of low hygroscopicity [18, 19]. The values for voltage departure plotted in these curves are those shown by the electrodes after 72 hours conditioning in distilled water. These results indicate the permanency as well as the magnitude of the inhibiting effect brought about by annealing after leaching.

Immersing these "dead" electrodes for a few seconds in hydrofluoric acid (1:1) restored their electrode function immediately, and their voltage departure values once again coincided with curve *A* of figure 1. These results showed that the loss of electrode function was confined to a very thin layer on the outer surface of the electrode bulb. If the swelling, 0.2 interference fringe [20], shown by Corning 015 glass for the period of time that the electrodes were leached in 0.1 *N* HCl is taken as an indicator of the maximum possible thickness of the inactivating layer, it can be no greater than 5.8×10^{-6} cm, calculated from the formula:

$$\text{Thickness} = \frac{\text{fringe displacement} \times \text{wave length of He light}}{2}.$$

TABLE 1. *Voltage departures (errors) of 5 glass electrodes after leaching in 0.1 N HCl, 6 hr at 80° C, followed in turn by annealing at 550° C and stripping with HF*

pH	Departure, millivolts														
	Electrode 1			Electrode 2			Electrode 3			Electrode 4			Electrode 5		
	0.1 *N* HCl	550° C	HF	0.1 *N* HCl	550° C	HF	0.1 *N* HCl	550° C	HF	0.1 *N* HCl	550° C	HF	0.1 *N* HCl	550° C	HF
1.9	0	0	0	0	0	0	0	0	0	0	0	0	0	0	0
5.3	0	150	0	0	139	0	0	134	0	0	118	0	0	113	0
7.6	0	240	0	0	223	0	0	208	0	0	194	0	0	180	0
9.2	0	309	0	3	296	0	0	261	0	2	244	0	0	217	0

2. Effect of Heat Treatment at Temperatures Other Than the Annealing Range

Another series of glass electrodes was prepared for the purpose of confirming the findings in the previous section and extending the investigation to temperatures other than the annealing region. Three electrodes from this series were heated to 550° C, annealed by the previous schedule, and then tested for voltage departure after 1 hour of soaking in distilled water. As in the previous case,

771185—48——2

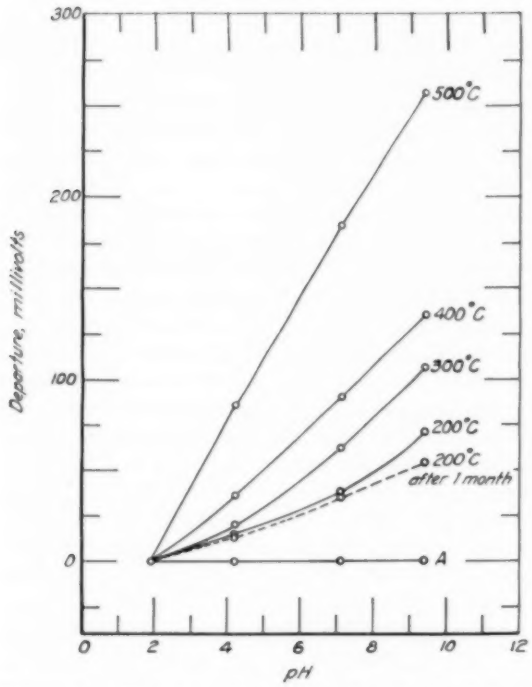

FIGURE 3. *Effect of heat treatment on the hydrogen electrode function of glass electrodes leached in 0.1 N* HCl, *6 hours at 80° C.*

there was no voltage departure brought about by the annealing (curve *A*, fig. 3). The remaining electrodes were leached for 6 hours at 80° C in 0.1 *N* HCl. Three of these, when heated to 550° C and cooled slowly through the annealing region, lost much of their hydrogen electrode function, which they regained immediately upon treatment with hydrofluoric acid. It is of passing interest to note that much of the pH response was restored to these "dead" electrodes by the application of HF to the smallest possible area.

These electrodes, annealed as in the earlier series, served not only to confirm the previous results but also acted as the control experiments for the present series.

Five of the leached electrodes were then heat-treated as a series in temperature steps of 100° C over the range from 100° to 500° C, inclusive. The data from table 2 plotted in figure 3 show the voltage-departure curves resulting from these heat treatments. The effect of the heat treatment at 100° C was not sufficiently permanent or steady to make satisfactory readings possible. However, for the other temperatures the effect had not disappeared after the electrodes had stood for 1 month in distilled water. The voltage departure, remaining after 1 month's soaking in distilled water for the electrode treated successively at 200° C, table 3, is shown as a broken line in figure 3.

TABLE 2. *Voltage departures (errors) of a series of glass electrodes after leaching in 0.1 N* HCl, *6 hr, at 80° C, followed by heat treatments at various temperatures*

pH	Voltage departure after heat treatment at—					
	Room temperature	100° C	200° C	300° C	400° C	500° C
	mv	*mv*	*mv*	*mv*	*mv*	*mv*
1.9	0	0	0	0	0	0
4.2	0	(a)	15	20	36	85
7.1	0	(a)	38	62	90	184
9.4	0	(a)	71	106	136	257

[a] Satisfactory readings not possible.

TABLE 3. *Voltage departures (errors) of a leached glass electrode showing the effect of successive reheating to 200° C*

pH	Voltage departures after reheating to 200° C.					
	First reading	Second reading	Third reading	Fourth reading	Fifth reading	
					1 hr	1 mo [a]
	mv	*mv*	*mv*	*mv*	*mv*	*mv*
1.9	0	0	0	0	0	0
4.2	15	12	13	14	14	13
7.1	38	41	46	48	46	35
9.4	71	78	76	80	82	54

[a] Continuous soaking in distilled water at room temperature.

When the values of voltage departure are plotted against temperature of heat treatment from table 2 or figure 3, the resulting curves (fig. 4) present a sharp increase in effect on the electrode function beyond 400° C. This can be readily rationalized with the critical temperature and annealing region indicated by the expansion curves of figure 2. It shows that the electrode function is destroyed much more strongly by heating near the critical temperature. If the procedure adopted in earlier publications [16, 19] of plotting the pH response as millivolts per pH in acid buffers is followed, the extent to which the electrode function of the glass has been adversely affected by heat treatment is apparent at a glance (table 4 and fig. 5).

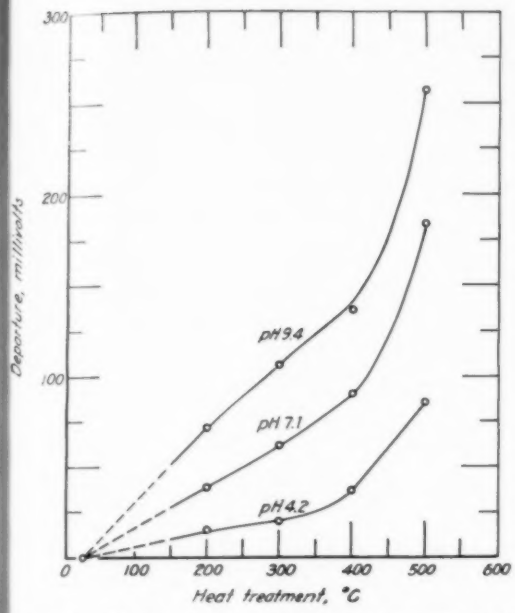

FIGURE 4. *Effect of the temperature of heat treatment on the hydrogen electrode function of glass electrodes at constant pH values.*

Data from figure 3 and table 2.

TABLE 4. *pH response of unleached and leached glass electrodes after heat treatment at various temperatures*

[The pH response values for the leached electrodes were calculated from the voltage departure data for pH 1.9 and pH 4.2 given in table 2]

Heat treatment	pH response	
	Unleached	Leached
	mv/pH	*mv*/pH
Room temperature	59	59
200° C	59	53.4
300° C	59	50.3
400° C	59	43.4
500° C	59	22.0

3. Effect of Heat Treatment on the Hygroscopicity of the Glass

Voltage anomalies (errors) of glass electrodes are normally associated with the hygroscopicity [16, 19], and changes in the chemical durability [18, 20] of the electrode glass. In the present investigation, as all pH measurements have been confined to a pH range over which little or no voltage departure can be accredited to durability shift of the glass, it seems reasonable to expect that the changes in hydrogen electrode function

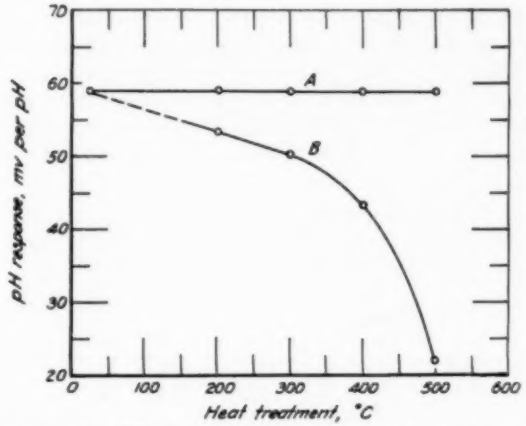

FIGURE 5. *Effect of heat treatment on the* pH *response of glass electrodes.*

A, Unleached; *B*, leached in 0.1 *N* HCl for 6 hours at 80° C. (Values calculated from the data in table 2, fig. 3 for pH 1.9 and pH 4.2).

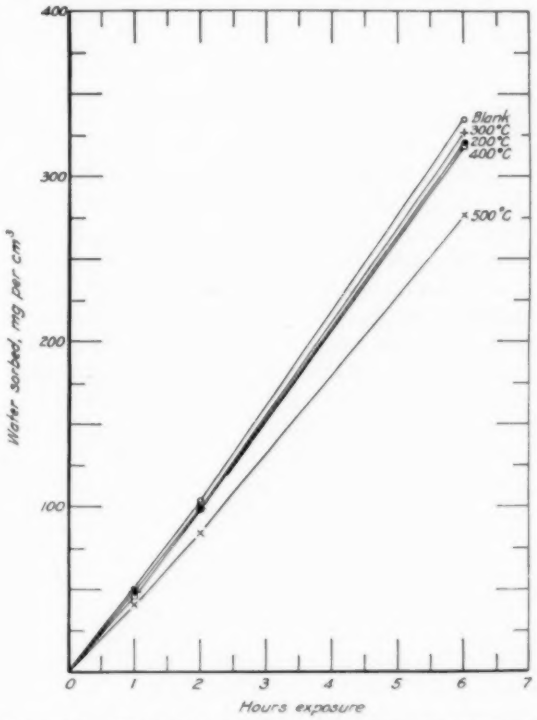

FIGURE 6. *Effect of heat treatment at various temperatures on the hydroscopicity of unleached powdered Corning 015 glass.*

caused by the various heat treatments of the electrodes might be associated with changes in hygroscopicity. Table 5 and figure 6 illustrate

the effect of heat treatment on the quantity of water sorbed by unleached powdered samples of Corning 015 glass. The effect of temperature up to 400° C was small with the sequence of curves for 200° C and 300° C being in a reverse order. The curve for 500° C, although displaced from the group, still indicates a glass of high hygroscopicity. These results correlate well with the fact that the annealing had little effect on the hydrogen electrode function of virgin glass electrodes.

TABLE 5. *Hygroscopicity of unleached powdered Corning 015 glass after various heat treatments*

Heat treatment	Water sorbed for exposures of—		
	1 hr	2 hr	6 hr
	mg/cm²	mg/cm²	mg/cm²
Room temperature	50	103	334
200° C	49	99	320
300° C	48	99	326
400° C	46	98	318
500° C	41	84	276

The displacement of the hygroscopicity curve for 500° C probably is not due entirely to a change in hygroscopicity of the glass, but largely due to a reduction of exposed surface from sintering at the high temperature. This sintering at 500° C was very evident at the time the sample was removed from the annealing furnace. However, this displacement indicated for 500° C was small in comparison with the effect of identical heat treatment on powdered samples that had been leached before heat treatment (table 6 and fig. 7). In this series, the powdered glass had been leached with 200 ml of 0.1 *N* HCl for 6 hours at 80° C, then washed, and dried at 110° C before heat treatment. The results showed a conspicuous lowering of the hygroscopicity that paralleled, in a remarkable fashion, the reduction in hydrogen electrode function of glass electrodes given similar treatment. (Compare figs. 3, 5, and 7.)

TABLE 6. *Hygroscopicity of leached powdered Corning 015 glass after various heat treatments*

Samples leached in 200 ml of 0.1 *N* HCl, 6 hr at 80° C

Heat treatment	Water sorbed for exposures of—		
	1 hr	2 hr	6 hr
	mg/cm²	mg/cm²	mg/cm²
Room temperature [a]	59	126	334
200° C	77	126	182
300° C	64	114	163
400° C	65	84	117
500° C	49	71	82

[a] Unleached specimen included as comparison control.

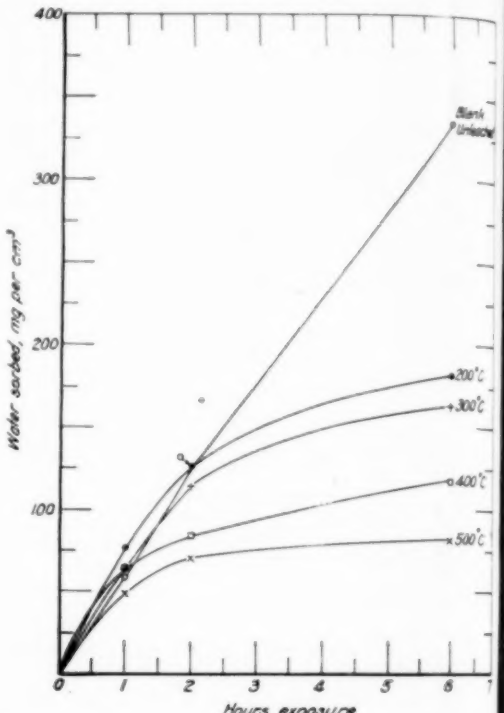

FIGURE 7. *Effect of heat treatment at various temperatures on the hydroscopicity of samples of powdered 015 glass leached in 0.1 N HCl, 6 hours at 80° C.*

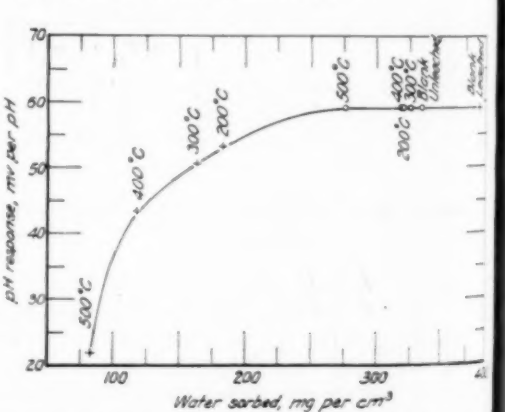

FIGURE 8. *Comparison of pH response of heat treated leached and unleached glass electrodes with the hydroscopicity of the glass after similar treatments.*

○, Unleached; +, leached.

An over-all view of the effect of heat treatment on the pH response of glass electrodes and the accompanying effect on the hygroscopicity of the glass is given in table 7 and figure 8. It emphasizes strongly that the pH response of the heat-treated electrodes is dependent on the accompany hygroscopicity of the glass surface as affected by leaching and not on the temperature of treatment alone.

TABLE 7. *Effect of heat treatment on the* pH *response and hygroscopicity of leached and unleached samples of Corning 015 glass*

Heat treatment	pH response		Water sorbed	
	Unleached	Leached	Unleached	Leached
	mv/pH	*mv/pH*	*mg/cm²*	*mg/cm²*
Room temperature	[a] 59	[a] 59	[b] 334	392
200° C	59	53.4	320	[c] 182
300° C	59	50.3	326	163
400° C	59	43.4	318	117
500° C	59	22.0	276	82

[a] Values from table 4.
[b] Values from table 5.
[c] Values from table 6.

Figure 7 showed that in most cases the sorption of moisture during the first hour of exposure by the leached powder was more rapid than for the fresh glass. This property is more strongly emphasized by the data presented in table 8 and figure 9. In obtaining these data, additional HCl was added to maintain the solution acid during the period of leaching. The behavior of the powder was noticeably different, with an increase in volume and more rapid rate of settling. The marked increase in the sorption of moisture by this treated glass during the early hours of exposure in the humidity chamber compared with the fresh glass sample, is undoubtedly the result of the difference in the chemical and physical nature of the surfaces presented, the desiccating property of silica gel becoming a decided factor.

TABLE 8. *Hygroscopicity of leached samples of Corning 015 glass after various heat treatments*

The leaching solution was maintained acid by repeated additions of HCl.

Heat treatment	Water sorbed after exposures of—		
	1 hr	2 hr	6 hr
	mg/cm²	*mg/cm²*	*mg/cm²*
Room temperature (unleached)	61	140	360
Room temperature (leached)	131	204	418
200°C	103	169	274
300°C	100	170	257
400°C	88	135	222
500°C	74	103	148

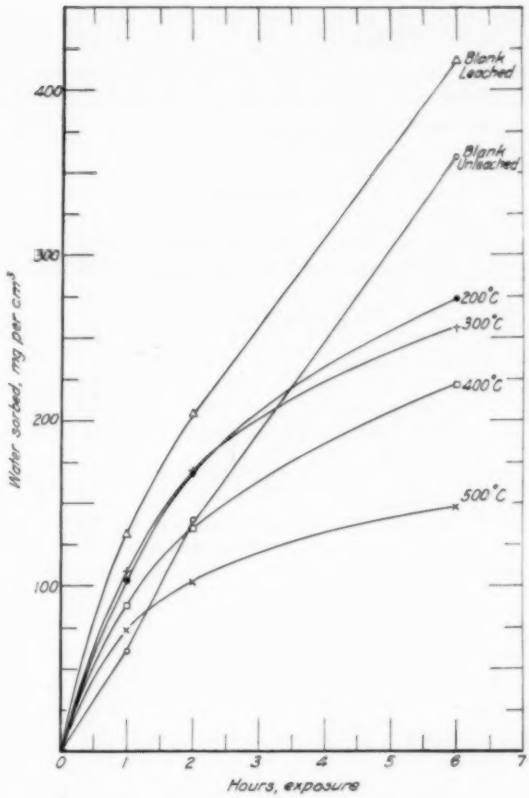

FIGURE 9. *Effect of heat treatment at various temperatures on the hydroscopicity of leached, powdered Corning 015 glass.*

The acid solution that normally becomes alkaline was maintained acid by repeated additions of HCl.

IV. Summary

New unleached glass electrodes were given annealing and other heat treatments without reducing their pH function, whereas electrodes leached in hydrochloric acid lost much of their pH response upon identical heat treatment. This reduction in pH response brought about by heat treatment was found to be accompanied by a reduction in the hygroscopicity of the glass. By treating these "dead" electrodes with hydrofluoric acid, it was possible to restore their hydrogen

electrode function and to show that the inhibiting effect was confined to a thin layer on the outer surface of the electrode bulbs. An estimate of 5.8×10^{-6} cm as the maximum thickness of these inhibiting films was made by means of the interferometer.

V. References

[1] George W. Morey, Amerian Chemical Society Monograph Series, No. 77. (Reinhold Publishing Corporation, New York, N. Y.).

[2] M. So, Proc. Tokyo Math. Phys. Soc. **9,** 426 (1918).

[3] L. H. Adams and E. D. Williamson, J. Franklin Inst. **190,** 597 (1920).

[4] C. G. Peters and C. S. Cragoe, BS Sci. Pap. **16,** 449 (1920) S393.

[5] W. E. S. Turner and F. Winks, J. Soc. Glass Tech. **14,** 84 (1930).

[6] Arthur Q. Tool, J. Research NBS **34,** 199 (1945) RP1637.

[7] L. W. Elder, Jr., J. Am. Chem. Soc. **51,** 3266 (1929).

[8] W. S. Hughes, J. Chem. Soc. 491 (1928).

[9] F. Haber and Z. Klemensiewicz, Z. physik. Chem. **67,** 385 (1909).

[10] D. G. MacInnes and M. Dole, J. Am. Chem. Soc. **52,** 29 (1930).

[11] M. R. Thompson, BS J. Research **9,** 833 (1932) RP511.

[12] H. T. S. Britton, Hydrogen ions, 2d ed., table 57 (c) p. 255 (D. Van Nostrand Co., Inc., New York, N. Y. 1932).

[13] W. Mansfield Clark, The determination of hydrogen ions (Williams & Wilkins Co., Baltimore, Md.

[14] James W. McBain, Phil. Mag. [6] 18, 916 (1909); Z. physik Chem. **68,** 471 (1909).

[15] Herbert Freundlich, Colloid and capillary chemistry, English Translation, p. 109 (E. P. Dutton & Co., Inc., New York, N. Y.).

[16] Donald Hubbard, J. Research NBS **37,** 223 (1946) RP1743.

[17] James B. Saunders, J. Research NBS **23,** 179 (1939) RP1227.

[18] Donald Hubbard and Gerald R. Rynders, J. Research NBS, **39,** 561 (1947) RP1848.

[19] Donald Hubbard, J. Research NBS **36,** 511 (1946) RP1719.

[20] Donald Hubbard, Edgar H. Hamilton, and A. X. Finn, J. Research NBS **22,** 339 (1939) RP1187

WASHINGTON, October 1, 1947.

U. S. Department of Commerce
National Bureau of Standards

Research Paper RP1860
Volume 40, February 1948

Part of the Journal of Research of the National Bureau of Standards

Infrared Radiation From a Bunsen Flame[1]

By Earle K. Plyler

The infrared emission spectrum of the flame of a Bunsen burner has been measured with prisms of LiF, NaCl, and KBr. In the region of 2.7 μ, the emission band has been resolved into two bands, 2.5 and 2.7 μ, and a series of 15 lines from 2.8 to 3.1 μ. These emission lines are separated by about 22 cm^{-1} and fall in the spectral region where the rotational-vibrational band of OH should occur. The spacing between lines, however, is too small for the changes in the energy levels of the OH molecule. This separation agrees very well with the calculated value for certain rotational states of the H_2O molecule. The long wavelength band at 15 μ has been observed in both CO burned in the air and the Bunsen burner flame. The present detection of this band represents the first confirmation of the original observations of Rubens and Aschkinass. Several bands have been observed with a grating instrument, and their frequencies check well with known energy transitions. The region from 12 to 24 μ has been measured with a KBr prism for the Bunsen flame. It contains a large number of the pure rotational lines of water vapor. In addition to the H_2O lines, there are two strong bands, 14 and 15 μ, which are produced by CO_2.

I. Introduction

Many observers have studied the infrared emission of a Bunsen flame [1].[2] The strongest band occurs at about 4.4 μ and is produced by carbon dioxide. Other bands have been found at 0.95, 1.45, 2.0, and 2.8 μ, and are attributed to carbon dioxide and water vapor. Very little radiation has been observed in the region beyond 7 μ.

In the visible and ultraviolet regions of the spectrum, considerable progress has been made in the study of flames [2]. By the use of instruments with good resolution and by detecting with photographic plates that average out the fluctuations of the flame, many band systems have been identified. The band systems include such atomic groups as OH, CN, NO, CH, and NH.

The question may be asked why the spectra of such groups have not been observed in the infrared region. The probable reason is that sufficiently high resolution has not been applied in the infrared region to separate properly the spectra of the different groups. Also, slight fluctuations in the flames make it difficult to obtain accurate measurements with radiometric detectors. An advantage in the study of the infrared spectra of flames is that a large percentage of the energy emitted by the flame falls in this region. The present study is mainly confined to the flame of the Bunsen burner. Both natural and mixed manufactured-natural gases were used.

II. Experimental Method and Results

A Perkin-Elmer infrared spectrometer was used in the measurement of the spectra, with prisms of LiF, NaCl and KBr for the different regions of the spectrum. A Bunsen burner with a steady flame was substituted for the globar source. Observations were made on the flame in the region of the cone, about two thirds of the distance from the bottom of the cone. Although the flame appeared steady, there was some variation in the total radiation that may have been produced by small fluctuations in the gas pressure. In many cases, a region was observed five or six times, and an average curve calculated from the various observations. The spectra shown have been averaged. As a rule, a single trial would not yield such a smooth curve. However, no emission band was included unless it could be redetermined several times. For this

[1] Part of the subject matter of this paper was presented at the Cincinnati meeting of the Optical Society of America on October 23 to 25, 1947.

[2] Figures in brackets indicate the literature references at the end of this paper.

reason, there may be more structure in the bands than is actually shown.

Figure 1 shows the energy curve for the Bunsen burner as obtained with a NaCl prism in the region from 1 to 5 μ. The lowest curve was observed with slits 60 μ wide, and the slits were 100 μ wide for the upper curve from 1.5 to 4.0 μ. In the region from 1 to 1.5 μ,200-μ slits were necessary to observe the bands. In the region of 4.25 μ, there is a drop in the energy curve produced by the absorption of the carbon dioxide in the air. The strong band at 4.39 μ is somewhat irregular at the point of greatest energy and can be observed better under higher resolution.

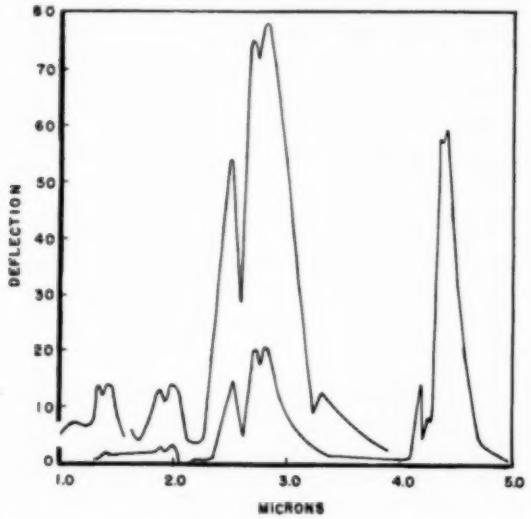

FIGURE 1. *Infrared emission of a Bunsen flame measured with a* NaCl *prism.*

The upper curve was measured with wider slits than the lower.

The region from 1.7 to 3.6 μ has been observed under higher resolution by the use of a LiF prism. The results are shown in figure 2. The slits used were 60 μ wide.

These results were obtained with natural gas containing about 88 percent of methane. The small bands in the region of 1.8 to 2 μ are produced by water vapor and CO_2. The band at 2.49 μ is probably due to water vapor, and the bands in the region of 2.7 μ are attributed to CO_2. The fine structure in the region from 2.8 to 3.1 μ may be produced by H_2O. This fine structure extends over to the 2.7-μ region, but because of the absorption of water vapor in the air and the band at 2.79 μ in the LiF prism, it could not be observed with sufficient accuracy to be included. Hence, a smooth curve was drawn thru the observed points in the 2.7- to 2.8-μ region. A small band observed in the region of 3.32 μ is probably produced by CH. This band is of low intensity, and it is not possible to determine whether it arises from CH, CH_2, CH_3 or CH_4. It is removed by about 12 cm^{-1} from the position of the methane absorption band.

In figure 3 is shown the emission band in the region of 4.36 μ. The solid line gives the actual

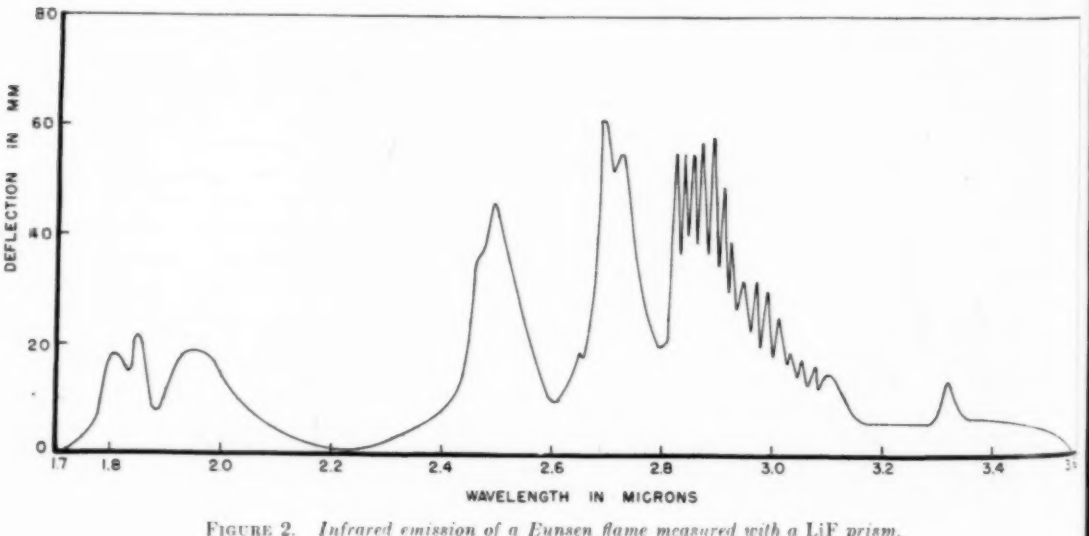

FIGURE 2. *Infrared emission of a Bunsen flame measured with a* LiF *prism.*

deflections. The reversal of the CO_2 absorption band in the air causes the low energy in the region of 4.22 and 4.28 μ. The easily recognized doublet band of CO_2 can be identified. The broken line in figure 3 indicates the amount of energy that would be present if the CO_2 in the air did not absorb any of the radiation emitted by the flame. The corrections to the observed curve were averaged from six observations of the absorption of CO_2 in this region. As the flame changes the amount of CO_2 in the air, it was found necessary to take a reading of the radiation of the flame and, immediately afterward at the same wavelength, a reading of the radiation from the globar source. This method of measurement was carried out at frequent settings of the wavelength drum, and the resultant curve was obtained. Barker [3] has obtained a curve of this type by the use of a grating spectrometer. The value of the maximum energy was found by Barker to be 4.37 μ.

The absorption by the flame of radiation in the region from 4.0 to 4.8 μ is small. The flame of the Bunsen burner was placed in the path of the radiation from the globar source, but in a position where its flame was not in focus and hence its radiation could produce very little effect on the detector. At 4.36 μ where the maximum emission of CO_2 occurs, the globar radiation was reduced very little, and no appreciable absorption

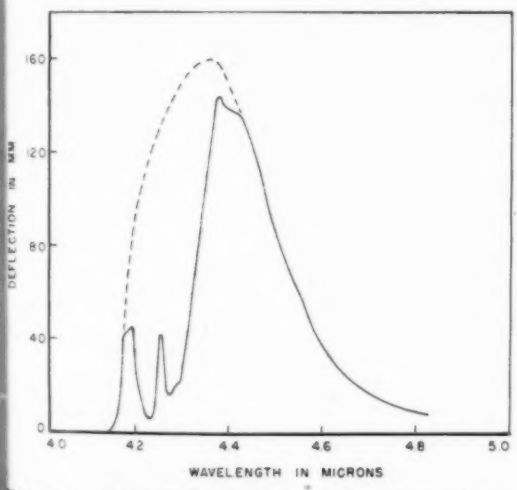

FIGURE 3. *The 4.36-μ emission band of a Bunsen-burner flame.*

The broken line represents the probable form of the energy curve after applying corrections for absorption of CO_2 in the air.

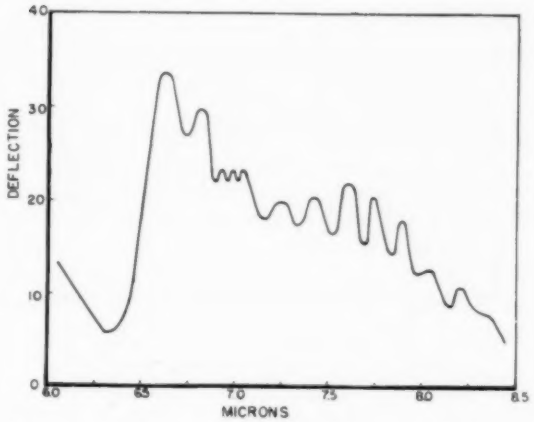

FIGURE 4. *Infrared emission of a Bunsen flame in region 6 .o 8.5 μ measured with a* NaCl *prism.*

due to the flame was found in any part of this spectral region.

In figure 4 is shown the emission spectrum from 6 to 8.5 μ. The energy is low in this region so that slits of 300 μ were used. This band is somewhat distorted and is part of the bending vibration of H_2O. In absorption this water-vapor band occurs at 6.26 μ. Some lines of the rotational-vibrational band stand out clearly in the region of 7.5 and 8 μ. The region from 5 to 6 μ could not be studied in detail because of the overlapping of the strong CO_2 band. This band was measured with a NaCl prism. No doubt, a greater detail of structure could be observed by the use of a CaF_2 prism or a grating.

Rubens and Aschkinass [4] in their study of the emission of water vapor, were able to find both branches of this vibrational-rotational band, because they did not have the tremendous overlapping of the CO_2 emission band. In the emission curve that they obtained from the Bunsen burner they were able to obtain only the long wavelength portion of the band, as is shown in figure 4 of the present paper. Their instrument was not of sufficient resolution to observe the individual rotational lines. However, their work was remarkably accurate and the bands check well in intensity with the results obtained in the present study.

In figure 5 the rotational lines of water vapor have been observed from 8.5 to 14.5 μ with a NaCl prism and slits of 0.45-mm width. The energy is very small in this region, and from 9

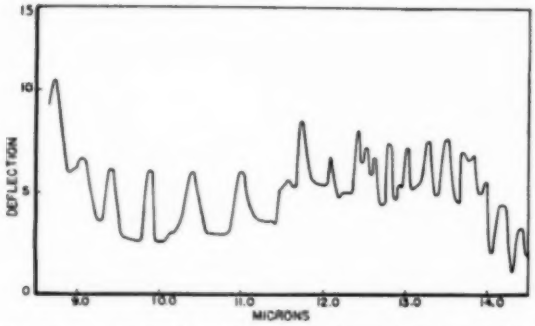

FIGURE 5. *Infrared emission of a Bunsen flame in region 9 to 14 μ measured with a* KBr *prism.*

to 11 μ it falls to a minimum. This is the part of the spectrum where water vapor has the least absorption, and is also that part of the spectrum where the pure rotational lines of H_2O begin to appear. The energy increases from 11.5 to 13.5 μ and then starts to decrease again. The decrease in energy is caused by the absorption of CO_2 in the air and the absorption of the prism. In addition to the water-vapor lines in this region, there is a possibility that the two difference bands, $\nu_3-2\nu_2$ and $\nu_3-\nu_1$ are present in low intensities. These bands occur in absorption at 9.40 and 10.41 μ. There are two distinct maxima observed in this region, but whether they are produced by H_2O or CO_2 has not been determined because both substances are present in the Bunsen-burner flame. This question can be answered when spectra of burning hydrogen and burning CO are measured separately in this region. That the decrease in energy is caused by the CO_2 and the absorption of the prism is clearly demonstrated when this region is studied with a KBr prism.

In figure 6 is shown the energy curve from 12 to 24 μ. From 12 to 19.5 μ the slits were 0.5 mm in width; from 19.5 to 21.5 μ, 0.7 mm; and 21.5 to 24 μ, 1.0 mm. In contrast with the measurements with the NaCl prism, which does not give large deflections for this part of the spectrum, the energy observed with the KBr prism increases from 12 to 15 μ. The broken line curve at about 15 μ in figure 6 is a measure of the energy after corrections have been made for the absorption of CO_2 in the air. The absorption of CO_2 in the air was measured with the same slit width used in the emission measurements, and then corrections to the observed curve were made. The maximum of radiation occurs at 15.0 μ. This emission band is no doubt one of the long wavelength CO_2 bending vibrations. In the region from 13 to 17 μ, there is a considerable number of lines of water vapor, which overlap the CO_2 emission. However, the two intense peaks at 13.9 and 15.0 μ are produced by CO_2.

In 1944 an unpublished study was made by the author at the University of Michigan on the emission of burning CO, using a grating spectrometer with a KBr foreprism. The CO was generated by two different methods. In one case a furnace was used that had a tube in the center filled with charcoal. Oxygen was passed slowly through the heated tube, and the CO was burned at the end of the tube. In the second case the CO was generated by dropping formic acid onto heated sulfuric acid. The radiation of the burning CO was measured, and in each instance, two peaks were found—one at 14.0 μ and the other at 15.0 μ. As a further proof that the observed bands were produced by CO_2, the charcoal was removed from the tube and CO_2 gas was passed slowly through the heated tube. Under these conditions, the radiation in the 15-μ region was also detected.

The results obtained with the grating instrument are shown in figure 7. The slits of the spectrometer were 1 mm wide and a 1,200 line per inch grating with an area of 108 in.^{2} was used in the spectrometer. The energy of the thermocouple was amplified by a Moll thermal relay, and the deflections of a high sensitivity galvanometer were read on a scale at a distance of 3 meters from the galvanometer. Very low levels of radiant energy could be detected with this system, but even so, wide slits were necessary in order to detect these bands. In addition to the bands shown in figure 7, there are probably several other smaller maxima in this region that were not detected. The

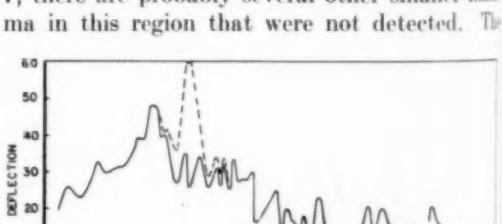

FIGURE 6. *Infrared emission of a Bunsen flame in region 12 to 24 μ measured with a* KBr *prism.*

The broken line represents the probable form of the energy curve after applying corrections for absorption of CO_2 in the air.

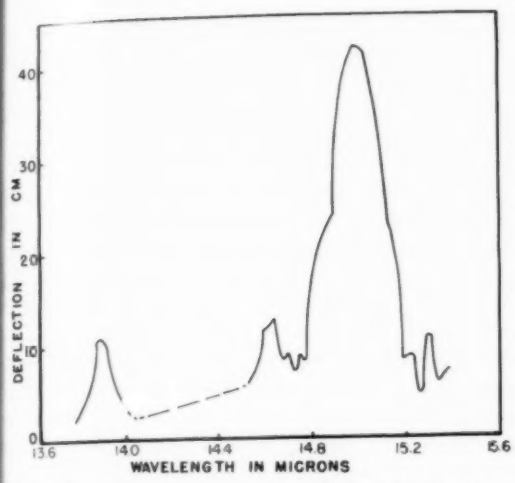

FIGURE 7. *Infrared emission of a* CO *flame burning in air measured with a grating spectrometer after applying corrections for absorption of* CO_2 *in the air.*

curve represents the probable emission curve after corrections to the deflections were made by taking into consideration the absorption of the CO_2 in the air.

Rubens and Aschkinass [4] in 1898 observed a band at 14.1 μ, but later observers were not able to find any band in this region. The intensities obtained by Rubens and Aschkinass for the bands of the Bunsen burner flame are in good agreement with results of this study. They measured the emission spectra to 23 μ with a KCl prism and found a definite peak in the region 13 to 14 μ, although their resolution was not great enough to show that this region contained many emission bands and lines. Their success in finding the band was due to the use of the KCl prism.

Garner and Johnson [5] in 1927 tried to observe this band but were not able to detect any energy in this region. They stated that, if the band was one-fiftieth as strong as the 4.4-μ band, it could be observed. The reasons for the low intensity of this band are discussed in section III.

The emission spectrum of the Bunsen burner from 6.5 to 24 μ has a large number of water vapor lines caused by rotation of the H_2O molecules. No doubt these lines continue beyond 24 μ. The separate emission lines are not quite at the same position in wavelength as the absorption lines. Also there are many other lines that fall between the ones shown in figure 6, but, because of the low resolution, they could not be observed in sufficient detail for measurement.

III. Discussion of Results

The infrared-absorption spectrum of CO_2 has been classified by Adel and Dennison [6], and, by means of their equations and certain observed bands, it is possible to calculate the frequency corresponding to the various quantum states. The notation followed in this discussion to designate the different types of vibration of CO_2 and H_2O is that used by Herzberg [7] in the classification of these molecules. For example, the ν_3 band, which is the asymmetrical vibration along the line of centers, for the quantum change from 0 to 1 gives rise to a band at 4.25 μ. For the quantum changes 1 to 2, the band falls at 4.30 μ, for 2 to 3 at 4.34 μ, and for 3 to 4 at 4.38 μ. In emission the quantum numbers change from large to small, but the energy changes are the same between the two states for absorption or emission. It is not possible to observe distinct bands corresponding to the different quantum jumps in the 4- to 5-μ region, as there is considerable overlapping of the various states. Also the quantum states of the other vibrations vary and produce a slight shift in the bands. The temperature measured from the inner cone to the outer surface of the flame varies considerably.

In addition, there is a change in the intensities of rotational lines as the temperature is increased. With all these effects on the energy emitted, it would be difficult to give a good approximation of the relative number of molecules represented in each state. The radiation of this band can be observed to about 5.0 μ, and this indicates that there is a considerable number of molecules in the higher rotational and vibrational states. The two bands, observed at 2.69 and 2.72 μ, arise from the combinations $\nu_3+\nu_1$, and $\nu_3+2\nu_2$. In absorption, three bands occur that arise from the combinations $\nu_3+4\nu_2$, $2\nu_2+\nu_1+\nu_3$, and $2\nu_1+\nu_3$, whose wavelengths are 2.05, 2.01, and 1.96 μ, respectively. All three bands are of the doublet type and do not have the strong zero branch that would make it possible to separate them. These three bands probably produce the one maximum that is observed at 1.95 μ

In the 15-μ region, the various states give rise to absorption bands with a zero branch. Therefore, the separate bands produced by different quantum

jumps are discernible. For example, the band at 13.88 μ is produced by the change (10^00) to the (01^10), that is $\nu_1 - \nu_2$. The appearance of this band with such a high relative intensity indicates that the energy of the inactive frequency ν_1, is transferred to the ν_2 level, where it can be radiated. The possibility of a transfer of the energy from one of the higher states of the inactive frequency to a state of an active frequency has been suggested by Gaydon [8].

The strong maximum shown in figure 7 probably arises from the transitions (02^20) to (01^10) and (01^10) to (00^00). Also the transitions (03^10) to (02^20) at 15.46 μ, (02^00) to (01^10) at 16.18 μ, and (03^10) to (02^20) at 16.75 μ, should appear in this region. There is some indication of these bands in the observations made with the grating spectrometer, but this region should be restudied to definitely establish the presence of these transitions.

The intensity of the bands of CO_2 in emission is different from the intensity in absorption. The probability coefficients of the population of states are well known and vary as the third power of the frequency in emission, although in absorption these coefficients are independent of frequency. That is, two absorption bands of equal intensity and having frequencies of 1,000 cm^{-1} and 2,000 cm^{-1}, respectively, would have an intensity ratio of 1 to 8 in emission. Shaefer and Phillips [9] state that the 4.25-μ band is about 28 times as strong as the 2.75-μ band in the absorption spectrum of CO_2. In the Bunsen flame the ratio is about 4 to 1 for the emitted energy of these two bands. However, when the factor $(3700/2300)^3$ is multiplied by 4, a value close to 17 is obtained. It is difficult to make accurate intensity measurements, and the values given above are rough or approximate figures. The check is sufficiently close to suggest that the same type of excitation is present in each band, and that it is not necessary to assume a chemical reaction rather than thermal excitation. However, the approximations made in this calculation are not accurate and the possibility of a combination of thermal and other excitations cannot be ruled out

When the long wavelength band at 665 cm^{-1} is considered, there is a large decrease in the energy emitted because of the dependence on the third power of the frequency. The ratio of intensities in absorption must be multiplied by $(2300/665)^3$ to obtain the ratio of intensities in emission. This gives a value of approximately 120 to 1 for the intensity ratio of the 4.36-μ band to 15.0-μ band. For a more accurate determination other factors would have to be taken in consideration, but as the intensity measurements are not very accurate small correction terms would not be significant. The value of 120 to 1 for the ratio of intensities of these bands probably explains why Garner and Johnson [5] did not observe this band as they stated that an intensity ratio of only 50 to 1 was necessary for detection. It should be emphasized that in calculating these intensities only rough approximations have been used, and a much more refined mathematical treatment, taking into consideration the various energy states involved, as well as other factors, is necessary before an accurate value can be arrived at. However, such estimates are valuable in predicting the order of magnitude to be expected in the intensity measurements.

In figure 6 the deflection as shown in the broken curve is the amount of energy emitted after making the correction for absorption of CO_2 in the air. This deflection is about equal to the deflection obtained in the 4.36-μ band. After taking into consideration the different dispersions of the NaCl and KBr prisms, and the different slit widths used in the two regions, the ratio of the observed energies in emission for the two bands is found to be roughly 100 to 1. This is approximately the same value as found in the calculated intensity ratio for emission. This suggests the possibility that this band is excited by the same mechanism as the 4.36-μ band. However, because of the roughness of the approximations, this calculation cannot be taken as proof of the nature of the energy.

Gaydon [8] calculated the radiative life, or time of transition, from one state to another from observed absorption measurements and found that for the ν_3 vibration this value is about 0.01 second, and that ν_2 has a time of transition of about 0.2 second. Because of the greater transition life of ν_2, he concludes that most of the energy of the 14.97-μ band is lost by collisions and does not enter into the radiation process. Gaydon further states that the failure to observe this band is proof that the emission is produced by chemical rather than thermal causes. If the excitation is thermal, the band should be present and have an intensity in accordance with theoretical calcula-

tions, because the population of the excited states would be increased and decreased by about the same amount in thermal exchanges. That thermal exchange could be the means of the energy radiation has been shown in the discussion of the ratio of the observed intensities of the ν_2 and the ν_3 vibrations. Gaydon has a very complete and interesting discussion in his book in regard to the combustion process and the influence of H_2O and other substances on the energy emitted by the flame.

The emission spectrum of water vapor consists of vibrational-rotational bands and pure rotational lines. The two OH vibrations in the water vapor molecule give rise to bands at 2.66 and 2.74 in absorption. In figure 2 the water band is well separated from the 2.7-μ region and has its maximum energy at 2.49 μ. There is an additional maximum on the short wavelength side of this band, but it is not well resolved. The change in frequency of the H_2O molecule in emission as compared to the corresponding frequency in absorption may be brought about by the molecule being in the higher rotational states. Randall, Dennison, Ginsburg, and Weber [10] have shown in accounting for the rotational lines in the absorption spectrum of water vapor that, for the higher energy states, there is a change in the angle of the water molecule. They state that the bond angle of the molecule changes from its equilibrium value of 104°36′ to 98°52′, and the OH distance changes from 0.9558 to 0.9640 A when $J=11$. Therefore, if the molecule at the temperature of emission is in the higher rotational states, it would not have the same spread between the maxima in the P and R branches as observed in absorption. The combination band $\nu_3+\nu_2$ is observed at 1.81 μ. This band corresponds to the band at 1.89 μ in absorption.

It is not possible to identify the exact location of the 6.26-μ band, but it is shifted to about 6.35 μ. By subtracting ν_3 from $\nu_3+\nu_2$, a value of 1508 cm^{-1} or about 6.63 μ is obtained, which corresponds approximately to the observed value. The 6.26-μ absorption band of H_2O has a greater intensity than the 2.66-μ band. However, in emission the 2.49-μ band is more intense than the 6.35-μ band. The change in intensity ratio between absorption and emission is explained by the third power of frequency that enters into the probability coefficients of emission. This effect has been discussed in connection with the intensities of the CO_2 emission bands and will not be repeated for the H_2O bands.

There are several small bands of CO_2 and H_2O in the region below 1.8 μ, but they have not been studied in detail and no attempt has been made to classify them. In figure 5 it is seen that the rotational-vibrational band of water vapor becomes very weak in the spectral region of 9 μ. In this region it is difficult to classify a line as part of the rotational-vibrational band or as a pure rotational line. The lines increase in intensity from 9 to 15 μ. The resolution is good with a NaCl prism at 12 and 13 μ, and much more detail of the lines can be seen than with a KBr prism. However, beyond 14 μ the KBr prism is more suitable. Some of the stronger emission lines have been compared with the absorption lines for the same spectral region, and it is found that the lines in emission do not appear at the same frequency as the absorption lines. This variation in frequency is probably caused by the emission lines being produced by transitions when the molecule occupies higher states, and the absorption lines being produced by lower energy transitions. These emission lines should be measured on a grating instrument. Then it may be possible to classify properly the emission lines, as has been done for rotational lines in absorption.

In figure 2 there are shown 15 rotational lines in the region between 2.8 and 3.2 μ. Some lines are also present below 2.8 μ, but because of the absorption of the water vapor in the air and the CO_2 emission band, the lines below 2.8 μ could not be measured accurately. The fifteen lines observed are spaced about 22 cm^{-1} apart. With higher resolution the band might show additional fine structure. These rotational lines, because of the large frequency spacing, evidently involve hydrogen. The OH band for many substances has been observed in the region of 2.8 μ. The moment of inertia of the OH group is such that a spacing somewhat different than that observed in these lines would be expected. The observed spacing of these rotational lines corresponds more closely to the spacing calculated for the H_2O molecule when the quantum changes are $\Delta k=0$ and $\Delta j=-1$. These lines correspond to the changes from $j=10$ to $j=24$. In the flame of burning hydrogen these lines are much more intense, and several additional lines have been

observed. These data will be presented in a subsequent article.

A small emission band has been observed in the region of 3.32 μ. This band is about 12 cm^{-1} less in frequency than the methane band. The intensity of the band is very low. The region of maximum energy has the appearance of a zero branch. As this is the part of the infrared spectrum, where characteristic vibrations of CH are found in absorption, this band is classified as being produced by the CH bond. As no rotational structure has been observed, it is not possible to distinguish between CH, CH_2, CH_3, or CH_4, and this band may arise from any one of these atomic groups.

Because of the strong emission of the CO_2 band in the region of 4.64 μ, no radiation that could be attributed to CO would be discerned unless it was of considerable intensity. As no bulge was observed, any energy that the CO molecule radiates in this region must be of low intensity. In the region of 2.3 μ, the flame is almost void of radiation, hence a low-intensity band due to the harmonic of CO could have been detected if it occurred. This leads to the conclusion that CO contributes very little to the total emission of the Bunsen burner.

The absence of a band in the region of 2.2 μ indicates that there is not a first harmonic of the ν_3 vibration of CO_2. This is in agreement with the selection rules that apply to absorption.

IV. Conclusion

In this work the infrared emission of a Bunsen flame has been measured from 1.8 to 24 μ and good resolution, obtained by a LiF prism, has been employed for the study of the region from 1.8 to 3.6 μ. Many bands have been resolved that have not been reported previously by other observers. It appears that a study of the infrared radiation with higher resolution than that used in this work would result in showing more detail that would be of great value in the formulation of a theory of combustion. This would also allow the more accurate calculation of the energy states. In addition to the need for better resolution, well-regulated sources should be used so that the various gases and the oxygen or air may be varied in known amounts. A vacuum spectrometer or one in which the air about it is free from CO_2 and water vapor would allow more accurate measurements in several regions of the spectrum.

V. References

[1] J. W. Ellis, Phys. Rev. **26**, 469 (1925); C. R. Bailey and K. H. Lih, Trans. Faraday Soc. **25** (1929).

[2] V. Kondratjew, Z. Physik **63**, 322 (1930); V. Kondratjew and M. Ziskin, Acta Physicochim. (USSR.) **7**, 65 (1937); W. M. Vaidya, Proc. Roy. Soc. [A] **162**, 513 (1934); A. G. Gaydon, Proc. Roy. Soc. [A] **173**, 439 (1942).

[3] E. F. Barker, Astrophys. J. **55**, 391 (1922).

[4] H. Rubens and E. Aschkinass, Ann. Physik u. Chem. **64**, 584 (1898).

[5] W. E. Garner and C. H. Johnson, Phil. Mag. [7], **3**, 97 (1927).

[6] A. Adel and D. M. Dennison, Phys. Rev. **43**, 716 (1933).

[7] G. Herzberg, Infrared and Raman spectra of polyatomic molecules (D. Van Nostrand & Co., Inc., New York, N. Y., 1945).

[8] A. G. Gaydon, Spectroscopy and combustion theory (Chapman & Hill, Ltd., London, 1942).

[9] C. Shaefer and B. Phillips, Z. Physik **36**, 641 (1926).

[10] H. M. Randall, D. M. Dennison, N. Ginsburg, and L. R. Weber, Phys. Rev. **52**, 160 (1937).

Washington, November 21, 1947.

U. S. Department of Commerce
National Bureau of Standards

Research Paper RP1861
Volume 40, February 1948

Part of the Journal of Research of the National Bureau of Standards

Perforated Cover Plates for Steel Columns; Compressive Properties of Plates Having Ovaloid, Elliptical, and "Square" Perforations

By Ambrose H. Stang and Bernard S. Jaffe

Tests were made to determine the mechanical properties of perforated cover plates intended to be used as a substitute for lattice bars or batten plates in built-up box-type columns. These tests supplement and extend the range of perforation shapes beyond that described in preceding reports.

This paper gives the results for seven plates having perforations of ovaloid shape, six with the long axis parallel to the load, and one with the short axis parallel to the load; three plates having elliptical perforations with the major axis parallel to the load; two plates having square perforations with rounded corners for one of which the load was parallel to the side of the square, and for the other of which the load was parallel to a diagonal. A column having a solid plate was also tested for comparison with the columns having perforated plates.

Tests were made to determine the stiffness of the perforated plate columns relative to that of the column having a solid plate, the distribution of stress on the edge of the perforation, and the strength of each column.

I. Introduction

This paper is the seventh of a series dealing with the experimental determination of the mechanical properties of perforated cover plates intended to be used as a substitute for lattice bars or batten plates in built-up box-type columns. The columns for which the results are here reported are additions to the original program.[1]

In that program, the ratio of perforation width to plate width was 0.45 for nearly all of the perforated plates. In this series, plates with ovaloid perforations with the load parallel to the long axis and having ratios of perforation width to plate width of 0.255 and 0.647 have been included to cover a wider range for this ratio. Plates having elliptical perforations with the major axis parallel to the load, ovaloid perforations with the short axis parallel to the load, "square" perforations with the side of the square in one plate and with the diagonal, in another plate, parallel to the load, have also been included.

II. Cover-Plate Columns

The details of the columns are shown in figures 1 and 2. The columns were riveted before delivery to the laboratory. The ends had been milled after assembly and were reasonably smooth and parallel. A piece of material 20 in. long, which had been cut from each plate and angle used in the columns, was delivered with the columns.

[1] Ambrose H. Stang and Martin Greenspan, J. Research NBS **28**, 609 (1942) RP1473; **28**, 687 (1943) RP1474; **29**, 279 (1942) RP1501; **30**, 15 (1943) RP1514; **30**, 177 (1943) RP1527; **30**, 411 (1943) RP1540.

TABLE 1. *Areas for the columns*

Column	Angle area	Plate area		Column area			
		Gross	Net	Gross, A_g	Net, A_n	Ratio, A_g/A_n	Ratio, A_n/A_t
	*in.*²	*in.*²	*in.*²	*in.*²	*in.*²		
C4D–A	11.454	9.514	9.514	20.968	20.968	1.000	1.00
C4E–1	11.461	9.644	7.138	21.105	18.599	1.135	0.86
C4E–2	11.461	9.644	7.128	21.105	18.590	1.135	.86
C4E–3	11.461	9.644	7.146	21.105	18.608	1.134	.86
C4F–1	11.638	9.677	3.416	21.316	15.054	1.416	.70
C4F–2	11.638	9.677	3.439	21.316	15.077	1.414	.70
C4F–3	11.638	9.677	3.391	21.316	15.029	1.418	.70
C4G–1	11.604	9.707	5.328	21.311	16.932	1.259	.78
C4G–2	11.604	9.707	5.329	21.311	16.933	1.259	.78
C4G–3	11.604	9.707	5.330	21.311	16.935	1.258	.79
C4H	11.630	9.836	5.354	21.466	16.984	1.264	.79
C4I	11.850	9.798	5.350	21.248	16.800	1.265	.79
C4J	11.486	9.831	5.306	21.317	16.792	1.269	.79

The dimensions given in figures 1 and 2 are nominal. There were the usual commercial variations in the thicknesses and widths of the plates. The variations in the dimensions of the perforations were considerably greater; for some plates, the differences between the maximum and minimum perforation length or width as well as the difference from the nominal dimensions was greater than 0.1 in.

As the columns were already riveted when delivered, the cross-sectional areas of the plates and angles of the columns were computed from the dimensions of the extra lengths of material rather than from measurements on the columns.

No distinguishing marks had been placed on the three columns of the same design or on the three extra lengths of material representing them. The dimensions of the extra lengths having the same mark were therefore averaged, and the gross cross-sectional areas of the three columns of the same design were taken as identical.

The cross-sectional areas of the plates and angles and of the columns, computed from the measured dimensions, are given in table 1.

III. Procedure

Coupons representing the plate and angle material were cut in the direction of rolling and tested in tension. Young's modulus of elasticity, Poisson's ratio, the upper and lower yield point, and tensile strength were determined.

A composite sample of the plate material and a composite sample of the angle material were analyzed for carbon, manganese, phosphorus, and sulfur.

The methods used in testing the columns were the same as those described in the references in footnote 1, except as noted below. The shortening under load in the elastic range was determined for each column.

The strains in the edge of the middle perforation were determined for each of the C4E and C4F columns, using a Berry hand-operated strain gage, 2-in. gage length. The values for each of the three similar columns were averaged. The strains in the edge of the middle perforation of columns C4G–2, C4H, C4I, and C4J were measured with Huggenberger tensometers, 1-in. gage length. The stress distribution on the edge of the perforations was calculated from the strain data and the values of Young's modulus obtained from the coupon tests.

Each column was tested to destruction. Data to complete the stress-strain curves and data for the stress-deflection curves were taken.

IV. Results

The average results of the tensile tests of the coupons are given in table 2, and the chemical composition of the coupon material is given in table 3.

The moduli, E', of the columns, and the effective-area factors, K, with respect to shortening under compressive load, for the plates, are given in table 4.[2]

[2] Ambrose H. Stang and Martin Greenspan, J. Research N.B.S. 28, (1942) RP1473.

TABLE 2. *Average results of tensile tests of coupons*

Column designation	No. of coupons	Thickness	Young's modulus	Poisson's ratio	Yield point		Tensile strength
					Upper	Lower	
PLATE COUPONS							
		in.	*kips/in.²*		*kips/in.²*	*kips/in.²*	*kips/in.²*
C4D-A	1	0.372	30,000	0.258	38.5	37.1	62.6
C4E	3	.376	29,900	.263	38.6	37.0	64.2
C4F	3	.378	30,000	.270	39.2	36.5	63.0
C4G	3	.380	29,900	.270	39.3	36.7	62.7
C4H	1	.385	29,500	.259	40.2	37.3	63.7
C4I	1	.382	29,600	.269	38.7	37.2	63.4
C4J	1	.383	29,900	.262	38.6	35.8	62.4
ANGLE COUPONS							
C4D-A	2	0.488	30,000	0.271	48.2	45.7	68.0
C4E	6	.488	29,900	.277	46.6	44.7	67.7
C4F	6	.496	29,200	.262	46.5	44.3	63.5
C4G	6	.496	29,500	.272	47.0	44.2	63.9
C4H	2	.496	29,400	.260	46.7	44.9	63.8
C4I	2	.488	29,800	.276	47.8	45.7	67.3
C4J	2	.486	29,600	.276	47.2	45.6	67.2

TABLE 3. *Chemical composition of coupon material*

Composite sample	Carbon	Manganese	Phosphorus	Sulfur
	Percent	*Percent*	*Percent*	*Percent*
Plates	0.24	0.39	0.010	0.040
Angles	.25	.39	.011	.033

The distribution of stress on the edge of the middle perforation is shown in figures 3, 4, 5, 6, 7, and 8.

The vertical axis of the graph in each figure is a development of one quadrant of the edge of the perforation. In the stress ratios, $\sigma_{u,v}/(P/A_n)$, A_n is the net area of the column, and σ_u and σ_v are the maximum and the minimum principal stresses, respectively.

The maximum stress ratios are given in table 4. The stress ratios based on gross area, $\sigma_{u,v}/(P/A_g)$, where A_g is the gross area of the column, may be calculated from the values in figures 3 to 8, by multiplying those values by the column area ratio, A_g/A_n, of table 1.

The axial shortening of the column was measured using eight compressometers located as shown in figure 7 of Research Paper RP1473.[3] These compressometers had a gage length equal to two bay lengths. The gage-length shortenings thus represented the shortening in the uniformly perforated portion of the plate. The strain for a given load was calculated by dividing the average shortening in the eight gage lengths by the average gage length. The stress-strain graphs for the columns, based on net areas, are shown in figure 9. The stresses on gross area may be obtained by multiplying the stresses on net area by the column area ratio, A_n/A_g, of table 1.

TABLE 4. *Moduli of columns, effective area factors of plates, and maximum-stress ratios*

Column designation	Based on gross area			Based on net area		
	Modulus, E'	Effective area factor, K	Ratio, maximum stress, P/A	Modulus, E'	Effective area factor, K'	Ratio, maximum stress, P/A
SOLID PLATE						
	kips/in.²			*kips/in.²*		
C4D-A	30,100			30,100		
PERFORATIONS OVALOID; LOAD PARALLEL TO LONG AXIS						
C4E-1	27,800	0.83		31,500	1.12	
C4E-2	27,600	.82		31,300	1.11	
C4E-3	27,800	.83		31,500	1.13	
Avg	27,700	0.83	−2.28	31,400	1.12	−2.01
C4F-1	21,700	0.39		30,800	1.10	
C4F-2	21,800	.40		30,800	1.11	
C4F-3	21,900	.40		31,000	1.14	
Avg	21,800	0.40	−2.39	30,900	1.12	−1.69
PERFORATIONS ELLIPTICAL; LOAD PARALLEL TO MAJOR AXIS						
C4G-1	25,200	0.64		31,700	1.17	
C4G-2	25,100	.64	−2.43	31,600	1.17	−1.93
C4G-3	25,100	.64		31,600	1.16	
Avg	25,100	0.64		31,600	1.17	
PERFORATIONS OVALOID; LOAD PARALLEL TO SHORT AXIS						
C4H	25,200	0.65	−3.94	31,900	1.19	−3.12
PERFORATIONS "SQUARE"; LOAD PARALLEL TO SIDE						
C4I	24,900	0.63	−3.82	31,500	1.15	−3.02
PERFORATIONS "SQUARE"; LOAD PARALLEL TO DIAGONAL						
C4J	25,700	0.69	−9.40	32,600	1.27	−7.41

[3] Ambrose H. Stang and Martin Greenspan, J. Research NBS **28**, 679 (1942) RP1473.

771185—48— 3

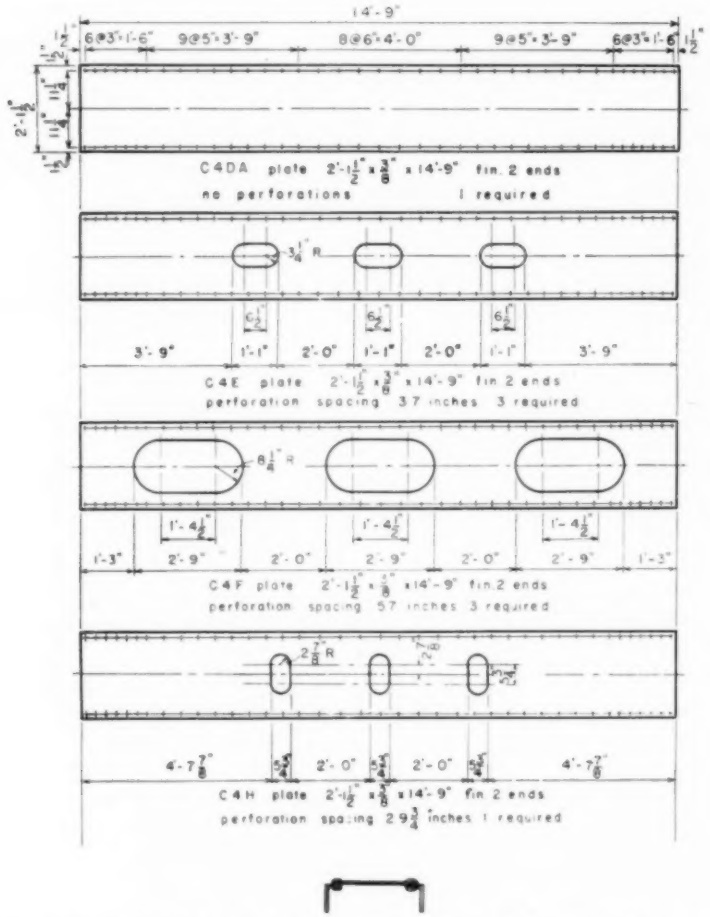

FIGURE 1. *Columns having a solid plate and plates with ovaloid perforations.*

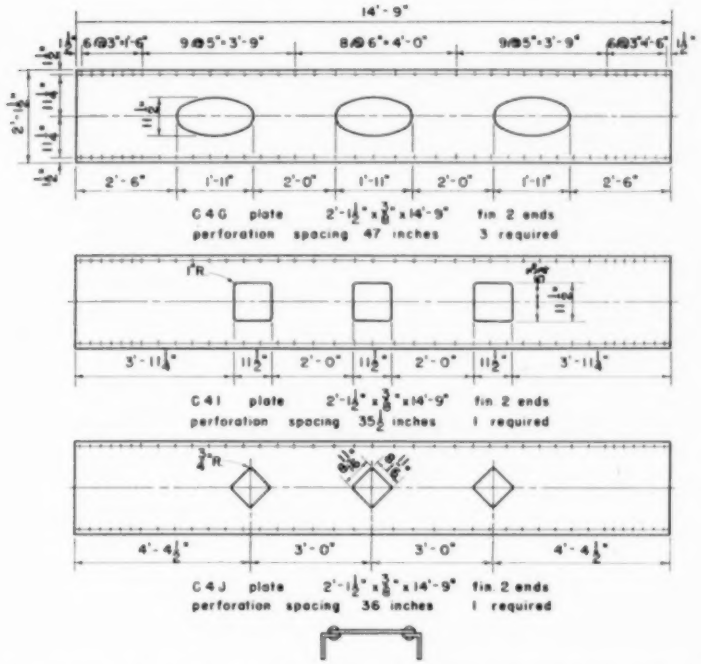
14'-9"
C4G plate 2'-1½" x ⅜" x 14'-9" fin 2 ends
perforation spacing 47 inches 3 required
C4I plate 2'-1½" x ⅜" x 14'-9" fin 2 ends
perforation spacing 35½ inches 1 required
C4J plate 2'-1½" x ⅜" x 14'-9" fin 2 ends
perforation spacing 36 inches 1 required

FIGURE 2. *Columns having plates with elliptical perforations and with "square" perforations.*

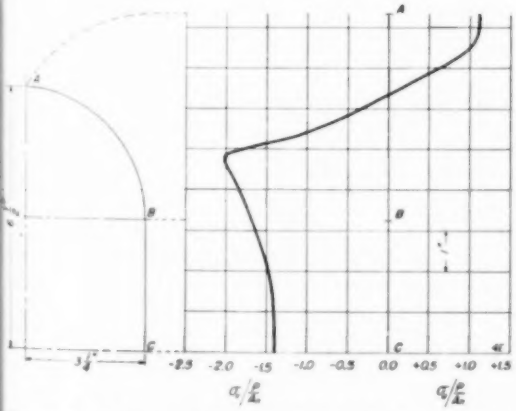

FIGURE 3. *Columns C4E, ovaloid hole, load parallel to long axis.*

Distribution of stress on the edge of the perforation. Based on net area

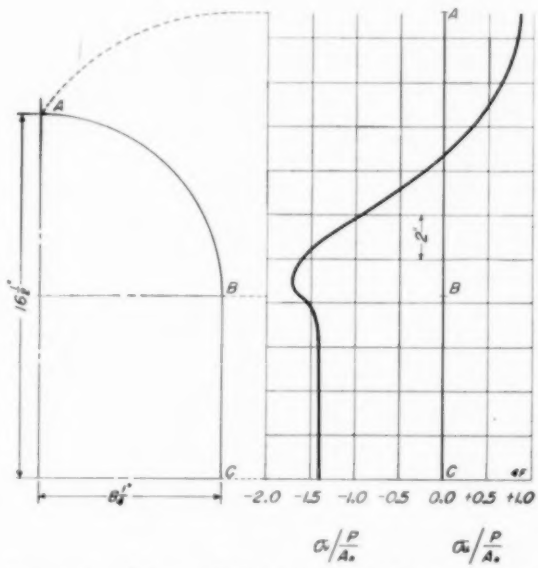

FIGURE 4. *Columns C4F, ovaloid hole, load parallel to long axis.*

Distribution of stress on the edge of the perforation. Based on net area.

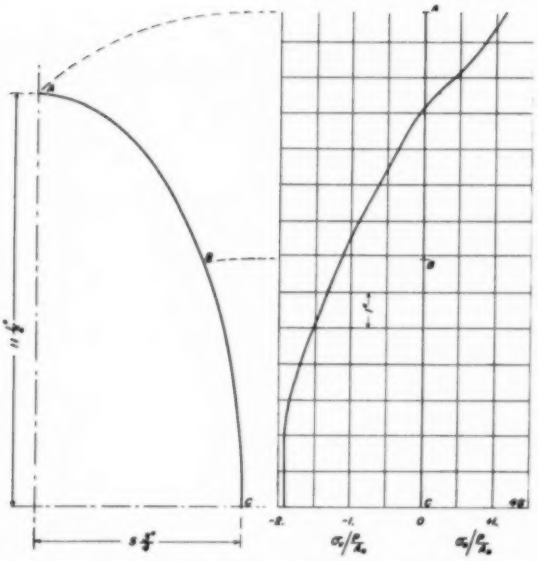

FIGURE 5. *Column C4G–2, elliptical hole, load parallel to major axis.*

Distribution of stress on the edge of the perforation. Based on net area.

The lateral deflections at midheight of the column, in planes at right angles to the principal axes of inertia of the cross section were measured at various loads. The deflections were determined to 0.01 in. by the taut-wire mirror-scale method. The distance between the supports for the wires was 14 ft 3 in. The stress-lateral-deflection graphs, based on net area, are shown in figure 10.

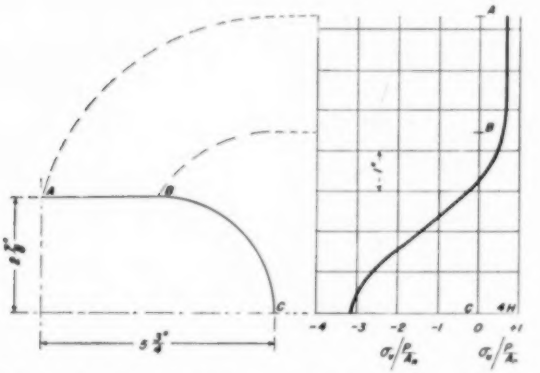

FIGURE 6. *Column C4H, ovaloid hole, load parallel to short axis.*

Distribution of stress on the edge of the perforation. Based on net area.

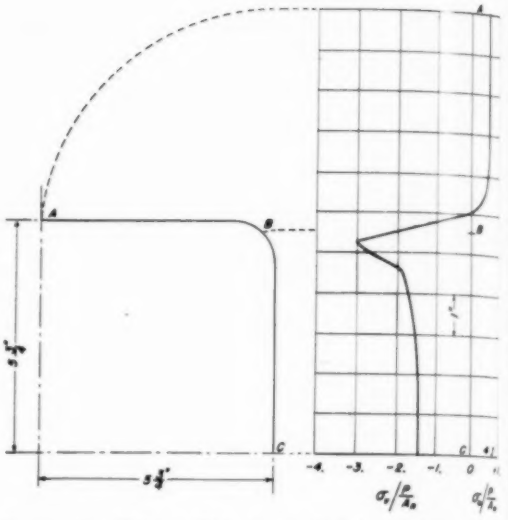

FIGURE 7. *Column C4I, "square" hole, load parallel to side.*

Distribution of stress on the edge of the perforation. Based on net area.

The maximum loads for the columns, the maximum average stress on the gross area and on the net area, and the effective-area factors[4] of the plates with respect to compressive strength, C_t, are given in table 5.

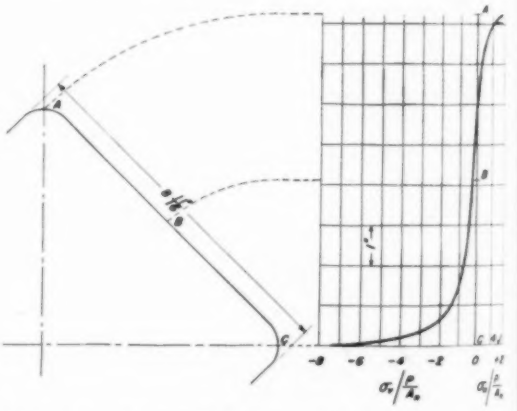

FIGURE 8. *Column C4J, "square" hole, load parallel to diagonal.*

Distribution of stress on the edge of the perforation. Based on net area.

[4] Ambrose H. Stang and Martin Greenspan, J. Research NBS 28, 653 (1942) RP1473.

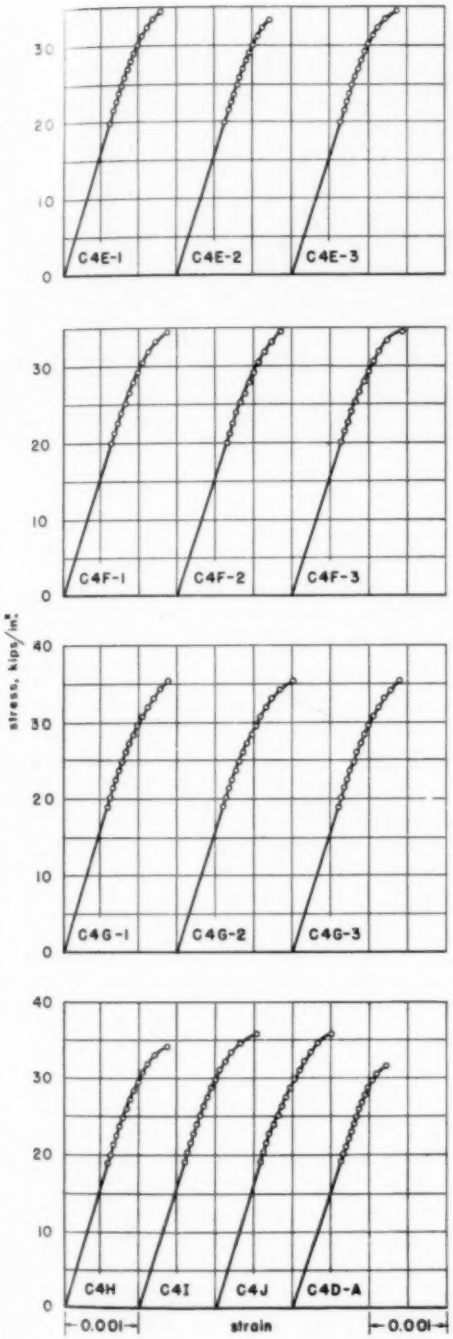

FIGURE 9. *Stress-strain graphs for the columns.*
Based on net area.

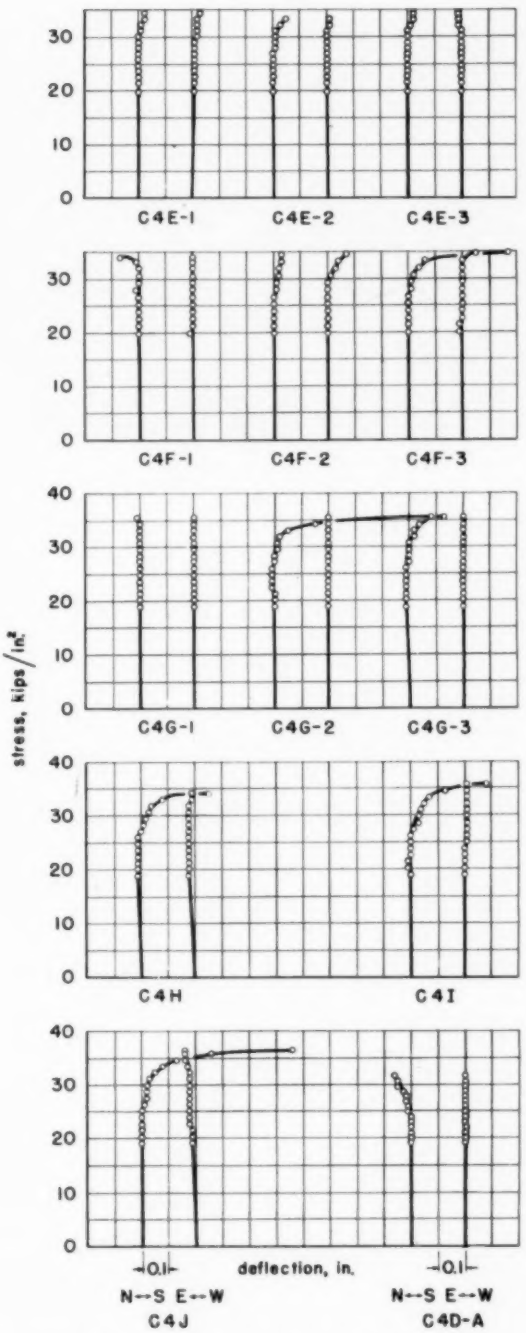

FIGURE 10. *Stress-deflection graphs for the columns.*
Based on net area. When the deflection is north, N, the bending stress is tensile on the plate side.

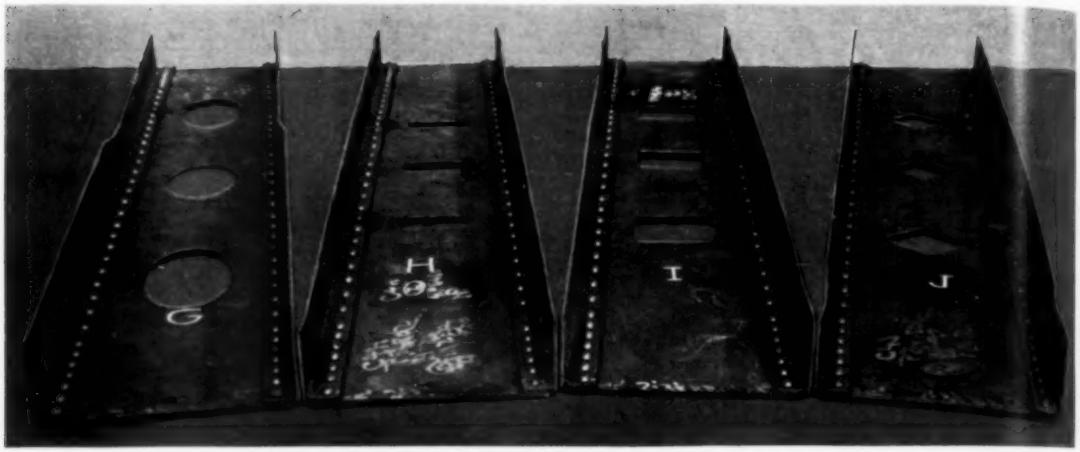

FIGURE 11. *Columns after maximum load tests.*
From left to right, the columns are C4G-1, C4H, C4I, and C4J.

TABLE 5. *Maximum loads for columns and effective area factors for plates*

Column designation	Maximum compressive load	Based on gross area		Based on net area	
		Maximum compressive stress	Effective area factor, C	Maximum compressive stress	Effective area factor, C
SOLID PLATE					
	kips	*kips/in.²*		*kips/in.²*	
C4D-A	678	32.3	1.00	32.3	1.00
PERFORATIONS OVALOID; LOAD PARALLEL TO LONG AXIS					
C4E-1	659	31.2	0.93	35.4	1.25
C4E-2	630	29.9	.83	33.9	1.13
C4E-3	655	31.0	.91	35.2	1.23
Aug	648	30.7	0.89	34.8	1.20
C4F-1	525	24.6	0.48	34.9	1.35
C4F-2	538	25.2	.52	35.7	1.45
C4F-3	520	24.4	.46	34.6	1.31
Avg	528	24.7	0.49	35.1	1.37
PERFORATIONS ELLIPTICAL; LOAD PARALLEL TO MAJOR AXIS					
C4G-1	613	28.8	0.76	36.2	1.28
C4G-2	600	28.2	.72	35.4	1.31
C4G-3	610	28.6	.75	36.0	1.36
Avg	608	28.5	.74	35.9	1.35
PERFORATIONS OVALOID; LOAD PARALLEL TO SHORT AXIS					
C4H	581	27.1	0.64	34.2	1.18
PERFORATIONS "SQUARE"; LOAD PARALLEL TO SIDE					
C4I	600	28.2	0.73	35.7	1.33
PERFORATIONS "SQUARE"; LOAD PARALLEL TO DIAGONAL					
C4J	610	28.6	0.75	36.3	1.39

The unperforated plate column, C4D–A, failed toward the plate side as would be expected from the double modulus column theory. The column bent as a whole with buckling of the outstanding legs of the angles near midheight.

The perforated plate columns, C4E–1, C4E–2, C4E–3, C4F–2, C4F–3, C4G–2, C4G–3, C4H, C4I, and C4J, failed away from the plate side as would be expected from the consideration that, in the neighborhood of a perforation, the gravity axis of the column is displaced away from the plate side. The perforated plate columns, C4F–1 and C4G–1, failed in the other direction, having suffered practically no deflection until the maximum load was approached. Local buckling of the outstanding legs of the angles and buckling of the plate near a perforation characterized the failures of the columns having perforated plates. Figure 11 shows columns C4G–1, C4H, C4I, and C4J after test.

V. Summary

The results of the tests of the columns reported here, as well as of the perforated plate columns for which properties have been previously reported, will be discussed in a forthcoming Research Paper. Comparisons will be made between the experimental results and values based on theories that have been developed during this investigation.

WASHINGTON, October 13, 1947.

U. S. Department of Commerce
National Bureau of Standards

Research Paper RP1862
Volume 40, February 1948

Part of the Journal of Research of the National Bureau of Standards

Behavior of Certain Sugars and Sugar Alcohols in the Presence of Tetraborates—Correlation of Optical Rotation and Compound Formation

By Horace S. Isbell, Joseph F. Brewster, Nancy B. Holt, and Harriet L. Frush

In the present investigation, the changes in the equilibrium specific rotation caused by the addition of either sodium or potassium tetraborate to solutions of D-glucose, D-fructose, L-sorbose, sucrose, mannitol, and sorbitol have been observed and the results interpreted. Measurements have been made for various concentrations of carbohydrates with fixed concentrations of borate, and for various concentrations of borate with fixed concentrations of carbohydrate. It was thus possible to observe independently the effect of variation in the concentration of either carbohydrate or borate. The results indicate that glucose, fructose, sorbose, and sorbitol form three borate compounds, that mannitol forms two, and sucrose one. The optical rotations of the compounds have been estimated, and the composition of the solutions discussed. Extensive tables have been included, giving the optical rotations of the above-mentioned carbohydrates in the presence of sodium and potassium tetraborate.

I. Introduction

In recent years large quantities of the polyhydric alcohols, sorbitol and mannitol, have been produced and have found use in many industries. The commercial applications make important the development of simple methods of analysis. The sugar alcohols, like nearly all sugar derivatives that do not contain an oxygen ring, have low optical rotatory power, but the addition of borates, molybdates, tungstates or certain other inorganic substances considerably increases the rotation and makes polarimetric methods of measurement possible. Although it has been more or less customary, since 1874, to characterize the sugar alcohols by their optical rotations in aqueous solutions containing borax [1],[1] there has been no uniform procedure and little emphasis on the effect of concentration. The purpose of this investigation was to obtain more comprehensive data concerning the effect of borates on the optical rotations of mannitol and sorbitol at various concentrations. As borates affect the optical rotations of the sugars as well as the sugar alcohols, similar studies appeared to be desirable on those sugars (glucose, fructose, sorbose, and sucrose) that are commonly associated with sorbitol and mannitol.

Another object of the investigation was to extend knowledge of the character of the borate-carbohydrate compounds, a subject of particular importance in relation to various polysaccharides. Thus, it is well known that the viscosity and physical properties of algins, plant gums, and mucilages are altered in striking manner by the addition of borates. It is believed that the information presented in this paper will be useful in interpreting the action of borates on these more complex substances.[2]

II. Reactions of Borates and Carbohydrates

1. Prior Work

It has been known for many years that polyhydroxy substances combine with boric acid any borates in solution with great ease and rapidity. The reactions are accompanied by extraordinarily

[1] Figures in brackets indicate the literature references at the end of this paper.

[2] The methods described in this paper are being applied to the study of other carbohydrates, including the uronic acids.

large changes in physical and chemical properties. Thus, the addition of mannitol to aqueous solutions of borax changes the reaction of the borax from strongly alkaline to strongly acid [2]. Information as to the character of the compounds formed has been derived from measurement of the changes in optical rotation, electrical conductivity, acidity, freezing point, solubility, and volume. Lambert first observed the effect of structure on compound formation [3], a subject that Magnanini studied extensively by conductivity measurements [4]. In a series of brilliant investigations extending over many years, Böeseken and coworkers developed Magnanini's method and ascertained the structural and configurational conditions necessary for the formation of borate compounds.[3] Originally Böeseken assumed that 1 molecule of a dihydroxy compound combines with 1 of boric acid with loss of water to form a cyclic compound (type A) having strong acid properties. The preparation by Hermans [6] of several crystalline compounds of this structure, but having only weak acid properties, led to a revision of the original concept and the conclusion that there are several classes of boric acid compounds differing widely in acid strength. The formulas that have been suggested are tabulated below

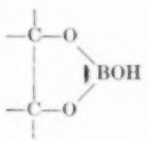
(A)

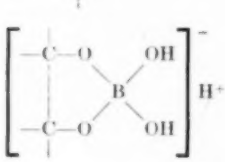
(BD)

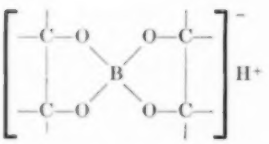
(BD_2)

For convenience they will be designated hereafter as types A, BD and BD_2, respectively. Hermans considered structure BD_2 as most probable for the strongly acid compounds, but recognized that compounds of the BD type may also be strongly acidic. Böeseken [7] justified the existence of compounds of pentavalent boron having four tetrahedrally arranged covalent bonds on the basis of the Lewis-Langmuir theory and pointed out the possibility of optical isomers for certain compounds of the BD_2 type. The resolution of the strychnine salt of borodisalicylic acid into two optically active isomers confirmed the idea of the tetrahedral arrangement of the boron valences and established the structure of the BD_2 type conclusively [8].

The first compounds known to be of type A were prepared by Hermans [6], who found that a weakly acid volatile substance,

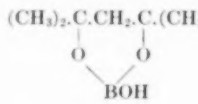

crystallizes readily from aqueous solutions containing equivalent quantities of boric acid and 2,4-dimethylpentane 2,4-diol. Several other representatives of this class were prepared. Ordinarily, compounds of type A are formed by dehydration of solutions containing the diol and boric acid or borate in proper proportion. Thus, by dehydration of mixtures of mannitol and boric acid,

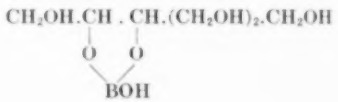

and

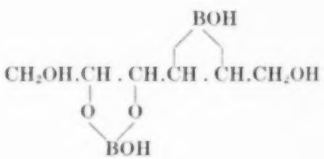

are obtained [9]. Partial hydrolysis of these compounds yields a crystalline acyclic mannitol borate considered to be 2-mannitol monoborate. Dehydration of boric acid mixtures containing ethylene glycol or 1,3-butylene glycol gives compounds of type A that are volatile [10]. Under like conditions glycerol gives a nonvolatile viscous mass the nonvolatility of which is attributed to the formation of a third ester linkage between two diesterified molecules.

The evidence for compounds of the BD type is not so convincing as that for compounds of type A

[3] A comprehensive list of Böeseken's early publications on this subject is found in footnote 3 on page 338 of [5].

Possibly the mannitol-boric acid compound of Fox and Gauge [11] having the empirical formula $C_6H_{15}O_9B$ belongs to this class, and also the *cis*-cycloheptane diol boric acid of Derx [12].

Numerous representatives of the BD_2 type in the form of crystalline salts have been prepared, [6, 8]. It was shown by Hermans that several compounds prepared by other workers (e. g., the salts of dipyrocatechol boric acid [13], potassium diborocitric acid [14], and possibly certain compounds prepared by Wohl and Neuberg [15] are of the BD_2 type. A few of the crystalline acids have been obtained by heating the aniline or pyridine salts in a vacuum [6, 8], and it is possible that certain crystalline compounds of fructose, mannitol, and xylose are also of the BD_2 type [16]. Vermaas [17] suggested that all 1,2, and 1,3 diols with hydroxyl groups in suitable positions are able to form compounds of type A, in which the valence angle of the trivalent boron is 120°. Compounds of types BD and BD_2, however, can be formed only when the hydroxyl oxygens are sufficiently close to allow the 4 covalencies of boron to assume a smaller angle, namely, 109°. This concept has been confirmed by X-ray diffraction measurements [18]. The *cis* diols [4] that Böeseken classified as "favorable" meet this requirement and give rise to borate compounds of types BD and BD_2 as well as to those of type A. But for any single diol, it has not been possible to separate all three borate compounds in crystalline form.

For determining the configurations of the reducing sugars, advantage has been taken of the fact that the only cyclic diols that form compounds that increase the acidity of boric acid solutions are those with adjacent *cis* hydroxyl groups. This principle has been used by Böeseken and coworkers for establishing the configurations of many sugars [21]. For example, it was found that α-D-glucopyranose increases the acidity of boric acid, whereas β-D-glucopyranose does not. Hence the hydroxyls of carbons 1 and 2 of the alpha pyranose modification of glucose are in the *cis* position [22]. Moreover, the selective combination of certain modifications of the sugars with borates causes a shift in the equilibrium state. The borate-sugar compound is decomposed by the addition of acid with regeneration of the sugar, and formation of a salt and boric acid. It was shown by Levy and Doisy [23] that this process is followed by a mutarotation caused by release of the sugar modification in the complex, and the subsequent establishment of the normal equilibrium state.

The prior work clearly shows the existence of borate-diol compounds of diverse types, but there is considerable uncertainty in regard to the character of the compounds present in aqueous solutions. Böeseken, Vermaas, and Küchlin [24] estimated the number of moles of polyol (n) which form a strongly acid complex with 1 mole of boric acid, (1) from the change in pH upon the addition of the polyol to a fixed amount of boric acid, (2) from the change in pH during the neutralization of polyol-boric acid solutions, and (3) from freezing point measurements of borate-polyol solutions. By the three methods, n was found to be 2 for fructose, mannitol, and α-mannitan. Tung and Chang, by potentiometric measurements of pH also found that n equals 2 for several substances, notably fructose, mannitol, and xylose [16]. In contradiction to this evidence, Levy [25], using the freezing point data of Kahlenberg and Schreiner [26], calculated that 1 mole of sodium borate enters into combination with 1 mole of mannitol, and presented data to show that a 1:1 combination takes place with other carbohydrates. Other proportions were suggested by Darmois and Peyroux [27], but Bancroft and Davis [28] questioned the existence of any of the compounds in solution. Other contradictory literature was cited by Rippere and La Mer [10].

Although borate-polyol systems are extremely complex, and there is some conflicting evidence, it appears that an equilibrium involving compounds of types A, BD and BD_2 accounts most adequately for the experimental facts. Equilibrium systems of this character have been considered by Vermaas [17] and Böeseken [20]. Vermaas presented the following reaction scheme:

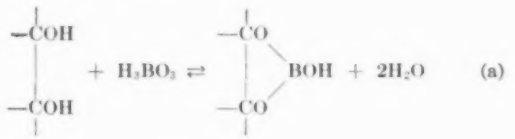

[4] Certain disaccharides having adjacent *cis* hydroxyl groups do not appreciably increase the conductivity of boric acid and may even cause a decrease [20]. Böeseken [20] ascribed the anomalous behavior to the particular conformation of the strainless ring in these compounds.

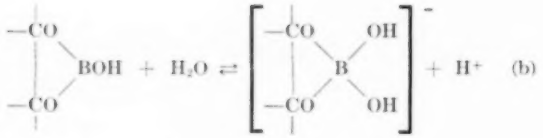

(b)

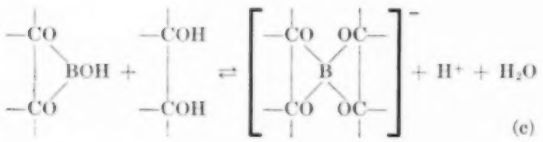

(c)

The primary reaction gives a compound of type A, which in turn is converted into substances of types BD and BD_2 by reaction with either a molecule of water or a second molecule of diol. Under suitable conditions the process of reaction (a) undoubtedly takes place, but it may include the stepwise formation of an acyclic intermediate of the type

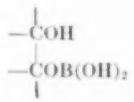

which Bremer [9] obtained by hydrolysis of a mannitol borate of type A. Reaction (c) seems questionable in light of the observation that the propylene glycol borate of type A does not combine with a second molecule of propylene glycol [10].[5] The inertness of the propylene glycol compound, however, may be due to an "unfavorable" structure rather than to the invalidity of the hypothetical reaction.

The following scheme was suggested by Böeseken [20].

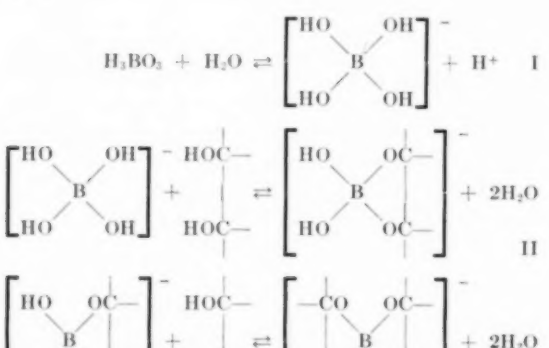

I

II

III

[5] See also p. 91 of [6].

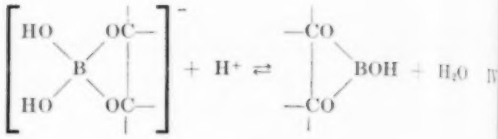

IV

The first reaction gives an ion containing quadricovalent boron, which combines with the diol to yield a compound of type BD directly. Reaction IV is the same as reaction (b) of Vermaas' scheme and appears to be relatively slow, at least with some diols.

In acid solutions the equilibrium for reaction I lies to the left. Consequently, only a small quantity of the quadricovalent borate ion is present and the tendency for the formation of ions BD^- and BD_2^- of reactions II and III is correspondingly small. The amounts of the complex acids formed from boric acid and a carbohydrate are sufficient to cause measurable changes in acidity but too small to detect by optical rotation measurements. In the presence of the alkali borates and tetraborates, however, the equilibrium for reaction I lies to the right, and the tendency for the formation of the ions BD^- and BD_2^- is high. Under these conditions large quantities of complex borates are formed, and it is possible to study compound formation of carbohydrates with borates or tetraborates by optical methods.

2. General Discussion of the Results of the Present Investigation

In this investigation, a study was made of the reactions of certain carbohydrates with sodium and potassium tetraborate. To obtain information concerning the compounds formed, solutions of D-glucose, D-fructose, L-sorbose, sucrose, mannitol, and sorbitol containing either sodium tetraborate or potassium tetraborate were studied polarimetrically. Measurements were made with solutions containing fixed amounts of the carbohydrate and various amounts of tetraborate, and with solutions containing fixed amounts of tetraborate and various amounts of carbohydrate.

As like molecular concentrations of sodium tetraborate and of potassium tetraborate were found to have like effects on the optical rotations of the substances investigated, the results obtained with the two salts are considered together. Sodium tetraborate is more readily obtained in pure condition and seems preferable for analytical pur-

poses, but potassium tetraborate is more soluble and can be used over a wider range of concentration.

It was shown by Kahlenberg and Schreiner [16] that sodium tetraborate in solution is equivalent to equimolecular amounts of sodium borate and boric acid. As compound formation of carbohydrates with boric acid is too slight to be observed polarimetrically, the presence of boric acid can be neglected, and 1 mole of tetraborate can be considered to be equivalent to 2 moles of borate. If it be assumed that compounds of the BD and BD_2 types are highly ionized and show little variation in ionization with concentration, and that a compound of type A is only slightly ionized, certain relationships can be drawn from Böeseken's equations, which appear to provide a reasonable interpretation of the complex changes observed in the optical rotations of carbohydrates in the presence of tetraborates.

The reactions may be expressed symbolically in the following manner: [6]

$$H_3BO_3 + H_2O \rightleftarrows B^- + H^+ \qquad I'$$

$$B^- + D \rightleftarrows BD^- + 2H_2O \qquad II'$$

$$BD^- + D \rightleftarrows BD_2^- + 2H_2O \qquad III'$$

$$BD^- + H^+ \rightleftarrows A + H_2O \qquad IV'$$

A system of this character would result in the equilibrium state represented somewhat arbitrarily in figure 1. This figure is similar to those used by Vermaas [17] and by Böeseken and Vermaas [29]. It includes, however, compounds of type A, and shows by the dotted lines, the direction of the changes that occur as the hydrogen ion concentration decreases. At a given tetraborate-diol ratio, the heights of the curves would be expected to vary widely with concentration and to depend on the characteristics of the diol in question.

From mass law it follows that: [7]

$$\frac{[BD_2^-]}{[BD^-]} = \frac{K_3[D]}{[H_2O]^2} \qquad (1)$$

$$[BD_2^-] = \frac{K_2[BD^-]^2}{K_2[B^-]} \qquad (2)$$

$$[A] = \frac{K_2K_4[H^+][B^-][D]}{[H_2O]^3} \qquad (3)$$

$$\frac{[BD^-]}{[A]} = \frac{K_4[H_2O]}{[H^+]} \qquad (4)$$

$$\frac{[BD_2^-]}{[A]} = \frac{K_3[D]}{K_4[H^+][H_2O]} \qquad (5)$$

From eq 1 and 2 it may be seen that the concentration of BD_2^- is favored by high concentrations of D and low concentrations of H_2O and B^-. Thus, compounds of the BD_2 type should be formed preferentially in concentrated solutions of the carbohydrate containing small amounts of borate. Consequently, the change in optical rotation caused by the addition of small quantities of tetraborate to a carbohydrate solution can be ascribed principally to the formation of a compound of the BD_2 type.

Compounds of types BD and A are favored by high borate concentrations according to eq 2 and 3. It follows from eq 1 and 4 that BD^- is favored over BD_2^- and A by dilution, and from eq 1 and 2 that BD^- is favored over BD_2^- by low concentrations of diol and high concentrations of borate. Hence, compounds of the BD type should predominate in dilute solutions containing large quantities of tetraborate and little carbohydrate.

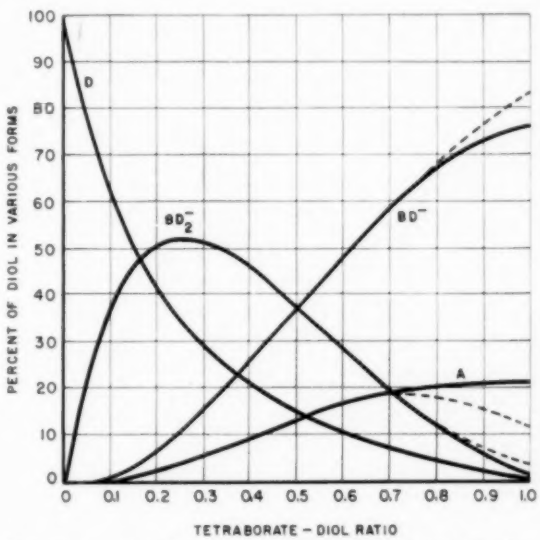

FIGURE 1. *Hypothetical equilibrium diagram for the tetraborate-diol system.*

D, Percentage of uncombined diol; BD_2, percentage of diol present as BD_2 compound; BD, percentage of diol present as BD compound; A, percentage of diol present as type A compound.

[6] D represents the carbohydrate (diol) and B^- the ion 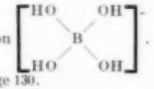 , BD^-, BD_2^-, and A represent the structures given on page 130.

[7] K_1, K_2, K_3, and K_4 are the equilibrium constants of equations I, II, III, and IV.

From eq 4, it is seen that in a system containing A and BD^-, [A] varies inversely with $[H_2O]$, and $[BD^-]$ varies directly. Hence, the proportion of compounds of type A is higher in concentrated solutions than in dilute, and the change in optical rotation with change in concentration at a constant tetraborate-carbohydrate ratio provides a means of judging the direction and magnitude of the optical rotation of the compounds of type A.

The relative amounts of compounds of types A, BD, and BD_2 also vary with the hydrogen ion concentration. The work of Hermans, Böeseken, Vermaas, and others has shown that compounds of type A are only weakly acidic; whereas, the hydrogen compounds of the BD_2 and BD types are strongly acidic. If, as we have assumed, compounds of type A are not ionized, and compounds of types BD_2 and BD are completely ionized, the relation between concentrations of hydrogen ion and of A, BD_2^-, BD^-, D, and B^- can be expressed by eq 3, 4, and 5. From eq 4 and 5, one would expect the ratios $[BD^-]$:[A] and $[BD_2^-]$:[A] to increase with decrease in hydrogen ion concentration. In general, as the tetraborate-carbohydrate ratio increases, the hydrogen ion concentration decreases, and $[BD^-]$ and $[BD_2^-]$ increase at the expense of [A]. This effect is indicated by the dotted lines of figure 1. In this study, consideration has not been given to the change in the degree of ionization of the borate with change in concentration or to differences between the optical rotations of the ionized and nonionized borate-di

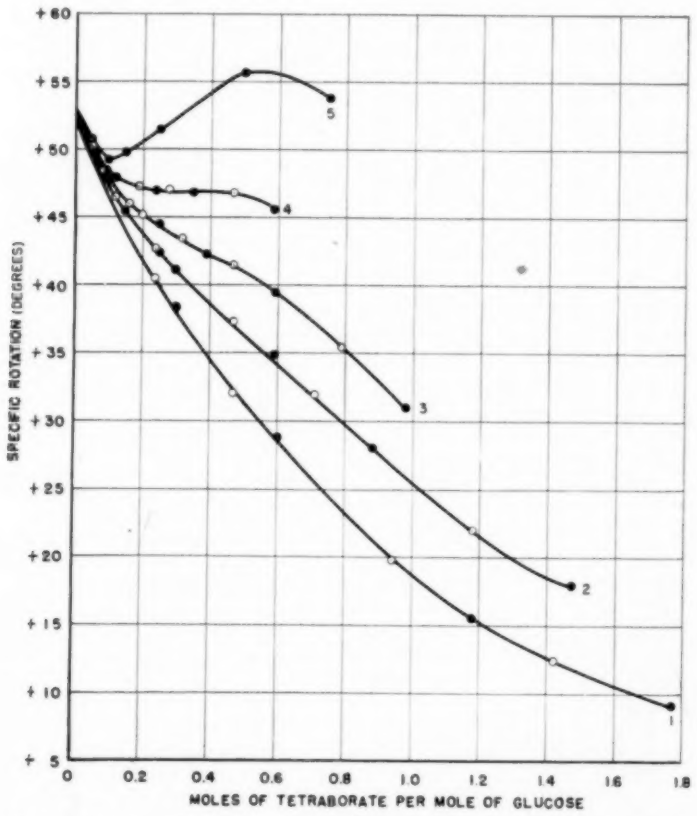

FIGURE 2. *Specific rotation of glucose in the presence of alkali tetraborates.*

○, Sodium tetraborate; ●, potassium tetraborate. 1, 2 g of glucose per 100 ml; 2, 4 g of glucose per 100 ml; 3, 6 g of glucose per 100 ml; 4; 10 g of glucose per 100 ml; 5, 25 g of glucose per 100 ml.

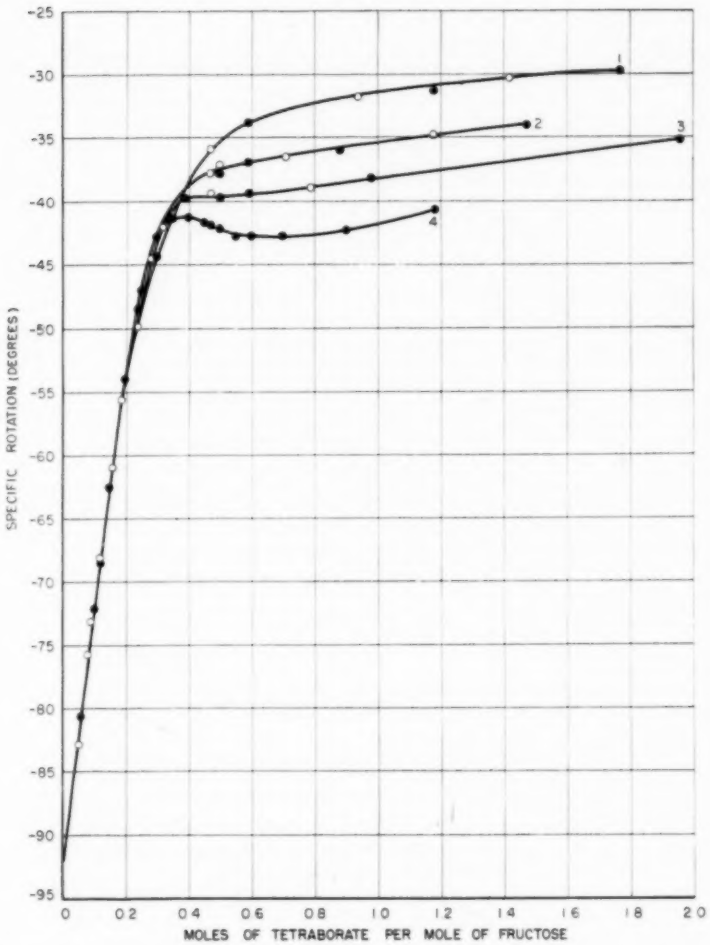

FIGURE 3. *Specific rotation of fructose in the presence of alkali tetraborates.*

○, sodium tetraborate; ●, potassium tetraborate. 1, 2 g of fructose per 100 ml; 2, 4 g of fructose per 100 ml; 3, 6 g of fructose per 100 ml; 4, 10 g of fructose per 100 ml.

mpounds. Although these factors are of im-rtance, they would not affect the qualitative nclusions that have been drawn.

It may be observed from the curves of figures 3, 4, 5, 6, and 7 that in the presence of tetra-rates, the optical rotations of certain carbohy-rates vary in striking manner with the tetra-rate-carbohydrate ratios and with the absolute ncentrations. The presence of a maximum and nimum in the curves for glucose and fructose, l the inflection in the curves for sorbose are vidence for the formation of three compounds from each of these substances. The general contour of the curves for sorbitol likewise suggests the presence of three compounds, but the curves for mannitol give evidence for two compounds and those for sucrose for only one. The proportions of the borate-carbohydrate compounds responsible for the changes in optical rotation appear to vary with the tetraborate-carbohydrate ratio essentially as indicated in the curves of figure 1. The several carbohydrate-tetraborate systems are considered in detail in succeeding sections.

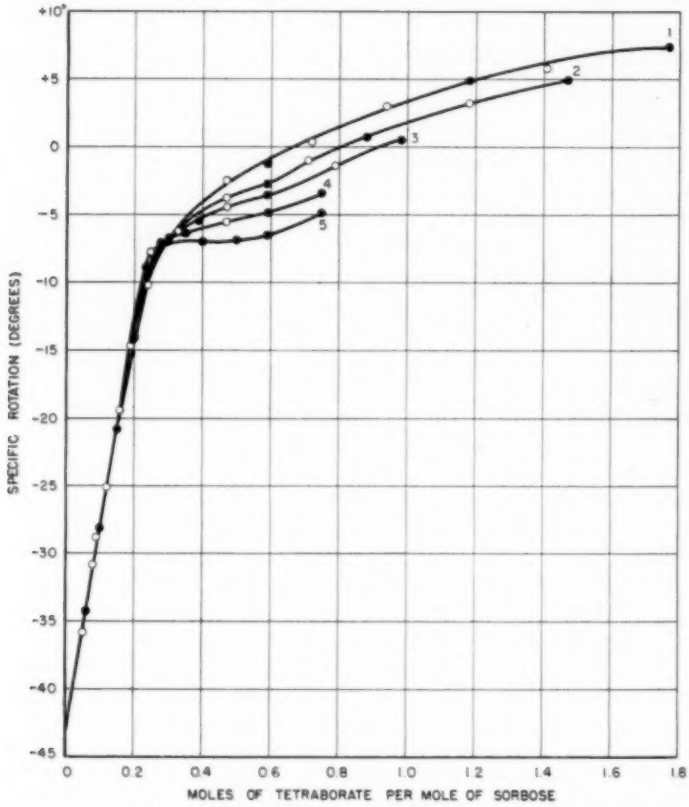

FIGURE 4. *Specific rotation of sorbose in the presence of alkali tetraborates.*

○, Sodium tetraborate; ●, potassium tetraborate. 1, 2 g of sorbose per 100 ml; 2, 4 g of sorbose per 100 ml; 3, 6 g of sorbose per 100 ml; 4, 10 g of sorbose per 100 ml; 5, 20 g of sorbose per 100 ml.

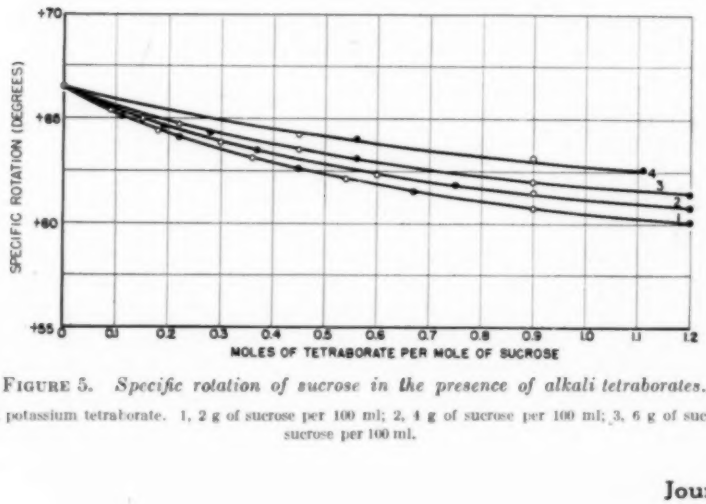

FIGURE 5. *Specific rotation of sucrose in the presence of alkali tetraborates.*

○, Sodium tetraborate; ●, potassium tetraborate. 1, 2 g of sucrose per 100 ml; 2, 4 g of sucrose per 100 ml; 3, 6 g of sucrose per 100 ml; 4, 10 g of sucrose per 100 ml.

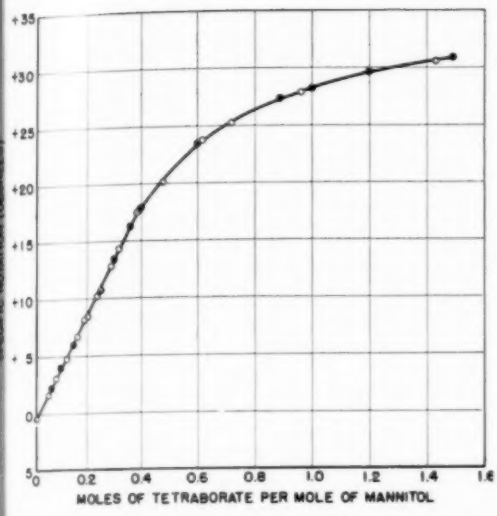

FIGURE 6. *Specific rotation of mannitol in the presence of alkali tetraborates.*

Data for solutions containing from 2 to 10 g of mannitol per 100 ml. ○, sodium tetraborate; ●, potassium tetraborate.

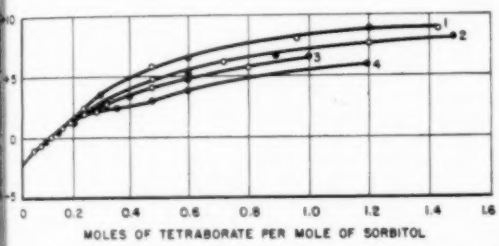

FIGURE 7. *Specific rotation of sorbitol in the presence of alkali tetraborates.*

○, Sodium tetraborate; ●, potassium tetraborate. 1, 2 g of sorbitol per 100 ml; 2, 4 g of sorbitol per 100 ml; 3, 6 g of sorbitol per 100 ml; 4, 10 g of sorbitol per 100 ml.

III. Optical Rotations of Carbohydrates in Solutions Containing Borates

1. D-Glucose

Although the effect of borates on the optical rotation of glucose was noted early, and has been studied by a number of investigators [22, 30, 31, 32, 33], prior work has not brought out the dependence of the optical rotation upon the relative and absolute concentration of both glucose and borate. The complex relationship is shown by the measurements reported in table 1 and figure 2. As already mentioned, α-D-glucopyranose combines selectively with boric acid and borates. Inasmuch as α-D-glucopyranose has one pair of adjacent *cis* hydroxyl groups, and a molecule of tetraborate furnishes 2 borate ions, formation of a compound of the BD_2 type requires 0.25 mole of tetraborate per mole of glucose. As this type of compound is favored by high concentrations of glucose, it may be assumed that the linearity of the change in optical rotation at tetraborate-glucose ratios of less than 0.1 is due to the substantially quantitative formation of the BD_2 compound. Extrapolation of this change in optical rotation to a tetraborate-glucose ratio of 0.25 gives a specific rotation of +40° for the BD_2 compound (expressed on the glucose content).

Compounds of the BD type are favored by dilute solutions at high tetraborate-diol ratios. Figure 8 shows that the specific rotation of glucose in the presence of either sodium tetraborate or potassium tetraborate approaches a limiting value of −9° as the concentration of the carbohydrate decreases, i. e., as the tetraborate-diol

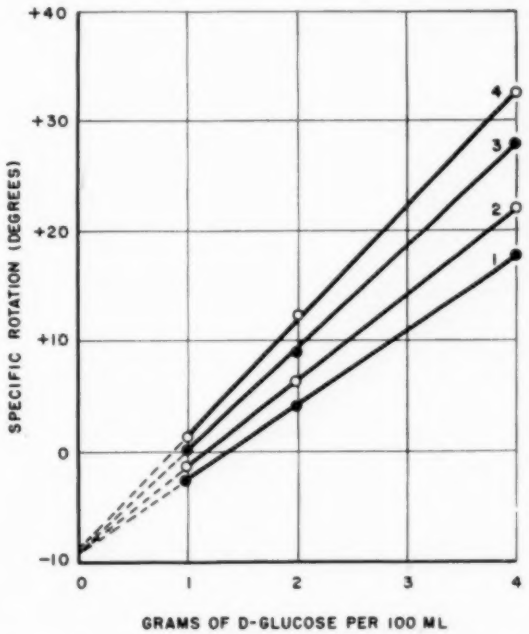

FIGURE 8. *Limiting value for the specific rotation of glucose at low concentration in the presence of tetraborates, for estimation of the specific rotation of the* BD *compound.*

○, Sodium tetraborate; ●, potassium tetraborate. 1, 10 g of $K_2B_4O_7.4H_2O$ per 100 ml; 2, 10 g of $Na_2B_4O_7.10H_2O$ per 100 ml; 3, 6 g of $K_2B_4O_7.4H_2O$ per 100 ml; 4, 6 g of $Na_2B_4O_7.10H_2O$ per 100 ml.

ratio increases.[8] As this value differs widely from the optical rotation of the free sugar (+52°) and does not vary appreciably with the concentration of the tetraborate, it may be assumed to correspond to the optical rotation of the BD compound. The existence of compounds having specific rotations of +40 and −9° will not account for the minimum and maximum observed in the rotations of concentrated solutions (figure 2, curve 5). Obviously, a compound at least as dextrorotatory as +58° (the maximum observed rotation) must be present. This compound is favored by high concentrations and a tetraborate-glucose ratio greater than 0.25. Hence, it is presumably of type A. The decrease in optical rotation with increasing tetraborate-glucose ratios above 0.5 can be ascribed to the formation of the BD compound by virtue of the decrease in hydrogen ion concentration (eq. 4, page 133).

TABLE 1. *Specific rotation of* D-*glucose in aqueous solutions containing tetraborate*

A. SODIUM TETRABORATE

D-Glucose	$Na_2B_4O_7.10H_2O$		$[\alpha]_D^{20}$	pH
g/100 ml	*g/100 ml*	*Moles per mole of glucose*		
1	6	2.84	+1.6	8.8
1	10	4.72	−1.8	9.1
2	0	0.00	+52.5	
2	1	.24	40.5	8.0
2	2	.47	32.1	8.1
2	4	.94	19.7	8.4
2	6	1.42	12.4	8.6
2	10	2.36	6.2	8.8
4	0	0.00	52.7	
4	1	.12	46.5	7.6
4	2	.24	42.7	7.5
4	2.12	.25	42.4	
4	4	.47	37.3	7.7
4	6	.71	32.0	8.0
4	10	1.18	22.0	8.3
6	0	0.00	52.7	
6	1	.08	48.5	7.2
6	2	.16	46.0	7.3
6	3.18	.25	44.5	
6	4	.32	43.4	7.4
6	6	.47	41.5	7.5
6	10	.79	35.4	7.9
10	0	.00	52.8	
10	1	.05	50.2	6.8
10	2	.09	48.4	6.8
10	4	.19	47.2	6.9
10	6	.28	47.0	7.0
10	10	.47	46.8	7.2

[8] A levorotation, (−8°) for certain glucose-borate mixtures was reported by Coleman and Miller [34].

TABLE 1. *Specific rotation of* D-*glucose in aqueous solutions containing tetraborate*—Continued

B. POTASSIUM TETRABORATE

D-Glucose	$K_2B_4O_7.4H_2O$		$[\alpha]_D^{20}$	pH
g/100 ml	*g/100 ml*	*Moles per mole of glucose*		
0.5	6	7.08	−4.3	
2	0	0.00	+52.5	
2	1	.30	38.3	
2	2	.60	28.8	
2	4	1.18	15.6	
2	6	1.77	9.2	
2	10	2.95	4.2	
4	0	0.00	52.7	
4	1	.15	45.4	
4	1.70	.25	42.4	
4	2	.30	41.2	
4	4	.59	34.9	
4	6	.88	28.0	
4	10	1.47	17.9	
6	0	0.00	52.7	
6	1	.10	47.7	
6	2	.20	45.1	
6	2.54	.25	44.6	
6	4	.39	42.3	
6	6	.59	39.5	
6	10	.98	31.0	
6	20	1.96	17.3	
10	0	0.00	52.8	
10	1	.06	49.6	
10	2	.12	47.9	
10	4	.24	46.9	
10	6	.35	46.8	
10	10	.59	45.6	
15	12.72	.50	50.6	
20	8.48	.25	50.6	
20	10.0	.30	51.3	
25	2.12	.05	50.7	
25	4.24	.10	49.1	
25	6.36	.15	49.9	
25	10.6	.25	51.4	
25	21.2	.50	55.7	
25	31.8	.75	53.8	
30	25.44	.50	57.0	
35	29.68	.50	57.4	
40 [a]	33.92	.50	57.6	

[a] Read at 35° C.

The complex relationships in the optical rotation shown in the curves of figure 2 arise from change in the proportions of the free sugar and the three borate compounds, essentially as shown in figure 1. At low tetraborate-glucose ratios, the concentration of the sugar is relatively high, and BD_2^- is the principal product. As the tetraborate-glucose ratio increases, the concentration of the free sugar decreases, and hence, the ratios $[BD_2^-]:[BD^-]$ and

$[BD_2^-][A]$. The formation of the compound of type A shifts the optical rotation in the dextro direction and accounts for the increase in optical rotation on the right-hand side of the minimum in curve 5 of figure 2. As the tetraborate-glucose ratio increases further, the hydrogen ion concentration decreases. This factor leads to the formation of the BD compound, partially at the expense of A, and accounts for the decrease in optical rotation following the maximum in curve 5.

At a fixed tetraborate-glucose ratio, changes in concentration affect the relative amounts of the three compounds. In concentrated solutions compounds of type A and BD_2 are present in larger amount, and account for the higher dextrorotations of these solutions; in dilute solutions at high tetraborate-glucose ratios the BD compound predominates to the exclusion of the others. The variation in the proportions of the several compounds with concentration accounts for the striking differences in the character of the curves obtained at different concentrations of glucose.

2. D-Fructose

The effect of boric acid and borates on the optical rotation of D-fructose has been studied by a number of workers [27, 31, 35]. It has been shown that fructose markedly increases the hydrogen ion concentration of aqueous boric acid, and that the effect is greatest at a concentration of 2 moles of fructose per mole of boric acid [36]. Other measurements have indicated that a difructose borate predominates under the conditions employed in the volumetric anaylsis of boric acid, and that a monofructose borate is present only when the concentration of fructose is less than 2 moles per mole of borate [37].

As fructose establishes an equilibrium containing both pyranose and furanose modifications [38], it might be expected to form derivatives of either modification. Levy and Doisy [23] observed that acidification of a solution containing fructose and borax results in a rapid mutarotation in the levo direction. The direction of the change is opposite to that of the mutarotation of crystalline β-D-fructopyranose. Hence, the predominating borate compound must contain an alpha fructopyranose, a fructofuranose, or an open-chain modification of the sugar. In light of the numerous possibilities, a definite structure cannot be assigned to the sugar component of any of the borate compounds at present.

The equilibrium specific rotations of fructose obtained in solutions at several concentrations in the presence of various amounts of sodium or potassium tetraborate are given in figure 3 and table 2. The specific rotations of solutions containing less than 0.25 mole of tetraborate per mole of fructose vary nearly linearly with the tetraborate-sugar ratio and show little change with change of concentration. These facts indicate that the product formed at low tetraborate-fructose ratios is relatively stable, and that its amount is nearly proportional to the borate present. As the proportion of tetraborate is low, the compound is presumably of the BD_2 type, and requires 0.25 mole of tetraborate per mole of fructose. The optical rotation can be estimated, as in the case of glucose, by extrapolation of the rotations observed at low tetraborate-fructose ratios to a ratio of 0.25. The result so obtained indicates a specific rotation of approximately $-45°$ based on the fructose content. The specific rotations in dilute solutions approach a limit at high tetraborate-fructose ratios of -22 to $-23°$ expressed on the fructose content (fig. 9). This value corresponds to the optical rotation of a compound presumably of the BD type. At tetraborate-fructose ratios above 0.3, the specific

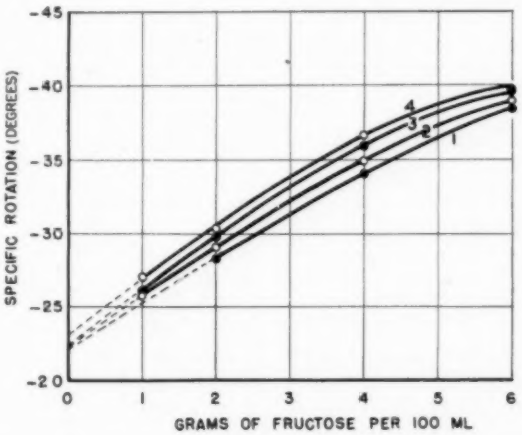

FIGURE 9. *Limiting value for the specific rotation of fructose at low concentration in the presence of tetraborates, for estimation of the specific rotation of the* BD *compound.*

○, Sodium tetraborate; ●, potassium tetraborate. 1, 10 g of $K_2B_4O_7{\cdot}4H_2O$ per ml; 2, 10 g of $Na_2B_4O_7{\cdot}10H_2O$ per 100 ml; 3, 6 g of $K_2B_4O_7{\cdot}4H_2O$ per 100 ml; 4, 6 g of $Na_2B_4O_7{\cdot}10H_2O$ per 100 ml.

771185—48——4

rotations vary markedly with concentration (fig. 3). As in the case of glucose, the variation may be caused by the formation of a compound of type A and by a shift in the relative proportion of BD_2^- and BD^-. It follows from eq 1 that at a given tetraborate-fructose ratio there must be relatively more BD_2^- in concentrated solutions than in dilute. This accounts in part for the more levo rotations of concentrated solutions, but a system having only two compounds in addition to the free sugar will not account for both the maximum optical rotation found at a tetraborate-fructose ratio of 0.3 to 0.5, and the minimum, found at a ratio of 0.5 to 0.8. The decrease following the maximum, shown in curve 4, shows the existence of a third compound, presumably of type A, and having a levorotation of at least −45°. The increase following the minimum may be attributed to changes in the proportion of BD^- and A with decrease in hydrogen ion concentration, as the tetraborate-fructose ratio is increased.

TABLE 2. *Specific rotation of* D-*fructose in aqueous solutions containing tetraborate*

A. SODIUM TETRABORATE

Fructose	$Na_2B_4O_7.10H_2O$		$[\alpha]_D^{20}$	pH
g/100 ml	*g/100 ml*	*Moles per mole of fructose*		
1	6	2.84	−26.7	9.0
1	10	4.72	−25.7	9.2
2	0	0.00	−92.3	
2	1	.24	−49.8	6.7
2	2	.47	−35.8	8.0
2	4	.94	−31.8	8.6
2	6	1.42	−30.3	8.7
2	10	2.36	−29.0	9.0
2	20	4.72	−27.5	
4	0	0.00	−92.3	
4	1	.12	−68.1	6.0
4	2	.24	−48.6	6.3
4	4	.47	−37.8	7.7
4	4.23	.50	−37.2	
4	6	.71	−36.6	8.1
4	10	1.18	−34.8	8.5
4	20	2.36	−31.0	
6	0	0.00	−92.6	
6	1	.08	−75.7	5.3
6	2	.16	−60.9	5.7
6	4	.32	−42.0	6.7
6	6	.47	−39.3	7.4
6	10	.79	−38.9	8.1
10	0	0.00	−93.0	
10	1	.05	−82.7	4.6
10	2	.09	−73.1	5.0
10	4	.19	−55.6	5.5
10	6	.28	−44.6	6.1
10	10	.47	−41.9	7.1

TABLE 2. *Specific rotation of* D-*fructose in aqueous solutions containing tetraborate*—Continued

B. POTASSIUM TETRABORATE

Fructose	$K_2B_4O_7.4H_2O$		$[\alpha]_D^{20}$	pH
g/100 ml	*g/100 ml*	*Moles per mole of fructose*		
1	6	3.54	−25.9	
1	20	11.79	−25.4	
2	0	0.00	−92.3	
2	1	.30	−44.3	
2	2	.59	−33.8	
2	4	1.18	−31.3	
2	6	1.77	−29.7	
2	10	2.95	−28.2	
4	0	0.00	−92.3	
4	1	.15	−62.5	
4	2	.30	−42.7	
4	3.39	.50	−37.8	
4	4	.59	−36.9	
4	6	.88	−35.9	
4	10	1.47	−34.0	
6	0	0.00	−92.6	
6	1	.10	−72.1	
6	2	.20	−54.0	
6	4	.39	−39.7	
6	5.09	.50	−39.7	
6	6	.59	−39.4	
6	10	.98	−38.3	
6	20	1.96	−35.2	
8	10	.74	−41.1	
10	0	0.00	−93.0	
10	1	.06	−80.6	
10	2	.12	−68.5	
10	4	.24	−48.6	
10	4.24	.25	−47.0	
10	6	.35	−41.2	
10	6.78	.40	−41.2	
10	7.63	.45	−41.6	
10	8	.47	−41.6	
10	8.48	.50	−42.1	
10	9.33	.55	−42.8	
10	10.18	.60	−42.7	
10	11.87	.70	−42.8	
10	15.26	.90	−42.8	
10	20	1.18	−40.7	
12	10.17	.50	−42.8	
15	6.36	.25	−47.2	
20	8.48	.25	−47.2	

3. L-Sorbose

Insofar as known the effect of borates on the optical rotation of L-sorbose has not been previously investigated, although it has been shown [39] that L-sorbose greatly increases the conductivity of boric acid. The capacity of sorbose to combine with boric acid might arise from the favorable positions of the hydroxyls of carbons 1 and 2 in either the pyranose or the furanose modifications. In the alpha forms, the hydroxyl of carbon

is also in a favorable position for the formation of a complex borate.

The results given in table 3 and figure 4 show that the optical rotations of sorbose solutions change from a levo to a dextro direction with the addition of increasing amounts of tetraborate. The curves are similar to those obtained for fructose and may be explained in like manner. As with fructose, the linear relationship, between the specific rotations and the tetraborate-sorbose ratios is evidence that the compound formed at ratios of less than 0.25 is relatively stable. The rotations at low tetraborate-sorbose ratios extrapolated to a ratio of 0.25 indicate that the specific rotation of the BD_2 compound is approximately $-5°$. The specific rotation of the compound favored by high tetraborate-sorbose ratios and presumably of the BD type, was found from the curves of figure 10 to be approximately $+16°$ (expressed on the sorbose content). The inflec-

TABLE 3. *Specific rotation of* L*-sorbose in aqueous solutions containing tetraborate*

A. SODIUM TETRABORATE

Sorbose	$K_2B_4O_7.10H_2O$		$[\alpha]_D^{20}$	pH
g/100 ml	*g/100 ml*	*Moles per mole of sorbose*		
2	0	0.00	−42.9	
2	1	.24	−10.2	6.8
2	2	.47	−2.5	7.9
2	3	.72	+.3	
2	4	.94	3.0	8.3
2	6	1.41	5.8	8.6
2	10	2.36	8.7	8.7
4	0	0.00	−42.9	
4	1	.12	−25.1	5.2
4	2	.24	−9.7	6.1
4	4	.47	−3.8	7.6
4	6	.71	−1.0	8.0
4	10	1.18	+3.2	9.0
6	0	0.00	−43.0	
6	1	.08	−30.8	4.7
6	2	.16	−19.3	5.2
6	4	.32	−6.2	6.4
6	6	.47	−4.5	8.0
6	10	.79	−1.3	8.1
10	0	.00	−43.2	
10	1	.05	−35.8	4.0
10	2	.09	−28.8	4.3
10	4	.19	−14.7	4.7
10	5.29	.25	−7.7	
10	6	.28	−6.9	6.2
10	10	.47	−5.5	7.1
10	10.58	.25	−7.5	

TABLE 3. *Specific rotation of* L*-sorbose in aqueous solutions containing tetraborate*—Continued

B. POTASSIUM TETRABORATE

Sorbose	$K_2B_4O_7.4H_2O$		$[\alpha]_D^{20}$	pH
g/100 ml	*g/100 ml*	*Moles per mole of sorbose*		
2	0	0.00	−42.9	
2	.88	.26	−8.3	
2	1	.30	−6.7	7.2
2	2	.59	−1.3	8.0
2	4	1.18	+4.8	8.5
2	6	1.77	7.4	8.6
2	10	2.95	9.8	8.9
4	0	0.00	−42.9	
4	1	.15	−20.8	5.4
4	1.70	.25	−8.6	
4	2	.30	−6.7	6.8
4	4	.59	−2.7	7.3
4	6	.88	+0.7	8.1
4	10	1.47	4.9	8.5
6	0	0.00	−43.0	
6	1	.10	−28.1	4.7
6	2	.20	−14.0	5.8
6	2.65	.26	−8.1	
6	4	.39	−5.5	7.1
6	6	.59	−3.5	7.5
6	10	.98	+.5	8.0
10	0	.00	−43.2	
10	1	.06	−34.2	4.0
10	2	.12	−25.3	4.3
10	4	.24	−9.7	5.4
10	4.24	.25	−8.5	
10	4.41	.26	−8.0	
10	4.75	.28	−7.3	
10	6	.35	−6.4	6.5
10	10	.59	−4.9	7.3
10	12.72	.75	−3.4	
20	8.14	.24	−9.3	
20	8.48	.25	−8.6	
20	8.82	.26	−8.1	
20	13.17	.40	−7.0	
20	16.96	.50	−6.9	
20	20.00	.59	−6.5	
20	25.44	.75	−5.0	
30	15.26	.30	−7.4	
30	25.44	.50	a−6.9	

a Read at approximately 33° C.

tions of the curves of figure 4 for high concentrations of sorbose indicate the presence of a third compound. As this compound is favored by high concentrations at tetraborate-sorbose ratios of more than 0.25, it is presumably of type A. To account for the alteration in optical rotations with concentration in the region of a tetraborate-sorbose ratio of 0.5, the compound must be at least as levorotatory as $-7°$. The increase in the slope of the curves as the tetraborate-sorbose

ratio is increased above 0.5 can be attributed to a change in the ratio [BD]:[A] caused by a decrease in the hydrogen ion concentration.

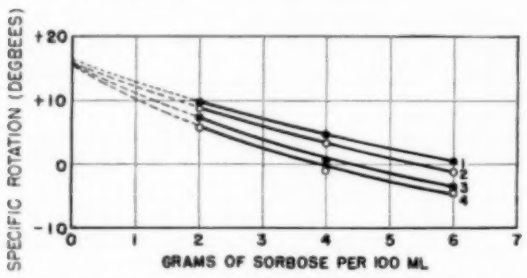

FIGURE 10. *Limiting value for the specific rotation of sorbose at low concentration in the presence of tetraborates, for estimation of the specific rotation of the* BD *compound.*

○, Sodium tetraborate; ●, potassium tetraborate, 1, 10 g of $K_2B_4O_7.4H_2O$ per 100 ml; 2, 10 g of $Na_2B_4O_7.10H_2O$ per 100 ml; 3, 6 g of $K_2B_4O_7.4H_2O$ per 100 ml; 4, 6 g of $Na_2B_4O_7.10H_2O$ per 100 ml.

4. Sucrose

It was noted by Müntz in 1876 [40] that the addition of borax to solutions of sucrose causes a lowering of optical rotation. The change is not nearly so large as that found for most sugars, yet it is substantial and cannot be explained merely by the action of the alkali or by a salt effect. Sucrose has no adjacent *cis* hydroxyl groups, and consequently it cannot form compounds of the BD and BD_2 types. Presumably for this reason, it does not appreciably affect the conductivity of boric acid solutions.[9] The results, given in table 4 and figure 5, show that the change in optical rotation varies with the concentration of both sugar and borate, but in contrast to the results obtained with glucose, fructose, and sorbose, the change is greatest in the most concentrated solutions. The optical rotations can be explained by the formation of a single sucrose-borate compound, which in dilute aqueous solutions dissociates in part. Presumably the compound is of type A and is analogous to the compounds formed by 1,3-diols.

TABLE 4. *Specific rotation of sucrose in aqueous solutions containing tetraborate*

A. SODIUM TETRABORATE

Sucrose	$Na_2B_4O_7.10H_2O$		$[\alpha]_D^{20}$	pH
g/100 ml	*g/100 ml*	*Moles per mole of sucrose*		
2	0	0.00	+66.5	
2	1	.45	64.2	9.1
2	2	.90	63.1	9.1
2	4	1.80	61.5	9.1
2	6	2.69	60.4	9.2
4	0	0.00	66.5	
4	1	.22	64.7	8.9
4	2	.45	63.5	8.9
4	4	.90	61.9	9.0
4	6	1.35	61.0	9.2
6	0	0.00	66.5	
6	1	.15	65.0	7.4
6	2	.30	63.8	8.8
6	4	.60	62.3	9.0
6	6	.90	61.4	9.0
10	0	0.00	66.5	
10	1	.09	65.4	8.1
10	2	.18	64.4	8.2
10	4	.36	63.1	8.8
10	6	.54	62.1	8.9
10	10	.90	60.7	8.9

TABLE 4. *Specific rotation of sucrose in aqueous solutions containing tetraborate*—Continued

B. POTASSIUM TETRABORATE

Sucrose	$K_2B_4O_7.4H_2O$		$[\alpha]_D^{20}$	pH
g/100 ml	*g/100 ml*	*Moles per mole of sucrose*		
2	0	0.00	+66.5	
2	1	.56	64.0	8.1
2	2	1.12	62.6	8.2
2	4	2.24	60.9	8.2
2	6	3.36	60.0	8.1
2	10	5.60	58.4	8.1
4	0	0.00	66.5	
4	1	.28	64.4	8.0
4	2	.56	63.1	8.0
4	4	1.12	61.4	8.1
4	6	1.68	60.3	8.1
4	10	2.80	58.8	8.2
4	20	5.60	57.2	
6	0	0.00	66.5	
6	1	.19	64.6	8.1
6	2	.37	63.4	8.1
6	4	.75	61.8	8.1
6	6	1.12	60.7	8.1
6	10	1.90	59.3	8.1
6	20	3.80	57.5	
10	0	0.00	66.5	
10	1	.11	65.1	8.0
10	2	.22	64.1	8.7
10	4	.45	62.6	8.9
10	6	.67	61.5	8.9
10	10	1.12	60.0	9.2
10	20	2.24	57.8	
20	20	1.12	59.0	

[9] See footnote 4.

5. Mannitol

In 1874 Vignon [1] observed that the optical rotation of mannitol is enhanced by the addition of borax and made extensive studies of the effect of the concentration of both mannitol and borax. Subsequently, Muller [30] made similar measurements and applied them to the quantitative estimation of mannitol. It was observed early that the addition of mannitol to solutions of boric acid causes a marked increase in acidity [2] and electrical conductivity. The effect has been studied extensively, and a method has been devised for the determination of boric acid by titration in the presence of mannitol [41].

Several mannitol-borates have been crystallized, but there is conflicting evidence in the literature as to the number and nature of the mannitol-borate compounds in solution. Fox and Gauge [11] reported a crystalline compound having acid properties, and the empirical formula $C_6H_{15}O_8B$, but did not assign a structural formula. It has since been considered to be of the BD type [6]. A crystalline compound having 2 molecules of mannitol and one of borate was prepared by Tung and Chang [16], who suggested a formula of the BD_2 type. Bremer [9] has disclosed the preparation of two amorphous mannitol-borate compounds of type A, in one of which two diol groups of the mannitol are combined with borate. As noted before, a crystalline acyclic mannitol borate considered to be 2-mannitol monoborate is formed by partial hydrolysis of the compounds of Bremer.[10]

From the optical rotations of a series of solutions containing increasing amounts of mannitol in the presence of decreasing amounts of borate, Böeseken and Vermaas [29] concluded that the solutions contained substances of the BD and BD_2 types having molar rotations of +6.80 and +3.26°, respectively. These values correspond to specific rotations of +37.4 and +8.96°, based on the weight of mannitol.

The data given in table 5 and figure 6 show that mannitol has an exceptionally high capacity for combination with borates. The mannitol-borate solutions are characterized first, in that the equilibrium specific rotation varies linearly with the tetraborate-mannitol ratio over a much wider range than that found for other carbohydrates, and second, in that the specific rotation is substantially independent of concentration at all tetraborate-mannitol ratios. The approximately linear relationship between the specific rotation and the tetraborate-mannitol ratio extends to a ratio of about 0.5. This is evidence for the formation of a relatively stable mannitol-borate compound having 1 molecule of mannitol for each borate group. The intercept of the linear curve with the ordinate corresponding to a tetraborate-mannitol ratio of 0.5 indicates that the specific rotation of the compound is approximately +22°.

TABLE 5. *Specific rotation of mannitol in aqueous solutions containing tetraborate*

A. SODIUM TETRABORATE

Mannitol	$Na_2B_4O_7.10H_2O$		$[\alpha]_D^{25}$	pH
g/100 ml	*g/100 ml*	*Moles per mole of mannitol*		
1	10	4.77	+34.5	
2	0	0.00	−0.5	
2	1	.24	+10.2	7.4
2	2	.48	20.1	8.1
2	4	.96	27.8	8.5
2	6	1.43	30.5	8.9
2	10	2.39	33.2	8.9
3	10	1.59	31.0	
4	0	0.00	−0.5	
4	1	.12	+4.7	5.9
4	2	.24	10.2	6.7
4	4	.48	20.2	7.8
4	6	.72	25.2	8.1
4	10	1.20	29.5	8.4
6	0	0.00	−0.4	
6	1	.08	+3.0	7.3
6	2	.16	6.4	8.0
6	4	.32	14.3	8.4
6	6	.48	20.1	8.5
6	10	.80	26.0	8.8
8	10	.60	23.4	
10	0	.00	−0.4	
10	1	.05	+1.7	4.9
10	2	.10	3.8	5.0
10	4	.19	8.1	5.7
10	6	.29	12.8	6.5
10	8	.38	17.5	
10	10	.48	20.3	7.9
10	12.8	.61	23.5	
12	10	.40	17.7	
14	10	.34	15.6	

[10] At the April 1939 meeting of the American Chemical Society in Baltimore, Md., W. H. Holst reported the preparation and identification of this mannitol borate. He showed that the compound is different from the mannitol boric acid of Fox and Gauge, which has the same empirical formula. He considered the latter compound to be 1-mannitol monoborate. However, the evidence does not appear to preclude the cyclic 1,2 structure proposed by Hermans [6] for the Fox and Gauge compound. To date, Holst's work has not been published.

TABLE 5. *Specific rotation of mannitol in aqueous solutions containing tetraborate*—Continued

B. POTASSIUM TETRABORATE

Mannitol	$K_2B_4O_7.4H_2O$		$[\alpha]_D^{25}$	pH
g/100 ml	*g/100 ml*	*Moles per mole of mannitol*		
1	0	0.00	−0.7	
1	1	.60	+22.4	
1	2	1.19	27.8	
1	4	2.39	31.9	
1	6	3.58	33.2	
1	10	5.96	34.5	
1	20	11.92	36.4	
2	0	0.00	−0.5	
2	1	.30	+13.3	7.3
2	2	.60	23.7	8.0
2	4	1.19	29.6	8.4
2	6	1.79	31.8	8.6
2	10	2.98	34.3	8.8
3	10	1.97	32.3	
4	0	0.00	−0.5	
4	1	.15	+5.9	5.8
4	2	.30	13.1	6.8
4	4	.60	23.4	7.8
4	6	.89	27.4	8.1
4	10	1.49	30.9	8.5
6	0	0.00	−0.4	
6	1	.10	+3.8	5.2
6	2	.20	8.2	5.8
6	4	.40	17.6	7.0
6	6	.60	23.1	7.5
6	10	1.00	28.1	8.0
6	18	1.80	31.9	8.9
8	10	.75	25.6	
10	0	0.00	−0.4	
10	1	.06	+2.2	4.6
10	2	.12	4.9	4.9
10	4	.24	10.4	5.7
10	6	.36	16.1	6.4
10	8	.48	20.3	
10	10	.60	23.3	
10	20	1.20	29.3	
10	30	1.80	32.1	
12	10	.50	21.0	
14	10	.43	18.8	

The compound might be of type A, but this seems improbable because the proportion of the compound does not depend on concentration. It will be recalled that with glucose, fructose, and sorbose the amount of the type A compound varied widely with concentration. In view of the general character of the curve, it seems probable that the compound having a specific rotation of +22° is of the BD_2 type in which D is only one-half of the mannitol molecule. That is, the mannitol molecule acts as a di-diol, and 4 hydroxyls instead of 2 are combined with borate, as represented in formula 1.[11]

Figure 11 shows that the optical rotation of mannitol in the presence of sodium tetraborate approaches a limiting value of approximately −36° with decreasing mannitol content. It is believed that this value approximates the optical rotation of a compound of the BD type (formula 2), again involving 4 hydroxyl groups of the mannitol molecule.

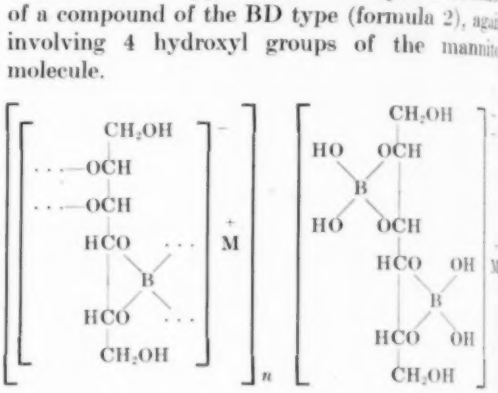

1. 2.

The nearly complete absence of a concentration factor for the optical rotations at constant tetraborate-mannitol ratios is most surprising and has been found only for mannitol. The marked changes in the optical rotations of tetraborate-

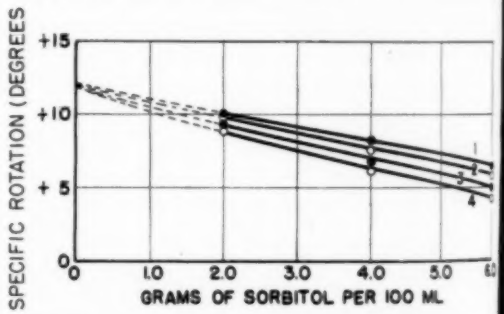

FIGURE 11. *Limiting value for the specific rotation of mannitol at low concentration in the presence of tetraborates, and estimation of the specific rotation of the* BD *compound.*

○, Sodium tetraborate; ●, potassium tetraborate. 1, 10 g of $K_2B_4O_7.4H_2O$ per 100 ml; 2, 10 g of $Na_2B_4O_7.10H_2O$ per 100 ml; 3, 6 g of $K_2B_4O_7.4H_2O$ per 100 ml; 4, 6 g of $Na_2B_4O_7.10H_2O$ per 100 ml.

[11] As joining molecules by quadricovalent boron would increase the molecular weight, it may explain the striking effect of borates on the viscosity and other properties of polyuronides such as algin and certain gums, which contain a pair of *cis* hydroxyl groups in the repeating unit. The marked effect of boric acid on the physical properties of high molecular weight compounds not having neighboring *cis* hydroxyl groups may arise from polymerization by ester linkage through tribasic boric acid.

glucose, tetraborate-fructose, and tetraborate-sorbose solutions with change in concentration were attributed to changes in the proportions of compounds of the BD_2, BD, and A types. The lack of a marked change in the optical rotation of tetraborate-mannitol solutions with alteration in concentration may arise from a fortuitous compensation of optical rotations and from the lack of a substantial quantity of a compound of type A in the solutions investigated.

One of the objects of the present investigation was to obtain data for use in the quantitative analysis of polyhydric alcohols. In the pharmaceutical trade, it has been customary to ascertain the purity of mannitol by measuring the optical rotation of 10 g in a solution containing 12.8 g of borax, and sufficient water to make a volume of 100 ml. Under these conditions, $[\alpha]_D^{20}$ is reported to be $+23$ to $+24°$ [42]; we have found that $[\alpha]_D^{20} = +23.5° \pm 0.1$. Although 12.8 g of borax can be held in solution by 10 g of mannitol in a volume of 100 ml at 20° C, with smaller quantities of mannitol this quantity of borax will not dissolve. Less difficulty was experienced with solutions containing 10 g of borax per 100 ml, and this quantity was used with various quantities of mannitol to obtain the data reported in table 6 and figure 12. The optical rotations do not vary linearly with the concentration of the mannitol, but by extrapolation between values, the concentration of mannitol corresponding to any observed reading can be ascertained with an accuracy of about 1 part in 200.

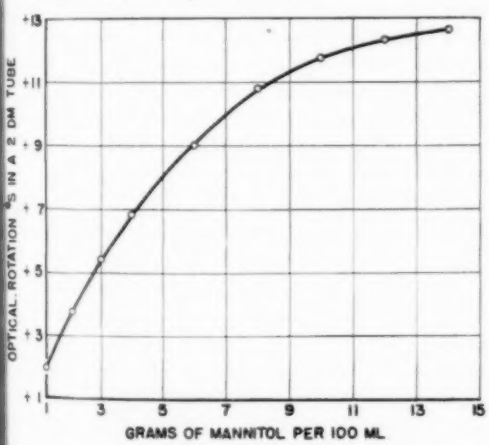

FIGURE 12. *Optical rotation of mannitol in the presence of 10 g of* $Na_2B_4O_7.10H_2O$ *per 100 ml of solution.*

TABLE 6. *Optical rotation of mannitol in the presence of 10 g of* $Na_2B_4O_7.10H_2O$ *per 100 ml of solution*

Mannitol	Observed reading in a 2-dm tube [a]	$[\alpha]_D^{20}$
g/100 ml	°S	
1	+1.99	+34.5
2	3.84	33.2
3	5.37	31.0
4	6.82	29.5
6	9.01	26.0
8	10.81	23.4
10	11.73	20.3
12	12.27	17.7
14	12.62	15.6

[a] Angular degrees = 0.3462 × °S.

6. Sorbitol

The effect of borax on the optical rotation of sorbitol was reported by Fischer and Stahel [43]. Böeseken and Vermaas [29] studied the optical rotations in a system in which both the sorbitol and borate were varied simultaneously. It has been found that the rotations of fixed quantities of sorbitol in the presence of increasing quantities of tetraborate are shifted in the same direction as those of mannitol, but the results differ in (1) the length and character of the linear portion of the curve, (2) the effect of concentration at fixed tetraborate-polyol ratios; and (3) the magnitude of the effect of tetraborate upon the rotation (fig. 7 and table 7). The curves for sorbitol are linear to a tetraborate-sorbitol ratio of only 0.16, whereas the mannitol curves are linear to a tetraborate-mannitol ratio of approximately 0.5. Hence, there is no reason to assume that sorbitol acts as a di-diol, as does mannitol. Extrapolation of the optical rotations obtained at low tetraborate-sorbitol ratios to a ratio of 0.25 gives a value of $+3°$, which presumably corresponds to the specific rotation of a compound of the BD_2 type. At high tetraborate-sorbitol ratios, the rotations approach a limit of $+11$ to $+12°$ (fig. 13). Presumably, this value corresponds to the specific rotation of a compound of the BD type. The specific rotation at fixed tetraborate-sorbitol ratios above 0.2 decreases with increasing concentration. This indicates the formation of a compound of type A which is less dextrorotatory than the compound of either the BD_2 or the BD type.

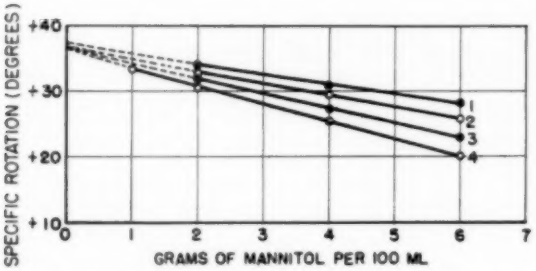

FIGURE 13. *Limiting value for the specific rotation of sorbitol at low concentration in the presence of tetraborates, for estimation of the specific rotation of the* BD *compound.*

○, Sodium tetraborate; ●, potassium, tetraborate. 1, 10 g of $K_2B_4O_7.4H_2O$ per 100 ml; 2, 10 g of $Na_2B_4O_7.10H_2O$ per 100 ml; 3, 6 g of $K_2B_4O_7.4H_2O$ per 100 ml; 4, 6 g of $Na_2B_4O_7.10H_2O$ per 100 ml.

TABLE 7. *Specific rotation of sorbitol in aqueous solutions containing tetraborate*

A. SODIUM TETRABORATE

Sorbitol		$Na_2B_4O_7.10H_2O$	$[\alpha]_D^{25}$	pH
g/100 ml	*g/100 ml*	*Moles per mole of sorbitol*		
1	10	4.78	+10.9	
2	0	0.00	−2.2	
2	1	.24	+2.4	6.9
2	1.05	.25	2.5	
2	2	.48	5.7	8.1
2	2.09	.50	5.7	
2	4	.96	8.0	8.6
2	6	1.43	8.9	8.8
2	10	2.39	9.8	8.9
3	10	1.59	8.7	
4	0	0.00	−2.2	
4	1	.12	+0.2	5.5
4	2	.24	2.0	6.4
4	2.10	.25	2.2	
4	4	.48	4.7	7.8
4	6	.72	6.1	8.2
4	10	1.20	7.7	8.6
6	0	0.00	−2.2	
6	1	.08	−0.6	5.6
6	2	.16	+0.9	6.5
6	4	.32	2.8	7.8
6	6	.48	4.1	8.2
6	6.27	.50	4.2	
6	10	.80	5.7	8.5
8	10	.60	4.0	
10	0	.00	−2.0	
10	1	.05	−1.0	4.6
10	2	.10	−0.2	4.8
10	4	.19	+1.3	5.1
10	5.26	.25	1.8	
10	6	.29	2.2	6.3
10	10	.48	2.9	7.3
10	10.47	.50	3.0	
12	10	.40	2.4	
14	10	.34	2.0	
20	10.47	.25	1.6	
20	20.94	.50	2.6	

TABLE 7. *Specific rotation of sorbitol in aqueous solutions containing tetraborate*—Continued

B. POTASSIUM TETRABORATE

Sorbitol		$K_2B_4O_7.4H_2O$	$[\alpha]_D^{25}$	pH
g/100 ml	*g/100 ml*	*Moles per mole of sorbitol*		
1	10	5.96	+10.5	
2	0	0.00	−2.2	
2	1	.30	+3.5	
2	2	.60	6.5	
2	4	1.19	8.8	
2	6	1.79	9.3	
2	10	2.98	10.0	
3	10	1.99	9.0	
4	0	0.00	−2.2	
4	1	.15	+0.4	
4	2	.30	2.6	
4	4	.60	5.2	
4	6	.89	6.6	
4	10	1.49	8.2	
6	0	0.00	−2.2	
6	1	.10	−0.2	
6	2	.20	+1.3	
6	4	.40	3.3	
6	6	.60	4.6	
6	10	1.00	6.5	
8	10	0.75	5.0	
10	0	.00	−2.0	
10	1	.06	−0.8	
10	2	.12	+0.2	
10	4	.24	1.7	
10	6	.36	2.4	
10	10	.60	3.9	
10	20	1.19	5.9	
12	10	0.50	2.9	
14	10	.43	2.4	

From a study of optical rotations and other data Böeseken and Vermaas [29] concluded that the sorbitol-sodium borate system is not so simple as the mannitol-sodium borate system, and that at high borate-sorbitol ratios there is evidence for the existence of a bivalent ion, $B_2D^{=}$. Although this substance may be formed, the results of the present investigation do not provide clear evidence for its presence. If formed, it would be analogous to compound 2, page 142, which is suggested for the mannitol system.

The quantitative determination of sorbitol at various concentrations by measurement of optical rotations in the presence of borax is not possible because the values are small, and the change in the observed optical rotation at constant tetraborate concentration shows a reversal with increasing amounts of sorbitol. This anomalous behavior is illustrated by the data of table 8.

TABLE 8. *Optical rotation of sorbitol in the presence of 10 g of* $Na_2B_4O_7.10H_2O$ *per 100 ml of solution*

Sorbitol	Observed reading in a 2-dm tube [a]	$[\alpha]_D^{20}$
g/100 ml	°S	
	+0.63	+10.9
	1.13	9.8
	1.51	8.7
	1.78	7.7
	1.98	5.7
	1.85	4.0
	1.68	2.9
	1.66	2.4
	1.62	2.0

[a] Angular degrees = 0.3462 × °S.

IV. Experimental Details

1. Purification of Tetraborates

(a) Sodium tetraborate ($Na_2B_4O_7.10H_2O$)

Borax, C. P. grade, was recrystallized from water by following the procedure recommended for standard borax for use in acidimetry [44].

(b) Potassium tetraborate ($K_2B_4O_7.4H_2O$)

Potassium tetraborate hydrates having 4, 5, and 5.5 molecules of water of crystallization have been reported [45]. The commercial product, labeled a pentahydrate, ordinarily has an indefinite amount of water. The potassium tetraborate used in this investigation contained 4 molecules of water of crystallization and was prepared in the following manner: 500 g of boric acid was suspended in 750 ml of water, and treated with 295 g of C. P. potassium hydroxide dissolved in 600 ml of water. The mixture was heated to dissolve the boric acid and was then filtered. The filtrate was evaporated to 750 ml, cooled to 0° C, seeded with potassium tetraborate tetrahydrate, and allowed to crystallize under constant agitation. After 3 hours the crystals were separated and washed with ice water. The product was recrystallized by dissolving it in a minimum quantity of hot, 5-percent aqueous potassium hydroxide. The substance was allowed to crystallize as before, separated by filtration, washed thoroughly with cold water, and dried at room temperature in air. The product so obtained gave the following analysis [46]: Calculated for $K_2B_4O_7.4H_2O$: K_2O, 30.83; B_2O_3, 45.59. Found: K_2O, 31.0; B_2O_3, 45.7.

2. Purification of Sugars and Sugar Alcohols

The glucose and sucrose used in the investigation were NBS Standard Samples, dried at 65° C in a vacuum oven. The levulose was purified by crystallization from a 90-percent aqueous solution with the addition of ethyl alcohol, and the sorbose and mannitol were recrystallized from water. The sorbitol was purified in the following manner: 1 part by weight of commercial sorbitol was dissolved in 3 parts of pyridine by heating on the steam bath. The solution was filtered through a Büchner funnel coated with a decolorizing carbon. The filtrate was seeded with crystals of the sorbitol-pyridine complex, stirred for several hours at room temperature, and placed in a refrigerator overnight. The crystalline material that formed was collected on a Büchner funnel and washed with a mixture of 2 parts of ether and 1 part of pyridine. The pyridine complex was recrystallized twice from 3 parts of hot pyridine and then decomposed by heating for 18 hours at 65° C in a vacuum oven. The product thus obtained was recrystallized from 3 parts of hot 95-percent ethyl alcohol by allowing the solution after seeding to cool over a period of 24 hours without stirring. Under these conditions anhydrous sorbitol crystallizes in large rosettes of fragile needles that can be readily separated by filtration.[12] The crystals were collected on a funnel and after a second crystallization, were air-dried, and finally dried to constant weight at 65° C in a vacuum oven.

3. Measurement of Optical Rotation

The solutions for the measurement of optical rotation were prepared by weighing the required amounts of carbohydrate and tetraborate into a volumetric flask. The mixture was dissolved in water, and the volume of the solution was adjusted at 20° C. In a few cases it was necessary to warm the solution slightly to effect complete dissolution of the materials. In all cases, the solutions were allowed to stand at 20° C for at least 2 hours or until the optical rotation had become constant. Readings were made with a Bates saccharimeter, in a water-jacketed, 4-dm tube at 20° C and were checked by a second observer. The values given in the tables were obtained from at least two separate determinations, in which the observed rotations

[12] If crystallization occurs rapidly, bulky masses of microscopic needles form, which are difficult to separate from the mother liquor.

agreed within 0.1° S. The saccharimeter readings were converted to angular degrees by use of the conventional factor, 0.3462. Some of the measurements reported in the tables were made on supersaturated solutions, but in these cases, care was taken to be certain that the solutions remained optically clear until the measurements were completed.

V. Summary

The present study indicates that the addition of either sodium or potassium tetraborate to a solution containing glucose gives rise to a diglucose borate having a specific rotation of about +40° (expressed on the glucose content). This substance exists in equilibrium with a monoglucose borate having a specific rotation of about −9° and a third compound whose rotation is at least +58°. The proportion of the diglucose borate having a rotation of +40° is highest when the tetraborate-glucose ratio is about 0.25. As the ratio is increased above 0.25, the proportion of this compound decreases with the formation of the levorotatory monoglucose borate and the substance whose rotation is at least +58°. The former compound is favored by dilute solutions and high tetraborate-glucose ratios; the proportion of the latter compound is highest in concentrated solutions at a tetraborate-glucose ratio of about 0.5, and decreases as the tetraborate-glucose ratio increases, presumably because of the accompanying decrease in the hydrogen ion concentration. According to the concentration, and the tetraborate-glucose ratio, the equilibrium specific rotation of D-glucose in the presence of tetraborate varies from +58 to −9°.

Similar studies with D-fructose, L-sorbose, and sorbitol show that these substances react with tetraborates in essentially the same manner as D-glucose. In each case, evidence was obtained for the existence of three complex borates. The compounds favored by a tetraborate-carbohydrate ratio of 0.25 have specific rotations of approximately −45°, −5° and +3°, based on the weights of fructose, sorbose, and sorbitol, respectively; the compounds of the same carbohydrates favored by dilution and high tetraborate-carbohydrate ratios have specific rotations of approximately −22°, +16°, and +12°. In each case, inflections in the curves and the effect of concentration indicate the presence of a third compound.

The mannitol-tetraborate system differs markedly from the other systems investigated in that the specific rotation depends almost completely on the tetraborate-mannitol ratio, and at a fixed ratio does not vary with concentration. The change in optical rotation with increasing tetraborate-mannitol ratio is linear to a ratio of 0.5. This is evidence that a relatively stable compound having a mannitol-borate ratio of 1:1 and a specific rotation of +22° is formed. It is believed that four hydroxyl groups of mannitol are involved, and that mannitol acts as a di-diol. At high tetraborate-mannitol ratios. the optical rotation approaches a limit of +36°. Presumably this rotation corresponds to that of a second mannitol-borate compound. A table for the quantitative determination of mannitol from measurements of optical rotations in the presence of tetraborates is given.

The optical rotation of sucrose is somewhat decreased by the addition of either sodium or potassium tetraborate. The alteration is greatest in concentrated solutions, and is explained by compound formation. There is no evidence for more than one sucrose-borate compound.

VI. References

[1] L. Vignon, Ann. Chim. Phys. [5] **2,** 440 (1874).
[2] D. Klein, Bul. soc. chim. [3] **29,** 357 (1878).
[3] A. Lambert, Compt. rend. **108,** 1016 (1889).
[4] G. Magnanini, Z. physik. Chem. **6,** 58 (1890).
[5] P. H. Hermans, Z. physik. Chem. **113,** 338 (1924).
[6] P. H. Hermans, Z. anorg. Chem. **142,** 83 (1925).
[7] J. Böeseken, Proc. Akad. Amsterdam **26,** 97 (1923).
[8] J. Meulenhoff, Z. anorg. Chem. **142,** 373 (1925).
[9] C. Bremer, U. S. Patent 2,223,948 (1940); U. S. Patent 2,224,011 (1940).
[10] R. E. Rippere and V. K. La Mer, J. Phys. Chem. **47,** 204 (1943).
[11] J. J. Fox and A. J. H. Gauge, J. Chem. Soc. **99,** 1053 (1911).
[12] H. G. Derx, Rec. trav. chim. **41,** 340 (1922).
[13] J. Böeseken, A. Obreen, and A. van Haeften, Rec. trav. chim. **37,** 184 (1917).
[14] E. Scheibe, Pharm. Z. Russ. **18,** 257, 289 (1879); **19,** 513 (1880); Pharm. J. Trans. [3] **11,** 389 (1880).
[15] A. Wohl and C. Neuberg, Ber. deut. chem. Ges. **32,** 3488 (1899).
[16] J. Tung and H. Chang, J. Chinese Chem. Soc. **9,** 127 (1942).

[17] N. Vermaas, Rec. trav. chim. **51,** 67 (1932).
[18] P. H. Hermans, Rec. trav. chim. **57,** 333 (1938).
[19] I. R. Verschuur, Rec. trav. chim. **47,** 123, 423 (1928).
[20] J. Böeseken, Rec. trav. chim. **61,** 82 (1942).
[21] J. Böeseken, A. H. Kirstjens, and C. E. Klamer, Proc. Akad. Amsterdam **18,** 1654 (1916); J. Böeseken, and H. Couvert, Rec. trav. chim. **40,** 354 (1921); J. Böeseken, Rec. trav. chim. **61,** 77 and 663 (1942).
[22] J. Böeseken, Ber. deut. chem. Ges. **46,** 2622 (1913).
[23] M. Levy and E. A. Doisy, J. Biol. Chem. **84,** 749 (1929).
[24] J. Böeseken, N. Vermaas, and A. T. Küchlin, Rec. trav. chim. **49,** 711 (1930).
[25] M. Levy, J. Biol. Chem. **84,** 763 (1929).
[26] L. Kahlenberg and O. Schreiner, Z. physik. Chem. **20,** 547 (1896).
[27] E. Darmois and R. Peyroux, Compt. rend. **193,** 1182 (1931).
[28] W. D. Bancroft and H. L. Davis, J. Phys. Chem. **34,** 2479 (1930).
[29] J. Böeseken and N. Vermaas, Rec. trav. chim. **54,** 853 (1935).
[30] J. A. Muller, Bul. soc. chim. **11,** 329 (1894).
[31] E. Rimbach and O. Weber, Z. physik. Chem. **51,** 473 (1905).
[32] M. Murgier and E. Darmois, Atti X° congr. int. chim. **2,** 737 (1938).
[33] Y. Tuzuki, Bul. Chem. Soc. (Japan) **16,** 23 (1941).
[34] G. H. Coleman and A. Miller, Proc. Iowa Acad. Sci. **49** 257 (1942).
[35] F. I. Berenshtein and A. U. Shpakovskii, Ukrain. Khem. Zhur. **11,** 433 (1936).
[36] F. I. Berenshtein and L. N. Aisenberg, Ukrain. Khem. Zhur. **8,** 307 (1933).
[37] H. Schäfer, Z. anorg. allgem. Chem. **247,** 96 (1941).
[38] H. S. Isbell and W. W. Pigman, J. Research NBS **20,** 773 (1938) RP1104.
[39] J. Böeseken and J. L. Leefers, Rec. trav. chim. **54,** 861 (1935).
[40] A. Müntz, Z. Verein. Rübenzucker Ind. **26,** 735 (1876).
[41] L. C. Jones, Am. J. Sci. [4] **7,** 147 (1899).
[42] Merck Index, p. 338 (Merck & Co., Inc., Rahway, N. J., 1940).
[43] E. Fischer and R. Stahel, Ber. deut. chem. Ges. **24,** 2144 (1891).
[44] Methods of Analysis, 6th ed., p. 805 (Assoc. Official Agr. Chem., Washington 4, D. C., 1945).
[45] A. Atterberg, Z. anorg. Chem. **48,** 367 (1906); A. Laurent, Ann. chim. phys. [2] **67,** 218 (1838); M. Dukelski, Z. anorg. Chem. **50,** 38 (1906).
[46] F. P. Treadwell and W. T. Hall, Analytical chemistry v. **II,** p. 533 (John Wiley & Sons, Inc., New York, N. Y., 1935).

WASHINGTON, October 7, 1947.

U. S. Department of Commerce
National Bureau of Standards

Research Paper RP1863
Volume 40, February 1948

Part of the Journal of Research of the National Bureau of Standards

Effect of Inhibitors on the Corrosion of Zinc in Dry-Cell Electrolytes

By Clarence K. Morehouse,[1] Walter J. Hamer, and George W. Vinal

This paper deals with a study of substitutes for mercury and chromate films in curtailing the corrosion of the zinc anode of Leclanché dry cells at high temperatures. Organic compounds containing the carbonyl group (such as furfural), heterocyclic nitrogen-containing compounds like quinaldine, and certain commercial products were found to be effective in retarding the corrosion of zinc in dry-cell electrolytes.

Although these types of materials retarded the corrosion of zinc, dry cells made with them did not have the expected increase in shelf-life or electrical output. The inhibitors either reacted with the paste wall to decrease its strength, or formed an insoluble film over the entire surface of the zinc anode that contributed to its internal resistance. No parallelism was observed between the electrical output of the cells and the percentage of inhibitor used in their construction. On the other hand, the paste wall of the dry cell, which is usually a starch-flour gel, was found to have inhibiting properties. Starch was inert, but flour had inhibiting properties. The active inhibiting agent of the flour is gluten. The constituents of gluten, namely, glutenin, and gliadin and mesonin in different states of aggregation were isolated, and the last two were found to be effective in retarding the corrosion of zinc. These materials can be incorporated in dry cells and increase their capacity at moderate temperatures.

I. Introduction

When the Leclanché type of dry cell is subjected to high-temperature storage, one of the sources of failure is the increased rate of corrosion of the zinc anode [1].[2] The zinc anode also corrodes at normal temperatures (18° to 30° C), and it is common practice either to amalgamate the zinc or to use chromate films to curtail local action. At high temperature neither of these methods is so effective as to yield good shelf life. In this paper alternate methods are described, including the use of inhibitors and modifications of the paste wall to increase its inhibiting properties.

The theory of corrosion inhibitors is still in the formative stage, and their choice is largely a matter of trial and error. However, the principles postulated for the corrosion of steel may be considered. In the dry cell the reactions are of two types: (1) the cell discharge reaction, which gives the available electrical energy, and (2) the corrosion reaction (local action), which is a side reaction, and from which no electric energy is available. These two reactions may be formulated as follows:

1. The dry-cell reaction [2, 3] in which no H_2 gas is formed:

$$Zn+2\ MnO_2=ZnO.Mn_2O_3.$$

2. Corrosion reaction in which H_2 gas is formed:

Reaction at anodic areas: $Zn \rightleftharpoons Zn^{++}+2\epsilon$,

Reaction at cathodic areas:

$$Zn^{++}+2NH_4Cl+2\epsilon \rightleftharpoons Zn(NH_3)_2Cl_2+H_2,$$

Over-all corrosion reaction:

$$Zn+2NH_4Cl \rightarrow Zn(NH_3)_2Cl_2+H_2.$$

The corrosion reaction may also be considered more simply as the discharge of hydrogen ions that penetrate to the cathodic areas of the zinc can. The corrosion and the cell-discharge reactions are not the same, and it should be possible to retard the

[1] Now with Olin Industries, Western Cartridge Co., East Alton, Ill.
[2] Figures in brackets indicate the literature references at the end of this paper.

corrosion reaction without materially affecting the discharge reaction. In order to accomplish this, the cathodic areas of the zinc must be made more anodic, or the anodic areas must be rendered ineffective until current is drawn from the cell. Amalgamation of the zinc and chromate films function in this sense.

In the steel industry, organic substances are added to the acid pickling bath to inhibit the corrosion of the metallic iron. The theory of these inhibitors is that they form an ionizable salt with the acid, whereby positive inhibitor ions are formed that are attracted by electrical forces to the cathodic areas. They are not discharged but replace the iron ions in a Helmholtz double layer, and when a state of equilibrium is attained they form a protective layer over the metallic surface. The effectiveness of this layer depends on its ability to prevent hydrogen ions from penetrating to the cathodic areas where they are discharged. The size, nature, position on the metallic surface, and the closeness of packing of the inhibitor ions will determine the effectiveness of this protective layer.

These types of inhibitors are classified as cathodic inhibitors. Attention was given to this type, because in the dry cell it is desirable that the corrosion of the zinc be inhibited by stopping the corresponding cathodic reaction and not the anodic one, which is necessary for the production of electrical energy by the cell. An anodic inhibitor, unless used in adjusted amounts, would not be desirable in that it would not only stop the cell-discharge reaction but might lead to localized corrosion and cause perforation of the zinc can. Chromates act as anodic inhibitors, and experience with chromate films indicates that they either become ineffective when current is drawn from the cell, or that the chromates function differently in the presence of the paste wall (starch-flour gels).

In many corrosion problems it is possible to reduce and sometimes eliminate the corrosion by altering the existing environments. With dry cells, however, the environments are necessary from the standpoint of electrical output and little changes can be made in them. The electrolyte in the usual type of dry cell consists of aqueous solutions of ammonium and zinc chlorides. There is an abundance of chloride ions, which are small in ionic volume, very mobile, and highly penetrating. Dry cells have been made with electrolytes composed of salts of anions other than chloride but with little success. Chlorides are necessary from the standpoint of electrical output, because they prevent the anode from becoming passive when the cell is discharged. Therefore, studies were confined to concentrated aqueous solutions of ammonium chloride with or without additions of zinc chloride. The corrosion rate of the zinc anode may be altered somewhat, but not significantly, by changing the concentration of the chloride or by using zinc containing various percentages of other metals. In this work, commercial zinc containing 0.25 to 0.60 percent of cadmium, 0.20 to 0.60 percent of lead, and less than 0.0[illegible] percent of iron was used.

II. Experimental Procedure

The rate of corrosion of the zinc was determined by a method suggested and used by D. A. Craig, in which the amount of hydrogen that is evolved under controlled conditions is measured. The apparatus consisted of an inverted test tube closed by a rubber stopper through which passes a capillary tube (fig. 1). Within the test tube the sample of zinc and electrolyte were placed, the electrolyte completely filling the test tube and capillary tube. In the inverted position, the gas liberated at the zinc rises in the tube and expels an equal volume of electrolyte through the capillary tube. The tube was weighed from day to day, and the volume of gas evolved was calculated from the change in weight and the known density of the solutions. Measurements were made at 54° C, a temperature reached in storage in the tropics during the past war. In some experiments ther ate of corrosion was determined by a loss-in-weight method, considered later.

III. Results

Data given in tables 1 and 2 show the effects of amalgamation and of chromate films on the rate of corrosion of zinc in ammonium chloride maintained at 54° C. AA-size zinc cans (17/32 in. in diameter and 1⅞ in. in height) were used. Neither amalgamation of the zinc nor use of chromate films was as effective as desired at 54° C. An excess of mercury decreases the mechanical strength of the cans.

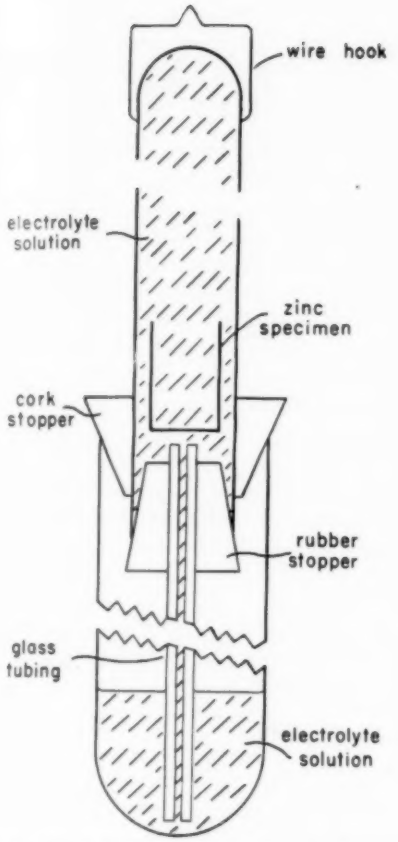

FIGURE 1. *Gas tube for measuring the rate of corrosion of zinc cans.*

TABLE 1. *Effect of amalgamation on the corrosion of zinc electrodes at 54° C*

[AA-size zinc cans totally immersed in 20% NH_4Cl solutions]

$HgCl_2$ per AA-size zinc can	Hydrogen evolved at 54° C for—	
	1 day	2 days
g	*ml*	*ml*
0.00	8.1	15.6
.01	4.8	11.1
.02	4.6	14.4
.04	3.1	9.1
.08	1.9	8.7
.10	1.9	7.2
.15	1.8	6.3
.20	1.7	7.2

The inhibiting properties of a large number of materials were studied. They may be classed as commercial or industrial by-products, organic compounds, inorganic compounds, and colloidal materials. The organic compounds may be subdivided into noncyclic and heterocyclic nitrogen-, oxygen-, or sulfur-containing compounds. Isocyclic compounds would not be expected to be effective inhibitors because of their symmetry. The one tried, salicyl aldoxime, was not effective, as anticipated.

Results obtained with D-size zinc cans (1¼ in. in diameter and 2¼ in. in height) immersed at 54° C in saturated aqueous solutions of ammonium chloride to which certain commercial products or organic compounds were added are given in tables 3 and 4. The data were extensive,

TABLE 2. *Effect of chromate films and dichromates on the corrosion of zinc electrodes at 54° C*

[AA-size zinc cans totally immersed in saturated NH_4Cl solutions]

Inhibitor	Hydrogen evolved at 54° C for—								
	1 day	5 days	10 days	15 days	20 days	25 days	30 days	35 days	40 days
	ml	*ml*	*ml*	*ml*	*ml*	*ml*	*ml*	*ml*	*ml*
Control (no film)	3.3	>13	(1)						
10-second Cronak treatment [2]	0.5	3.5	6.1	12.1	>13	(1)			
10-minute Cronak treatment [2]	.7	3.5	5.4	6.8	6.7	7.9	8.3	9.3	>13
0.5% $K_2Cr_2O_7$ added to solution	3.4	6.7	9.3	10.9	12.2	>13	(1)		
1.0% $K_2Cr_2O_7$ added to solution	2.7	6.4	8.9	10.9	12.2	>13	(1)		
2.0% $K_2Cr_2O_7$ added to solution	3.9	8.1	10.5			>13	(1)		

[1] Experiment was discontinued.

[2] The Cronak process, developed by the New Jersey Zinc Co., involves the treatment of the zinc with a solution containing sodium dichromate and sulfuric acid.

TABLE 3. *Effect of certain commercial inhibitors on the corrosion of zinc electrodes at 54° C*

(D-size zinc cans immersed in saturated solutions of ammonium chloride to which 1 percent of inhibitor was added)

Inhibitor	Duration of test	Rate of corrosion
	Days	*ml H_2/day*
None	1	3.5
Zinc dibutyl-dithiocarbamate	1	5.7
Piperdino pentamethylene dithiocarbamate	1	5.0
2-Mercaptobenzothiazole	1	4.3
Tetramethyl thiuram disulfide	5	1.7
Commercial oils [1]	1 to 20	1.3 to 0.5
Proprietary compounds of unknown composition [2]	1 to 160	10.4 to 0.023

[1] Three types.

[2] Eighteen types; most of these were believed to be heterocyclic organic compounds of the mercapto type.

and consequently only an average corrosion rate is listed for each material. This rate was obtained by dividing the total volume of gas evolved by the time (in days) of the test. The rates varied somewhat with the time, as shown in figure 2, for the better inhibitors. However, a preliminary choice of inhibitors and a comparison of their effectiveness may be made from the average rates. One percent of inhibitor was used in most cases. Lesser amounts were generally ineffective and larger amounts, as will be shown later, were undesirable in dry cells.

Of the commercial inhibitors, only tetramethyl thiuram disulfide, the commercial oils, and certain of the proprietary compounds of unknown composition were more or less effective. As the composition of these materials was unknown, no general principle for making a choice of possible inhibitors could be deduced from their study. Consequently, known organic and inorganic compounds were studied next.

The results obtained with organic compounds show that noncyclic compounds have little or no inhibiting action with the exception of crotonaldehyde. In fact most of these materials were corrosive. Crotonaldehyde exhibits resonance, has conjugated double bonds, and contains the carbonyl group (=C=O). Mann [4] has shown that the carbonyl group is effective in preventing corrosion of steel. He explained this by the formation of oxonium compounds, which ionize to give a positively charged ion as follows:

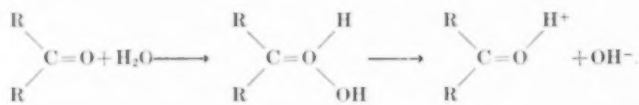

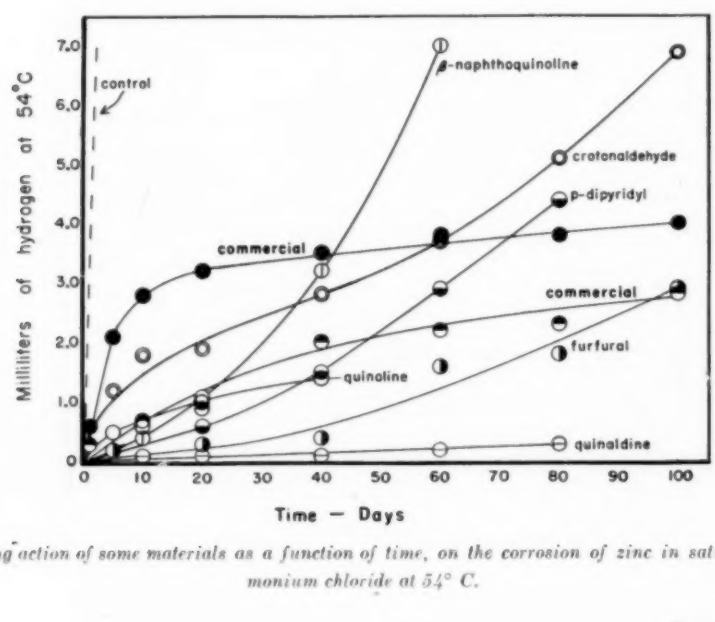

FIGURE 2. *Inhibiting action of some materials as a function of time, on the corrosion of zinc in saturated solution of ammonium chloride at 54° C.*

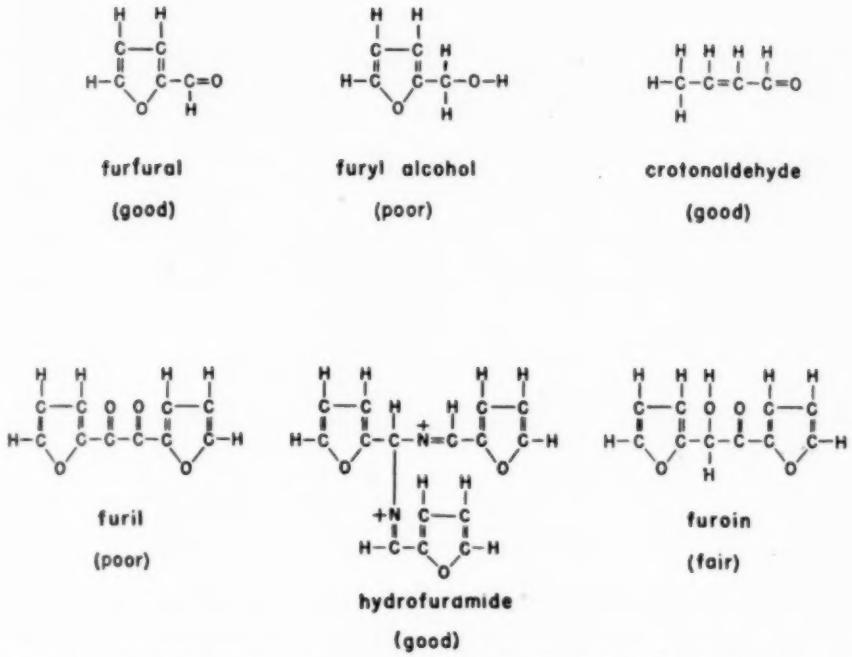

FIGURE 3. *Comparison of inhibiting action of compounds with and without the carbonyl group (=C=O) on the corrosion of zinc in saturated solutions of ammonium chloride at 54° C.*

TABLE 4. *Effect of organic compounds on the corrosion of zinc electrodes at 54° C*

(D-size zinc cans immersed in saturated NH_4Cl solutions to which 1 percent of inhibitor was added unless otherwise indicated)

Compound	Heterocyclic [1]			Compound	Noncyclic [1]	
	Number of rings	Duration of test	Rate of corrosion		Duration of test	Date of corrosion
NITROGEN-CONTAINING COMPOUNDS						
		days	*ml H_2/day*		*days*	*ml H_2/day*
Control		1	3.3	Control	1	3.3
8-Hydroxyquinoline [2]	2	1	4.3	Sulfanilic acid [3]	1	13
Quinaldinic acid	2	80	0.14	Anthranilic acid	1	13
8-Naphthoquinoline	3	60	.12	Benzidine	1	13
α-Dipyridyl	2	60	.048	Triethyl amine	1	12.9
Quinoline	2	60	.025	Diphenyl thiocarbazide [3]	1	12.4
8-Naphthoquinaldidine	3	60	.025	Diphenyl carbazone	1	11.5
Quinoline hydrochloride	2	60	.020	Aniline	1	10.8
Quinaldine	2	80	.004	Diphenyl carbazide	1	10.1
Pyridine [2]	1	1	13	Aldehyde ammonia [2]	1	10.0
Piperazine hydrate	1	1	6.4	Ethanol amine	1	8.2
α-Picoline	1	1	6.3	di-o-Tolylurea [3]	1	7.0
Brucine	6 or 7	1	5.9	Diethanol amine [2]	1	5.7
Salicyl aldoxime [2]	Isocyclic	1	5.8	Diphenyl guanidine	1	3.9
γ-Picoline	1	1	4.2			
Piperidine	1	1	3.0			

[1] Refers to the nitrogen, oxygen, or sulfur in the ring.
[2] Also contains oxygen.
[3] Also contains sulfur.

771185—48——5

TABLE 4. *Effect of organic compounds on the corrosion of zinc electrodes at 54° C*—Continued

Compound	Heterocyclic [1]			Compound	Noncyclic [1]	
	Number of rings	Duration of test	Rate of corrosion		Duration of test	Rate of corrosion
OXYGEN-CONTAINING COMPOUNDS						
Ascorbic acid		1	13	Formic acid	1	13
Brucine	6 or 7	1	5.9	Monochloracetic acid	1	11
Furil	2	5	2.2	Aldehyde ammonia [1]	1	10.0
Furyl alcohol	1	5	1.8	Hydroquinone	1	8.0
Furion	2	10	0.53	Resorcinol	1	7.1
Hydrofuramide [1]	3	100	.12	Pentane dione	1	4.8
Furfural	1	100	.029	Tannic acid	1	4.0
				Benzoic acid	5	1.4
				Crotonaldehyde	100	0.02
SULFUR-CONTAINING COMPOUNDS (ALL NONCYCLIC)						
Thiophenol	0	1	13	Sulfonated castor oil	1	3.8
Sulfanilic acid	0	1	13	Potassium ethyl xanthate	5	2.0
Diphenyl thiocarbazide	0	1	12.4	Ammonium sulfate (inorganic)	5	2.8

[1] Also contains nitrogen.

The positive ion is attracted to the cathodic areas of the steel and held there in a Helmholtz double layer, thereby increasing the hydrogen overvoltage of the cathodic areas.

The effect of the carbonyl group in retarding the corrosion of zinc is clearly shown for heterocyclic compounds in figure 3. Furfural contains the carbonyl group and is a good inhibitor. When the carbonyl group is converted to an alcoholic group by the addition of strong alkali, a compound, furyl alcohol, is obtained that has no inhibiting properties. It might be expected that furil would be an excellent inhibitor, as it contains two carbonyl groups. However, this is not the case, apparently because the carbonyl groups are effectively shielded from the zinc surface by the furan groups, or close packing of the positively charged ion on the zinc surface is not possible. The ineffectiveness of diphenyl carbazide, diphenyl thiocarbazide, or di-*o*-tolylurea as inhibitors may be explained on the same basis. The carbonyl or sulfonyl group in these compounds is shielded from the zinc surface by the phenyl or toluyl groups. Furoin inhibits slightly the corrosion of zinc, and therefore the carbonyl group in this compound must be attracted to the zinc surface. Hydrofuramide, which contains three furan groups, probably owes its inhibiting properties to the nitrogen and acts as a positively charged amine ion.

Heterocyclic compounds were the most effective inhibitors, providing a second or third ring was attached to the heterocyclic group. This is shown in figure 4. Pyridine, piperidine, α-picoline, and β-picoline, which are simple heterocyclic compounds containing nitrogen in the ring, had little or no inhibiting action, although these compounds may form addition compounds with acids or water and subsequently ionize to positively charged ions. On the other hand, phenyl and naphthalene derivatives, such as quinoline, *p*-dipyridyl, quinaldine, β-naphthoquinoline, and β-naphthoquinaldine do show inhibiting action. Here the positively charged ion is attracted to the cathodic areas at the nitrogen, and the large molecule, being unsymmetrical, is inclined at an angle to the zinc surface whereby a large area of the zinc surface is effectively covered. *p*-Dipyridyl is attracted to the zinc at both nitrogens and probably lies flat on the surface of the zinc and is therefore a good inhibitor. These conclusions agree, in the main, with those of Mann [4]. The better proprietary materials probably were heterocyclic compounds. The compound, 8-hydroxyquinoline shows no inhibiting properties, as the OH^- group favors orientation of the water molecule in its vicinity. This effect probably influences the position of the inhibitor ion in the Helmholtz double layer.

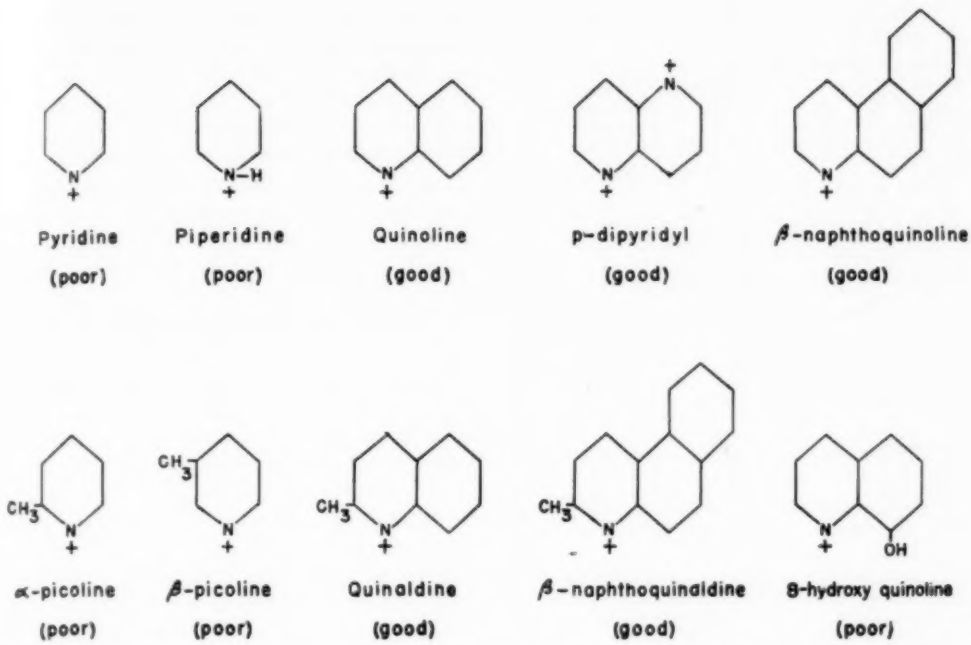

FIGURE 4. *Comparison of heterocyclic-nitrogen containing compounds showing the effect of molecular size on inhibition of corrosion of zinc in saturated solutions of ammonium chloride at 54° C.*

IV. Electrical Characteristics of Dry Cells Containing Inhibitors

In the foregoing it was shown that a number of organic compounds effectively curtail the local corrosion of zinc in saturated solutions of ammonium chloride. A few principles were outlined for making a choice of possible inhibitors. To determine whether these inhibitors could be successfully incorporated in dry cells, a number of D-size cells were made in the usual manner in which some of the better inhibitors were incorporated. The inhibitors were introduced into the cells in one of three ways: (1) by spinning an alcoholic solution of the inhibitor on the zinc can and removing the alcohol by evaporation, (2) by adding the inhibitor, if soluble, to the electrolyte of the paste wall, or (3) by grinding the inhibitor with the cereal (starch and flour) before the paste wall was gelatinized.

On the whole, dry cells made with inhibitors did not give the expected increase in shelf life or electrical output. The inhibitors either reacted with the paste wall and decreased its strength [5], or formed a high-resistant film on the zinc. In the latter case, these compounds probably form an insoluble precipitate over the entire surface of the zinc, which stifles not only the undesirable corrosion reaction, but also the cell-discharge reaction. In fact, Bartram and Kent [6] have shown that zinc and quinaldinic acid react to form an insoluble complex precipitate. Similar complex precipitates may be formed between the zinc and the other organic compounds.

In tables 5 and 6, the results of "light industrial tests" of the cells are given. The "light industrial test" gives the time in minutes of discharge to a cut-off voltage of 0.90 volt through a resistance of 4 ohms for 4-minute periods beginning at hourly intervals of 8 consecutive hours every day, with 16-hour rest periods intervening. At 21° C, the electrical output of cells made with or without inhibitors is approximately the same after 1 week of storage. At high temperatures, however, the cells containing the inhibitors gave less output, probably for the reasons cited above.

TABLE 5. *Light industrial tests of D-size dry cells containing inorganic or commercial inhibitors*

Inhibitor *	Discharge after storage at—			
	21° C, 1 week	54° C		
		1 month	2 months	3 months
	min	*min*	*min*	*min*
Control at 21° C, 0%	788	[1] 783	[1] 781	[1] 778
Control at 54° C, 0%	[2] 788	779	739	700
NH_4HF_2, 1.0%	776	3	----	----
$K_2Cr_2O_7$, 2.0%	779	699	3	----
Cronak treatment, 5 sec	----	708	614	192
Cronak treatment, 10 sec	----	694	640	[3] 240
Cronak treatment, 20 sec	----	706	650	[4] 280
Cronak treatment, 40 sec	----	681	637	384
Cronak treatment, 80 sec	----	669	733	262
Cronak treatment, 180 sec	----	718	708	288
Zinc dibutyl-dithiocarbamate, 5.0%	----	676	556	----
Commercial oils, 5.0%	----	622	488	[5] 363
Proprietary compounds of unknown composition, 1 to 10% [6]	754	544	207	49

* Inhibitor was mixed with the electrolyte of the paste wall or ground with the cereal. The electrolyte consisted of 22.78 g NH_4Cl, 6.1 g $ZnCl_2$, and 49.4 ml of H_2O. To this was added 7.15 g each of waxy cornstarch, Buffalo cornstarch, and Pillsbury XXXX wheat flour.

[1] Stored at 21° C. [2] Stored at 54° C.

[3] 192 minutes at the end of 4 months.

[4] 133 minutes at the end of 4 months.

[5] 105 minutes at the end of 4 months.

[6] Average of 20 tests on different inhibitors.

TABLE 6. *Light industrial tests of D-size cells containing organic inhibitors*

Inhibitor [1]	Discharge after storage at—			
	21° C, 1 week	54° C		
		1 month	2 months	3 months
	min	*min*	*min*	*min*
Control at 21° C, 0.0%	788	[2] 783	[2] 781	[3] 778
Control at 54° C, 0.0%	[2] 788	779	739	700
Furfural, 0.5%	802	644	368	34
Furfural, 1.0%	879	569	<3	----
Hydrofuramide, 0.5%	----	524	411	257
Crotonaldehyde, 1.0%	----	464	<3	----
Quinaldine, 1.0%	731	648	----	----
Quinaldine, 2.0%	871	664	----	----
Quinaldine. HCl, 1.0%	731	648	<3	----
Quinaldine. HCl, 10.0%	382	<3	----	----
Fatty acids of corn, 0.02%	429	----	----	----
Hydroquinone, 0.03%	----	<3	----	----

[1] The composition of the paste wall was the same as given in the footnote of table 5. The inhibitor was added to the electrolyte of the paste wall or was ground with the cereal.

[2] Stored at 21° C. [3] Stored at 54° C.

The amount of inhibitor to use in dry cells remains a moot question. Data obtained with the proprietary compounds and with Cronak treatments for various times did not show any correlation between electrical output and percentage of inhibitor. It is probable that there is an optimum concentration for each inhibitor. However, considerable work would be required to ascertain this optimum concentration, which may depend on the concentration of the electrolyte and the composition of the paste wall, because the inhibitors may react with the paste wall.

V. Inhibiting Characteristics of the Paste Wall

As the organic and other types of inhibitors for zinc did not improve the shelf life or electrical output of dry cells, studies were made of the organic substances commonly used in the paste wall (or separator) of the dry cell. It has been recognized that starch and flour not only provide a satisfactory separator for the dry cell, but also inhibit to some extent the local corrosion of the zinc electrode, without affecting the electrical output of the dry cell. These materials may be classed as water dispersible organic colloids. Most colloidal particles are positively charged in acid solutions and negatively charged in alkaline solutions. These positively charged particles in acid may then migrate to the cathodically active spots, which are thereby screened or poisoned.

In table 7 are given results obtained at 25° C with zinc immersed in saturated aqueous solutions of ammonium chloride to which colloidal materials were added. The natural starches had little protective value. The only modified starch that appears to have appreciable inhibiting properties was a modified starch prepared by H. S. Isbell of this Bureau. His method involved a treatment of starch with chlorine dioxide, whereby the aldehyde end groups of the starch are converted to aldehyde groups.

Cornmeal, zein, and starch glycerite all appear to have inhibiting properties. On the other hand, dextrose and the soluble starches, inulin and glycogen, accelerate the corrosion of zinc in saturated solutions of ammonium chloride. The starches apparently have no protective value, because they are not positively charged. In separating the amylose and amylopectin components of starch by the electrodialytic method, amylose migrates to the anode, and amylopectin remains stationary. Amylose is therefore negatively

charged and should be without effect on the corrosion of zinc. The high corrosive effect of amylose may be attributed to the butanol that is used to keep it in a soluble condition.

TABLE 7. *Results obtained with colloidal materials at 25° C*

[AA-size zinc cans immersed in saturated NH_4Cl solutions to which 2 percent of material was added]

Material	Duration of test	Rate of corrosion
NATURAL STARCHES		
	Days	*ml H_2/day*
Control	25	0.43
Inulin (dahlia)	5	2.20
Glycogen (animal)	10	1.23
Arrowroot	15	0.70
Sweetpotato	20	.64
Corn	20	.60
Maine potato	20	.54
Waxy corn	20	.53
Sago	25	.52
Rice starch	20	.44
Cassava	30	.39
Idaho potato	30	.39
NATURAL FLOURS		
Potato	30	0.40
Soybean	80	.14
Rice	100	.12
Buckwheat	90	.086
Wheat	100	.085
Rye	100	.081
Whole wheat	100	.080
MODIFIED STARCHES		
Control	25	0.43
Dextrose	10	1.27
Corn amylose [1]	1	1.10
Waxy corn amylopectin	10	0.91
Corn amylopectin	20	.60
H 20 cornstarch [2]	20	.60
4601 cornstarch [2]	25	.48
3406 cornstarch [2]	25	.48
Defatted cornstarch	30	.44
Zein	40	.31
Glycerite of starch	45	.27
H81 cornstarch [3]	50	.15
MODIFIED FLOURS		
Glutenin	30	0.36
α gliadin	30	.27
Mesonin I	50	.14
Gum gluten	100	.094
Gliadin	100	.087
Wheat flour	100	.085
Mesonin II	60	.063

[1] To keep amylose in a soluble form, it is kept moist with *n*-butanol. The high value for amylose may be caused by the presence of *n*-butanol, which may have a corrosive effect.

[2] Supplied by the National Starch Co.

[3] Supplied by R. W. Kerr, Corn Products Refining Co., Argo, Ill.

[4] Prepared by H. S. Isbell, National Bureau of Standards.

TABLE 7. *Results obtained with colloidal materials at 25° C*—Continued

MISCELLANEOUS MATERIALS

Material	Duration of test	Rate of corrosion
	Days	*ml H_2/day*
Ammonium alginate	1	11.3
Carpenter's glue	5	3.2
Hydroxyethyl cellulose	1	2.5
Carboxymethyl cellulose	20	0.57
Casein	40	.24
Agar agar	40	.21
Yellow corn meal	20	.17
Hemoglobin	70	.16
Amidex	80	.15
White corn meal	100	.11
Gelatin	100	.11
Powdered acacia	100	.11

The flours, with the exception of potato flour, which is low in protein content, all have inhibiting properties for the corrosion of zinc. It is evident from the data that the effective ingredient in flour is gluten, the protein-containing material. Gluten consists of glutenin, and gliadin and mesonin in different states of aggregation. Results obtained with these materials obtained from wheat flour by the combined methods of Stockelbach and Bailey [7] and Haugaard and Johnson [8] showed that with the exception of glutenin all were good inhibitors of the corrosion of zinc. When these materials are incorporated in dry cells they increase somewhat the capacity of dry cells at 21° C. as shown by the data of table 8. Current maintenance is defined as the ratio of the flash (or short-circuit) current after an interval of storage to the initial flash current. Many commercial cells give better current maintenance than the experimental controls given here. However, cells with and without proteins (experimental controls) were made under the same procedure, and comparisons should be made with the experimental controls and not with commercial cells. On hydrolysis the flour proteins give amino acids. Therefore, studies were made of the inhibiting properties of several amino acids, with the results given in table 9. The amino acids have no protective value; in fact most of them accelerate the corrosion of zinc.

Other colloidal materials, including gelatin, agar, acacia, casein, and hemoglobin likewise have inhibiting action. Carboxymethyl cellulose, hydroxymethyl cellulose, and ammonium alginate, which have been tried in the dry cell as substitutes

for starch and flour, have no inhibiting properties. Amidex, a degradation product of starch, has some inhibiting properties.

TABLE 8. *Effect of protein films on the current maintenance*[1] *of D-size dry cells at 21° C*

Type of paste wall	Number of cells	Current maintenance				
		1 month	3 months	6 months	1 year	15 months
		Percent	*Percent*	*Percent*	*Percent*	*Percent*
Control (cornstarch 67%, wheat flour 33%)	48	91	84	75	66	55
Cornstarch 67%-gum gluten 33%	3	91	87	77	61	51
Control+mesonin film[2]	9	94	90	79	81	71
Control+mesonin I film	9	95	88	84	.....	.....
Control+mesonin II film	2	91	91	82	.....	.....
Control+gliadin film	9	98	100	102	84	.....
Control+4° gliadin film	5	102	.....	88	94	.....
Control+(−10°)-gliadin film	7	94	.....	92	86	83
Control+neutralized 4° gliadin film	6	94	89	87	80	75

[1] Current maintenance is the ratio of the flash (or short-circuit) current after storage to the initial flash current.

[2] Many commercial cells give better current maintenance than these experimental controls, but comparisons must be made with the latter.

[3] All films covered the zinc can.

TABLE 9. *Effect of amino acids on the corrosion of zinc electrodes at 25° C*

Acid	Duration of test	Rate
	Days	*ml H_2/day*
Control	25	0.43
Leucine	5	2.32
Aspartic acid	5	2.06
Glutamic acid	5	1.84
Arginine	10	0.92
Tryptophane	10	.91
Control	25	.43
Serine	10	.86
Phenyl alanine	20	.75
Histidine.HCl	10	.50
Valine	40	.33
Alanine	40	.31

VI. Zinc-Corrosion Experiments by the Loss-in-Weight Method

As the conditions in the gas tubes are not entirely similar to conditions in the dry cell, and as solutions of higher concentrations of starch and flour could not be conveniently and satisfactorily tested in these tubes, a few corrosion experiments by a loss-in-weight method were undertaken.

TABLE 10. *Loss in weight of D-size zinc cans containing 30 ml of paste after storage at 54° C*

	Gel constituents	Loss in weight after storage at 54° C for—			
		48 hr	259 hr	284 hr	339 hr
		g	*g*	*g*	*g*
A[1]	100% water (distilled)				0.04
	5 parts NH_4Cl and 95 parts H_2O				.08
	20 parts NH_4Cl and 80 parts H_2O				.22
	30 parts NH_4Cl and 70 parts H_2O				.20
	40 parts NH_4Cl and 60 parts H_2O				.10
	Electrolyte mixture[1] (32.2% NH_4Cl; 4.12% $ZnCl_2$)	0.04	0.19	.....	.32
B[2]	21.5 g cornstarch	.05	.26	0.18	
	16.1 g cornstarch and 5.4 g wheat flour			.04	
	10.7 g cornstarch and 10.7 g wheat flour			.04	
	5.4 g cornstarch and 16.1 g wheat flour			.06	
	21.5 g wheat flour	.05	.05	.05	
C[2]	21.5 g waxy cornstarch			.12	
	21.5 g sweetpotato starch			.13	
	2.0 g carboxymethyl cellulose	.06	.36		
	2.5 g carboxymethyl cellulose			.18	
D[2]	21.5 g cornstarch and 21.5 g wheat flour				.07
	16.1 g cornstarch and 16.1 g wheat flour				.05
	10.7 g cornstarch and 10.7 g wheat flour				.08
	5.4 g cornstarch and 5.4 g wheat flour				.07
E[2]	21.5 g cornstarch and 2.0 g gliadin			.07	
	21.5 g cornstarch and 2.0 g gluten			.09	
	7.1 g cornstarch, 7.1 g waxy cornstarch and 7.1 g wheat flour			.04	
	2.5 g carboxymethylcellulose and 2.0 g gliadin			.07	
	2.5 g carboxymethylcellulose and 2.0 g gluten			.09	
	1.3 g carboxymethylcellulose and 10.7 g wheat flour			.05	

[1] The electrolyte mixture consisted of 46.1 g of NH_4Cl and 12.3 g of $ZnCl_2$ in 100 ml. of H_2O.

[2] Added to 93 ml of the electroylte mixture.

[3] 334 hours.

[4] Saturated; crystals of NH_4Cl on can.

A paste of electrolyte and cereal was poured into a D-size zinc can of known weight, and mineral oil was poured over the paste to prevent evaporation. After storage in an oven at 54° C, the can was thoroughly cleaned of paste and weighed. Results obtained by this method, given in table 10(A) show the corrosive effect of the electrolyte concentration. Concentrated solutions of ammonium chloride are more corrosive than dilute, and the addition of zinc chloride decreases the rate of corrosion, as expected. Results of table

10 also show that a flour paste has more inhibiting properties than a starch paste (B) or a carboxymethyl cellulose paste (C), in conformity with the results obtained with the gas experiments. The amount of flour in the paste (D) that is necessary to inhibit corrosion need not be very large. The results (E) also show that a starch or a carboxymethyl cellulose paste can be made less corrosive by the addition of small amounts of either flour, gum gluten, or gliadin.

VII. Conclusions

The results of this investigation have shown that the corrosion of zinc in saturated solutions of ammonium chloride may be curtailed by organic compounds containing the carbonyl group, by heterocyclic nitrogen-containing compounds with one or more rings attached to the heterocyclic group, by certain commercial products, and by colloidal materials. Of these the heterocyclic compounds were the best. For example, quinaldine, quinoline, furfural, *p*-dipyridyl, *β*-naphthoquinaldine, and *β*-naphthoquinoline were better inhibitors of the corrosion of zinc in dry-cell electrolytes at 54° C than mercury (amalgamation) or chromate films.

Of those materials found to retard the corrosion of zinc, only the colloidal materials could be incorporated in dry cells. Most of the noncolloidal materials either reacted with the paste wall of the dry cell or formed an insoluble film, like a varnish, over the entire surface of the zinc anode, and contributed to the internal resistance and reduced the electrical output of the dry cell.

It was found that the paste wall of the dry cell has inhibiting properties, provided it contains a colloidal protein like wheat flour. The active inhibiting agent of the flour was found to be gluten. The constituents of gluten, namely, glutenin, and gliadin and mesonin in different states of polymerization were isolated. Of these, gliadin and mesonin were found to be effective in retarding the corrosion of zinc in dry-cell electrolytes. When these materials are incorporated in dry cells, they increase somewhat the capacity of the cells.

The authors are indebted to Alfred Douty and George S. Gardner of the American Chemical Paint Co., to C. F. Prutton of the Lubrizol Corporation, and to D. G. Miller, of the Reilly Tar & Chemical Corporation, for their cooperation during the course of this investigation and for furnishing many of the commercial inhibitors.

VIII. References

[1] W. J. Hamer, J. P. Schrodt, and G. W. Vinal, Trans. Electrochem. Soc., Preprint 90-30, 367 (1946).
[2] L. C. Copeland and F. S. Griffith, Trans. Electrochem. Soc. **89,** 495 (1946).
[3] H. F. McMurdie, D. N. Craig, and G. W. Vinal, Trans. Electrochem. Soc. Preprint 90-31, 383 (1946).
[4] C. A. Mann, Trans. Electrochem. Soc. **69,** 115 (1936).
[5] W. J. Hamer. Unpublished.
[6] J. H. Bartram and P. J. C. Kent, Metallurgia **33,** 179 (1946).
[7] L. S. Stockelback and C. H. Bailey, Cereal Chem. **15,** 801 (1938).
[8] G. Haugaard and A. H. Johnson, J. Biol. Chem. **93,** 677 (1931).

Washington, October 1, 1947.

U. S. Department of Commerce
National Bureau of Standards

Research Paper RP1864
Volume 40, February 1948

Part of the Journal of Research of the National Bureau of Standards

Thermodynamic Functions for Molecular Oxygen in the Ideal Gas State

By Harold W. Woolley

The thermodynamic functions for molecular oxygen in the ideal gas state have been calculated using recent values of physical and spectroscopic constants. Values of $C_p°$, $H°-E_0°$, $-(F°-E_0°)/T$, and $S°$ are given, directly calculated or interpolated, for every twenty degrees up to 700°K and for every hundred degrees up to 5,000°K.

I. Introduction

A table of thermodynamic functions for molecular oxygen based on the latest spectroscopic data and values of physical constants was desired. Simple adjustment of the values published by Johnston and Walker [1, 2][1] seemed inadequate because of the complexity of the changes to be made in the spectroscopic constants. The new table is based entirely on newly computed values.

II. Spectroscopic Constants

The spectroscopic data used by Johnston and Walker have been revised to conform to the results of Curry and Herzberg [3] and Schlapp [4] for the ground state. For the $^1\Delta_g$ state, the constants used are based on the recent values of Herzberg and Herzberg [5]. Constants for the $^1\Sigma_u^-$ state and the $^3\Sigma_u^-$ state have been taken from the tables of Sponer [6]. For the $^3\Sigma_u^+$ state, approximate values of spectroscopic constants were selected, using a tentative identification of the Herzberg bands [7] proposed by Swings [8]. Several minor spectroscopic constants have been obtained with Dunham's formulas [9]. The improved theory of the ground state given by Schlapp introduces a slight shift in the calculated value of the unobserved lowest level. As this is the level to which all other levels are referred for purposes of thermochemical calculations, numerical values are altered slightly for all electronic states.

[1] Figures in brackets indicate the literature references at the end of this paper.

For states of diatomic molecules for which no splitting occurs due to spin or orbital interaction, the sum of electronic, vibrational, rotational, and vibrational-rotational interaction energies may be represented in wave numbers by the power series

$$W=\sum_{j,k} Y_{jk}\left(v+\frac{1}{2}\right)^j K^k(K+1)^k, \qquad (1)$$

using the notation of Dunham. Each electronic state has its own set of Y_{jk}'s. The electronic energy can be considered as represented by Y_{00}, the vibrational by

$$\sum_{j=1} Y_{j0}\left(v+\frac{1}{2}\right)^j,$$

and the sum of rotational and rotational-vibrational interaction energy by

$$\sum_{j=0,k=1} Y_{jk}\left(v+\frac{1}{2}\right)^j K^k(K+1)^k.$$

The vibrational quantum number, v, can assume any integral value, and the rotational quantum number, K, can assume various integral values. For a homonuclear molecule, such as O_2^{16}, there are half as many rotational states as for a comparable heteronuclear molecule. The ground state of O_2^{16} is a $^3\Sigma_g^-$ state with odd values of K. For the ground state, spin interactions are important, and triplet splitting occurs with the F_1 and F_3 components, averaging about 2 cm^{-1} lower than the F_2 component. The results of an adequate theoretical treatment of the splitting have been given by Schlapp, including inter-

actions neglected in the original treatment of Kramers [10]. The term values of the F_1, F_2, and F_3 components with $J=K+1$, K, and $K-1$, respectively, are given by the formulas

$$W_{K+1}=W_0+(2K+3)B-\lambda-[(2K+3)^2B^2+\lambda^2-2\lambda B]^{\frac{1}{2}}+\mu(K+1),$$
$$W_K=W_0, \qquad (2)$$
$$W_{K-1}=W_0-(2K-1)B-\lambda+[(2K-1)^2B^2+\lambda^2-2\lambda B]^{\frac{1}{2}}-\mu K,$$

with $B=1.438$ cm^{-1}, $\lambda=1.985$ cm^{-1}, and $\mu=-0.008$ cm^{-1}. W_0 is given by eq 1 with constants listed below for the $^3\Sigma_g^-$ state. In accord with these equations, the lowest state is the F_3 level for $K=1$ and is 3.96 cm^{-1} below the corresponding F_2 level, or 1.09 cm^{-1} below the nonexistent $K=0$ level.

For the $^1\Delta_g$ state, a double weighting due to Λ doubling provides single levels for both odd and even values of K, with levels beginning at $K=1$, the value of Λ. For the $^1\Sigma_g^+$ state, K has even values.

The states and spectroscopic constants used for O_2^{16} are

$^3\Sigma_g^-$ (ground state)

$Y_{00}=-786.08$ cm^{-1} $\quad$ $Y_{01}=1.4456$ cm^{-1}
$Y_{10}=1580.36$ cm^{-1} $\quad$ $Y_{11}=-0.0158$ cm^{-1}
$Y_{20}=-12.073$ cm^{-1} $\quad$ $Y_{02}=-4.838\times10^{-6}$ cm^{-1}
$Y_{30}=0.0546$ cm^{-1} $\quad$ $Y_{12}=-4.96\times10^{-9}$ cm^{-1}
$Y_{40}=-0.00143$ cm^{-1} $\quad$ $Y_{03}=0.1387\times10^{-12}$ cm^{-1}
$Y_{04}=-32.2\times10^{-18}$ cm^{-1}

$^1\Delta_g$

$Y_{00}=7132.1$ cm^{-1} $\quad$ $Y_{01}=1.4264$ cm^{-1}
$Y_{10}=1509.3$ cm^{-1} $\quad$ $Y_{11}=-0.0171$ cm^{-1}
$Y_{20}=-12.9$ cm^{-1} $\quad$ $Y_{02}=-4.86\times10^{-6}$ cm^{-1}

$^1\Sigma_g^+$

$Y_{00}=12409.2$ cm^{-1} $\quad$ $Y_{01}=1.4014$ cm^{-1}
$Y_{10}=1432.615$ cm^{-1} $\quad$ $Y_{11}=-0.0188$ cm^{-1}
$Y_{20}=-13.925$ cm^{-1} $\quad$ $Y_{02}=-5.36\times10^{-6}$ cm^{-1}

$^3\Sigma_u^+$

$Y_{00}=35{,}385$ $\quad$ $Y_{40}=-0.099$
$Y_{10}=791.5$ $\quad$ $Y_{01}=1.13$
$Y_{20}=-20.83$ $\quad$ $Y_{11}=-0.06$
$Y_{30}=0.83$ $\quad$ $Y_{02}=-9\times10^{-6}$

$^3\Sigma_u^-$

$Y_{00}=49{,}007$ $\quad$ $Y_{01}=0.820$
$Y_{10}=709.57$ $\quad$ $Y_{11}=-0.014$
$Y_{20}=-10.708$

Corresponding spectroscopic constants were obtained for lower states of the heteronuclear $O^{16}O^{17}$ and O^{16}-O^{18} molecules, for which both odd and even rotational levels are present in each state.

III. Method of Calculation

The thermodynamic functions for the ideal gas state at atmospheric pressure are obtained from the partition function Q by evaluating the formulas

$$\frac{H^\circ-E_0^\circ}{RT}=\frac{T}{Q}\frac{dQ}{dT}+\frac{5}{2}$$

$$-\frac{(F^\circ-E_0^\circ)}{RT}=\ln Q+\frac{3}{2}\ln M+\frac{5}{2}\ln T-3.6644$$

$$\frac{S^\circ}{R}=\frac{H^\circ-E_0^\circ}{RT}-\frac{F^\circ-E_0^\circ}{RT}$$

$$\frac{C_p^\circ}{R}=\frac{T^2}{Q}\frac{d^2Q}{dT^2}-\left[\frac{T}{Q}\frac{dQ}{dT}-1\right]^2+\frac{7}{2},$$

where T is temperature in degrees K; M is the molecular weight on the chemical scale, 31.9988 for O_2^{16}, 32.9955 for O^{16}-O^{17}, and 33.9956 for O^{16}-O^{18}; and Q, the partition function, or state sum, is given by $pe^{-\epsilon/KT}$, where $p=2J+1$ and $\epsilon=hcW$. The contributions of the different electronic states are included by evaluating $Q=Q_1+Q_2+Q_3+\ldots$ and its derivatives, where Q_1 is for the $^3\Sigma_g^-$ state, Q_2 for the $^1\Delta_g$ state, Q_3 for the $^1\Sigma_g^+$ state, etc.

In evaluating the Q's, or values of $\sum(2J+1)e^{-hcW/kT}$, the rotational energy is separated from the rest of the energy W, and the sum over rotation levels is expressed in terms of an integral. In this way it is found that the functions Q_i and their derivatives are given by the formulas

$$Q_i=g\sum fe^{-x} \qquad (7)$$

$$T\frac{dQ_i}{dT}=g[\sum Tf'e^{-x}+\sum fxe^{-x}] \qquad (7a)$$

$$T^2\frac{d^2Q_i}{dT^2}=g[\sum T^2f''e^{-x}+2\sum Tf'xe^{-x}-2\sum fxe^{-x}+\sum fx^2e^{-x}], \qquad (7b)$$

where x is G_vhc/kT, with G_v representing the sum of electronic and purely vibrational energy in cm^{-1}, and where the summation extends over all vibrational levels up to dissociation. G_v is thus that part of the total energy that is completely

independent of the rotational quantum number, and is given by

$$\sum_{j=0} Y_{j0}\left(v+\frac{1}{2}\right)^j$$

or its equivalent expressed as a polynomial in v. g is an average weight factor in addition to the factor $2J+1$ typical for the rotational levels of a simple rotating vibrator. For each electronic state, the quantity f, and its temperature derivatives, f' and f'', are functions of T and v obtained from

$$f=\frac{4}{315}\frac{c_2^2B_v^2}{T^2}+\frac{1}{15}\frac{c_2B_v}{T}+\frac{1}{3}+\frac{T}{c_2}\frac{1}{B_v}+\frac{T^2}{c_2^2}\left(\frac{-2D_v}{B_v^3}\right)+\frac{T^3}{c_2^3}\frac{12D_v^2-6B_vF_v}{B_v^5}+\frac{T^4}{c_2^4}\frac{120B_vD_vF_v-24B_v^2H_v-120D_v^3}{B_v^7}\cdots, \tag{8}$$

with $c_2=hc/k$, as in the derivation given in reference [11]. Convergence difficulties discussed in that paper for the hydrogens do not occur for such molecules as O_2. The spectrosopic constants B_v, D_v, F_v, and H_v, are given by $\sum_{j=0} Y_{jk}(v+1/2)^j$, with k taking the values 1, 2, 3, and 4, respectively.

In using the above expressions, the vibrational energy, G_v, is ordinarily to be evaluated with respect to the lowest level of the ground state. The partition function for the ground state, including the effect of triplet splitting, as detailed in eq. 2, may be represented as

$$\begin{aligned}
Q_r&=\sum_i\left\{f_e+\left[e^{-hc(2\lambda+\mu-2B)/kT}+2e^{-hc(\lambda+5\mu/2-2B)/kT}\right]\sum_{K=1,3\ldots}(2K+1)e^{\frac{-hcW}{KT}}\right\}\\
&=\sum_i\left\{f_e+\left[\frac{1}{3}e^{-hc(2\lambda+\mu-2B)/kT}+\frac{2}{3}e^{-hc(\lambda+5\mu/2-2B)/kT}\right]\frac{3}{2}f_0\right\}\\
&=\sum\left\{f_e+e^{-hc(4\lambda/3+2\mu-2B)/kT}3/2f_0\left[1+\frac{1}{9}\left(\frac{hc}{kT}\right)^2(\lambda-3\mu/2)^2-\frac{1}{81}\left(\frac{hc}{kT}\right)^3(\lambda-3\mu/2)^3+\ldots\right]\right\}\\
&=e^{-hc(4\lambda/3+2\mu-2B)/kT}\frac{3}{2}\sum\left\{\frac{2}{3}f_e\left[1+\frac{hc}{kT}(4\lambda/3+2\mu-2B)+\ldots\right]\right.\\
&\quad\left.+f_0\left[1+\frac{1}{9}\left(\frac{hc}{kT}\right)^2(\lambda-3\mu/2)^2-\frac{1}{81}\left(\frac{hc}{kT}\right)^3(\lambda-3\mu/2)^3\ldots\right]\right\}
\end{aligned} \tag{9}$$

Q_r represents the partition function that would be obtained for the ground state if the triplet splitting were negligibly small, and energies were reckoned from $K=0$. f_e is a small correction term to which the only significant contribution above very low temperatures comes from the $K=1$ levels:

$$f_e=3e^{\frac{-hc}{kT}[5B-(25B^2+\lambda^2-2\lambda B)^{1/2}+\lambda+3\mu-2B]}+1-6e^{\frac{-hc}{KT}[\lambda+5\mu/2-2B]}=\frac{1.963}{T}-\frac{1.48}{T^2}+\ldots \tag{10}$$

Equation 9 shows that the effect of the triplet splitting is most readily included for ordinary and elevated temperatures by introducing a small additive correction $4\lambda/3+2\mu-2B$, or -0.244 cm^{-1}, in the vibrational energy formula for the ground state and introducing small correction terms in the formula for f to take account of its trends toward lower temperatures.

Evaluation of the expressions as far as appears justified with the present data gives the following for the various states for O_2^{16}.

$^3\Sigma_g^-$ state, $g=\frac{3}{2}$

$$\begin{aligned}
G_v&=-0.244+1568.33v-11.993v^2+0.0517v^3-0.00143v^4\\
f&=-\frac{1.232}{T^2}+\frac{1.8902}{T}+\frac{1}{3}+(0.483562+0.005311v)T+(1.5746\cdot10^{-6}+0.0535\cdot10^{-6}v)T^2+14.89\cdot10^{-12}T^3+267\cdot10^{-18}T^4.
\end{aligned}$$

$^1\Delta_g$ state, $g=1$

$$\begin{aligned}
G_v&=7883.5+1496.4v-12.9v^2\\
f&=\frac{1}{3}+(0.49033+0.00599v)T+1.709\cdot10^{-6}T^2
\end{aligned} \tag{11}$$

$^1\Sigma_g^+$ state, $g=\frac{1}{2}$

$$G_v = 13122 + 1418.69v - 13.925v^2$$
$$f = \frac{1}{3} + (0.49944 + 0.006837v)T + 1.921 \cdot 10^{-6}T^2$$

$^3\Sigma_u^+$ state, $g = \frac{3}{2}$

$$G_v = 35776 + 771.2v - 19.74v^2 + 0.63v^3 - 0.099v^4$$
$$f = \frac{1}{3} + 0.632T/(1 - 0.0545v) + 6 \times 10^{-6}T^2$$

$^3\Sigma_u^-$ state, $g = \frac{3}{2}$

$$G_v = 49359 + 698.86v - 10.708v^2$$
$$f = \frac{1}{3} + (0.855 + 0.0145v)T$$

The values used for R and hc/k were 1.98714 (defined) cal deg^{-1}mole^{-1} and 1.4384 deg cm, respectively.

For all electronic states treated, each summation over rotational levels for a given vibrational level was broken off at the top of the predissociation region applying to the vibrational level, by using a suitable upper limit in the integration given in reference [11]. This complicating restriction, which requires special treatment, is significant only at the highest temperatures.

The contributions of the several electronic states to the partition function and its derivatives for O_2^{16} are listed in tables 1, 2, and 3. These values may facilitate any future revision of thermodynamic functions for oxygen if new spectroscopic data make it desirable. It is thought that in general these sums and their derivatives have been carried to more digits than correspond to the accuracy of the spectroscopic data. This is particularly the case for the $^1\Delta_g$ state for which the anharmonicity constant has not been determined experimentally. The values given in brackets are the additional contributions that would be obtained if the rotational sums were extended to infinite energy as has been customary instead of limiting them to the region of quantized levels. These additional contributions are given to more decimal places than were used for the entire sums because of possible theoretical interest in their magnitudes. The information necessary for a satisfactory calculation of the state sums for the vibrational states near the dissociation limit is not available. An analysis of the problem has been started in connection with this paper and previous work [11] and may be completed in a future publication.

TABLE 1. *Values of Q for* O_2^{16}

Temperature	$^3\Sigma_g^-$ (Q_1)	$^1\Delta_g$ (Q_2)	$^1\Sigma_g^+$ (Q_3)	$^3\Sigma_u^+$ (Q_4)	$^3\Sigma_u^-$ (Q_5)	Tota
°K						
100	73.344					
200	145.931					
300	218.705					
400	292.374					
600	447.681					
800	620.90	0.00				
1,000	816.90	.01				
1,250	1097.27	.09				
1,500	1418.91	.51	0.00			
1,750	1783.03	1.90	.01			
2,000	2190.46	5.26	.06			
2,500	3138.02	23.52	.61			
3,000	4266.61	68.37	2.96	0.00		
4,000	7086.4	293.7	23.97	.04	0.00	
	[.02]	[.01]	[.004]	[.024]		
5,000	10690.4	784.8	93.8	.76	.02	
	[.47]	[.24]	[.12]	[.06]		

TABLE 2. *Values of* TdQ/dT *for* O_2^{16}

Temperature	$^3\Sigma_g^-$ (TQ_1')	$^1\Delta_g$ (TQ_2')	$^1\Sigma_g^+$ (TQ_3')	$^3\Sigma_u^+$ (TQ_4')	$^3\Sigma_u^-$ (TQ_5')	Tota
°K						
100	72.551					
200	145.272					
300	219.098					
400	298.152					
600	489.366	0.000				
800	736.328	.005				
1,000	1041.33	.08				
1,250	1503.77	.91	0.00			
1,500	2056.30	4.62	.02			
1,750	2699.56	15.22	.17			
2,000	3434.68	38.16	.71			
2,500	5186.33	146.06	5.66			
3,000	7324.29	377.28	23.81	0.0		
	[.002]	[.001]				
4,000	12819.6	1370.2	157.6	.6	0.0	
	[.3]	[.14]	[.07]	[.4]		
5,000	20050.9	3267.1	534.2	8.8	.1	
	[6.3]	[3.2]	[1.6]	[8.9]		

The calculations which have been described were for O_2^{16}. Thermodynamic functions for ordinary oxygen may be obtained from those for O_2^{16} by making small adjustments in the values. In the naturally occurring mixture of isotopic oxygen, 99.526 percent of the molecules are O^{16}-O^{16}, 0.394 percent are O^{16}-O^{18}, and 0.080 percent are O^{16}-O^{17}, according to the isotope data given by Birge [12]. The tables of Gordon and Barrow [13] were used in calculating the minute changes in the thermodynamic functions due to the

presence of isotopic molecules and for some other calculations for which the tables were advantageous. The contribution to $S°$ and to $-(F°-E_0^°)/T$ due to the presence of both odd and even rotational levels in O^{16}-O^{17} and O^{16}-O^{18} amounts to 0.0065 cal deg^{-1} mole^{-1} in the final table. The entropy of mixing of isotopes, amounting to 0.0677 cal deg^{-1} mole^{-1}, was not included. Similarly, no entropy of nuclear spin has been included. The quantities that were added to the thermodynamic functions for O_2^{16} to obtain values for the isotope mixture are given in table 4.

TABLE 3. *Values of T^2d^2Q/dT^2 for O_2^{16}*

Temperature	$^3\Sigma_g^-$	$^1\Delta_g$	$^1\Sigma_g^+$	$^3\Sigma_u^+$	$^3\Sigma_u^-$	Total
	(T^2Q_1'')	(T^2Q_2'')	(T^2Q_3'')	(T^2Q_4'')	(T^2Q_5'')	(T^2Q'')
° K						
10	0.108	.....	.....	.....	.....	0.108
20	.466	.....	.....	.....	.....	.466
30	7.523	.....	.....	.....	.....	7.523
40	35.539	0.000	.....	.....	.....	35.539
50	164.969	.001	.....	.....	.....	164.970
60	367.677	.061	.....	.....	.....	367.738
70	628.33	.91	0.00	.....	.....	629.24
80	1033.40	7.85	.03	.....	.....	1041.28
90	1530.12	33.43	.30	.....	.....	1563.85
100	2123.25	95.23	1.75	.....	.....	2220.23
120	2817.34	211.16	6.54	.....	.....	3035.04
140	4525.96	662.84	42.32	0.0	.....	5231.12
160	6691.38	1469.47	150.44	.1	0.0	8311.39
	[.03]	[.02]	[.01]	[.1]		
180	12544.2	4278.8	772.6	7.6	.2	17603.4
	[4.0]	[2.1]	[1.1]	[5.6]		
200	20692.3	8769.0	2174.1	83.3	5.2	31693.9
	[72.5]	[37.4]	[18.9]	[104.5]		

TABLE 4. *Increments to functions for O_2^{16} to obtain functions for the naturally occurring isotope mixture*

T	$C_p°$	$(H°-E_0°)$	$-(F°-E_0°)/T$	
° K	cal deg^{-1} mole^{-1}	cal mole^{-1}	cal deg^{-1} mole^{-1}	cal deg^{-1} mole^{-1}
100	0	0.013	0.00770	0.00783
200	0	.013	.00776	.00782
300	0.00005	.015	.00779	.00784
400	.00011	.023	.00780	.00786
600	.00017	.053	.00783	.00792
800	.00016	.09	.00785	.00796
1,000	.00013	.12	.00788	.00800
1,250	.00010	.14	.00790	.00801
1,500	.00007	.16	.00792	.00802
1,750	.00006	.18	.00794	.00804
2,000	.00005	.20	.00795	.00805
2,500	.00003	.22	.00797	.00806
3,000	.00002	.23	.00799	.00807
4,000	.00002	.25	.00801	.00807
5,000	.00001	.26	.00802	.00807

TABLE 5. *Thermodynamic functions for the natural isotopic mixture of molecular oxygen in the standard ideal gas state at 20-degree intervals up to 700° K*

T	$C_p°$	$H°-E_0°$	$-(F°-E_0°)/T$	$S°$
° K	cal deg^{-1} mole^{-1}	cal mole^{-1}	cal deg^{-1} mole^{-1}	cal deg^{-1} mole^{-1}
20	6.984	136.39	23.373	30.193
40	6.964	275.81	28.130	35.025
60	6.960	415.03	30.930	37.848
80	6.958	554.20	32.922	39.850
100	6.958	693.36	34.469	41.402
120	6.958	832.52	35.733	42.671
140	6.958	971.67	36.803	43.743
160	6.958	1110.85	37.730	44.672
180	6.959	1250.0	38.547	45.492
200	6.961	1389.2	39.279	46.225
220	6.966	1528.5	39.941	46.889
240	6.974	1667.9	40.546	47.495
260	6.986	1807.4	41.102	48.054
280	7.002	1947.3	41.618	48.572
300	7.023	2087.6	42.097	49.056
320	7.050	2228.3	42.547	49.510
340	7.080	2369.6	42.969	49.938
360	7.115	2511.5	43.368	50.344
380	7.154	2654.2	43.745	50.730
400	7.196	2797.7	44.104	51.098
420	7.240	2942.1	44.445	51.450
440	7.286	3087.3	44.771	51.788
460	7.334	3233.5	45.083	52.113
480	7.382	3380.7	45.383	52.426
500	7.431	3528.8	45.671	52.728
520	7.480	3678.0	45.948	53.021
540	7.529	3828.0	46.215	53.304
560	7.577	3979.1	46.473	53.579
580	7.624	4131.1	46.723	53.845
600	7.670	4284.1	46.964	54.105
620	7.715	4437.9	47.199	54.357
640	7.759	4592.7	47.426	54.602
660	7.802	4748.3	47.648	54.842
680	7.843	4904.7	47.863	55.075
700	7.883	5062.0	48.072	55.303

Calculated with $R=1.98714$ cal deg^{-1} mole^{-1}

Values of the thermodynamic functions were computed in the manner described for every 20 degrees up to 200° and for temperatures 300°, 400°, 600°, 800°, 1,000°, 1,250°, 1,500°, 1,750°, 2,000°, 2,500°, 3,000°, 4,000°, and 5,000° K. Intermediate values were interpolated for $C_p^°$ at every 20 degrees up to 700° K and at every 100 degrees throughout the remainder of the temperature range covered. Using tabular integration, tables of $H°-E_0°$, $S°$ and $-(F°-E_0°)/T$ were built up from the $C_p^°$ table. Good agreement was obtained with the directly computed values at all the above reference temperatures. The results are given at 20-degree intervals up to 700° K in table 5 and at 100-degree

intervals up to 5,000° K in table 6 for the naturally occurring mixture of oxygen isotones.

TABLE 6. *Thermodynamic functions for the natural isotopic mixture of molecular oxygen in the standard ideal gas state at 100-degree intervals up to 5,000° K*

T	$C_p°$	$H°-E_0°$	$-(F°-E_0°)/T$	$S°$
° K	cal deg^{-1} mole^{-1}	cal mole^{-1}	cal deg^{-1} mole^{-1}	cal deg^{-1} mole^{-1}
100	6.958	693.36	34.469	41.402
200	6.961	1389.2	39.279	46.225
300	7.023	2087.6	42.097	49.056
400	7.196	2797.7	44.104	51.098
500	7.451	3528.8	45.671	52.728
600	7.670	4284.1	46.964	54.105
700	7.883	5062.0	48.072	55.303
800	8.063	5859.6	49.044	56.368
900	8.212	6673.7	49.912	57.327
1,000	8.336	7501.2	50.697	58.199
1,100	8.439	8340.1	51.416	58.998
1,200	8.527	9188.6	52.079	59.736
1,300	8.604	10045.2	52.695	60.422
1,400	8.674	10909.2	53.270	61.062
1,500	8.738	11779.8	53.810	61.663
1,600	8.800	12656.8	54.318	62.229
1,700	8.858	13539.7	54.799	62.764
1,800	8.916	14428.4	55.256	63.272
1,900	8.973	15322.8	55.691	63.756
2,000	9.029	16223	56.106	64.217
2,100	9.084	17129	56.503	64.659
2,200	9.139	18040	56.883	65.083
2,300	9.194	18956	57.248	65.490
2,400	9.248	19879	57.600	65.883
2,500	9.301	20806	57.939	66.261
2,600	9.354	21739	58.266	66.627
2,700	9.405	22677	58.582	66.981
2,800	9.455	23620	58.889	67.324
2,900	9.503	24568	59.185	67.657
3,000	9.551	25520	59.473	67.980
3,100	9.596	26478	59.753	68.294
3,200	9.640	27440	60.024	68.599
3,300	9.682	28406	60.289	68.896
3,400	9.723	29376	60.546	69.186
3,500	9.762	30350	60.797	69.468
3,600	9.799	31328	61.042	69.744
3,700	9.835	32310	61.280	70.013
3,800	9.869	33295	61.514	70.276
3,900	9.901	34284	61.742	70.532
4,000	9.932	35275	61.965	70.783

TABLE 6. *Thermodynamic functions for the natural isotopic mixture of molecular oxygen in the standard ideal gas state at 100-degree intervals up to 5,000° K*—Continued

T	$C_p°$	$H°-E_0°$	$-(F°-E_0°)/T$	$S°$
° K	cal deg^{-1} mole^{-1}	cal mole^{-1}	cal deg^{-1} mole^{-1}	cal deg^{-1} mole^{-1}
4,100	9.961	36270	62.183	71.029
4,200	9.988	37267	62.396	71.269
4,300	10.015	38267	62.605	71.505
4,400	10.039	39270	62.810	71.735
4,500	10.062	40275	63.011	71.961
4,600	10.084	41282	63.208	72.182
4,700	10.104	42292	63.401	72.399
4,800	10.123	43303	63.591	72.613
4,900	10.140	44316	63.777	72.821
5,000	10.156	45331	63.960	73.026

(Calculated with R=1.98714 cal deg^{-1} mole^{-1}

IV. References

[1] H. L. Johnston and M. K. Walker, J. Am. Chem. Soc. **55,** 172 (1933).

[2] H. L. Johnston and M. K. Walker, J. Am. Chem. Soc. **57,** 682 (1935).

[3] J. Curry and G. Herzberg, Ann. Physik **19,** 800 (1934).

[4] R. Schlapp, Phys. Rev. **51,** 342 (1937).

[5] L. Herzberg and G. Herzberg, Astrophys. J. **105,** 353 (1947).

[6] H. Sponer, Molecular spectra and their application to chemical problems. I. Tables. (Julius Springer, Berlin, 1935).

[7] G. Herzberg, Naturwissenschaften **20,** 577 (1932).

[8] P. Swings, Astrophys. J. **97,** 72 (1943).

[9] J. L. Dunham, Phys. Rev. **41,** 721 (1932).

[10] H. A. Kramers, Z. Physik **53,** 422 (1929).

[11] H. W. Woolley, J. Chem. Phys. **9,** 470 (1941).

[12] R. T. Birge, Rev. Modern Phys. **13,** 233 (1941).

[13] A. R. Gordon and C. Barnes, J. Chem. Phys. **1,** 297 (1933).

WASHINGTON, October 15, 1947.